Transport in quantum dots from the integrability of the Anderson model

Robert M. Konik
Department of Physics, University of Virginia, Charlottesville, Virginia 22903

Hubert Saleur
Department of Physics, University of Southern California, Los Angeles, California 90089-0484

Andreas Ludwig
Department of Physics, University of California, Santa Barbara, California 93106
(Received 29 June 2001; published 4 September 2002)

In this work we exploit the integrability of the two-lead Anderson model to compute transport properties of a quantum dot, in and out of equilibrium. Our method combines the properties of integrable scattering together with a Landauer-Buttiker formalism. Although we use integrability, the nature of the problem is such that our results are not generically *exact*, but must only be considered as excellent approximations which nonetheless are valid all the way through crossover regimes. The key to our approach is to identify the excitations that correspond to scattering states and then to compute their associated scattering amplitudes. We are able to do so both in and out of equilibrium. In equilibrium and at zero temperature, we reproduce the Friedel sum rule for an arbitrary magnetic field. From this we compute exactly the behavior of the zero-temperature linear-response conductance as a function of both the gate voltage and field. We also study transport quantities requiring knowledge of scattering states away from the Fermi surface. We compute the linear-response conductance at finite temperature at the symmetric point of the Anderson model and reproduce the numerical renormalization-group computation of this quantity of Costi *et al.* We then explore the out-of-equilibrium conductance for a near-symmetric Anderson model and arrive at quantitative expressions for the differential conductance, both in and out of a magnetic field. We reproduce the expected splitting of the differential conductance peak into two in a finite magnetic field H. We determine the width, height, and position of these peaks. In particular, we find that for $H \gg T_k$, the Kondo temperature, the differential conductance has maxima of e^2/h occurring for a bias V close to but smaller than H. The nature of our construction of scattering states suggests that our results for the differential magnetoconductance are not merely approximate, but become exact in the large-field limit.

DOI: 10.1103/PhysRevB.66.125304 PACS number(s): 73.23.Hk, 85.35.Gv, 72.15.Qm, 71.10.Pm

I. INTRODUCTION

The Kondo effect is a cynosure of modern condensed matter physics. Due to the strongly coupled nature of its IR fixed point, understanding its low-energy behavior has proven a major theoretical challenge. Typically, the phenomenon refers to the interaction of isolated magnetic impurities in a bulk metal. However, in the last several years the experimental study of single magnetic impurities has moved to a new arena: that of quantum dots connected to external leads.[1–5] In analogy to the traditional realization of the Kondo effect, the leads serve as the bulk metal and the dot as the magnetic impurity. The appearance of the Kondo effect in this new setting has brought a new set of theoretical challenges: how to compute transport quantities that form the main experimental signatures of these systems.

Quantum dots come in at least two forms. Semiconductor quantum dots[1–4] are a product of the continuing project of the miniaturization of solid-state devices. They are fabricated by confining electrons in a two-dimensional electron gas (2DEG) within a GaAs/AlGaAs structure using a combination of metallic gates. The region to which the electrons are confined is small enough that its energy levels may be considered discrete. The dot is connected to source and drain contacts (the two leads). Schematically, the quantum dot can be pictured as shown in Fig. 1.

The source and drain can be held at any relative voltage, thus enabling the study of both linear-response and out-of-equilibrium transport quantities. Beyond the gates that serve to confine the electrons of the 2DEG, additional gates can be deposited on the GaAs/AlGaAs heterostructure. Such gates capacitively couple to the quantum dot through a gate voltage V_g, thus allowing the chemical potential of the dot to be adjusted. This has two important consequences. By adjusting the gate voltage, one can tune the number of electrons in the

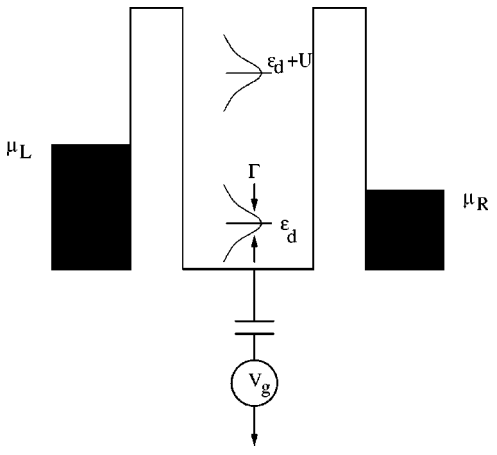

FIG. 1. Schematic of the quantum dot.

 ©2002 The American Physical Society

confined region to be odd so that there is a single unpaired electron. The presence of an unpaired electron allows the appearance of Kondo-like physics. Moreover, by tuning V_g, the unpaired electron's chemical potential can be adjusted, thus controlling the scale T_k where Kondo physics sets in. Such systems are thus said to possess a ''tunable'' Kondo effect.[2]

Quantum dots may also be fabricated from metallic carbon nanotubes.[5] By depositing metallic leads on top of a small section of a carbon nanotube, an effective quantum dot is made. Like their semiconductor counterparts, these dots are tunable: gates may be added to the semiconductor substrate upon which the nanotube and leads lie. Semiconductors dots typically carry 10–100 electrons. Nanotube dots, in contrast, have many thousands of electrons and yet still exhibit Kondo-like physics.

The transport quantities that lie at the focus of the experimental study of a tunable Kondo effect in quantum dots have been measured under a variety of conditions. Conductances of the lead-dot system have been determined both in and out of equilibrium and both in and out of the presence of a magnetic field. Remarkably, this wide variety of experimental phenomena is thought to be described by a conceptually simple theory: the Anderson model.

The Anderson model is fashioned from a chain of noninteracting spinful fermions (the leads) connected via hopping to a single-site impurity on which alone Coulomb repulsion is present. On a lattice, the Hamiltonian reads (with no bias and $H=0$)

$$H=\sum_{i\alpha} -t(c^{\dagger}_{i,\alpha}c_{i+1,\alpha}+\text{H.c.})+Un_{d\uparrow}n_{d\downarrow}+\sum_{\alpha}\,[V_1(c^{\dagger}_{-1,\alpha}d_{\alpha} + \text{H.c.})+V_2(c^{\dagger}_{1,\alpha}d_{\alpha}+\text{H.c.})]+\varepsilon_d(n_{d\uparrow}+n_{d\downarrow}). \tag{1.1}$$

Here $c^{\dagger}_{\alpha}$ and c_{α} are the lead electron creation and destruction operators, respectively, $d^{\dagger}$ and d the dot electron creation and destruction operators, respectively, and $n_d=d^{\dagger}d$. The dot is considered to reside at $x=0$. The index α indicates the spin species. The interaction on the dot is present in the term $Un_{d\uparrow}n_{d\downarrow}$. Although deceptively simple, the presence of a nonzero U makes the problem many body with all of its manifold complications.

U is pictured in Fig. 1 and represents the charging energy incurred when an electron is added to the dot. Roughly, it can be estimated as

$$U=\frac{e^2}{2C}+\Delta\varepsilon, \tag{1.2}$$

where C is the capacitance of the dot and $\Delta\varepsilon$ is the dot's energy level spacing. For the experiments at hand, $U\sim 1$ meV. The counterpart of the gate voltage V_g in the above Hamiltonian is ε_d, the parameter that controls the chemical potential of the electrons on the dot. By adjusting ε_d, the number of electrons on the model dot can be varied from 0 to 2. (Although there may be a large number of electrons on the actual dot, the concern here both theoretically and experimentally is of electrons in the highest-occupied energy level.) The final pair of parameters $V_{1,2}$ measure the height of the tunnel barriers between the leads and dot. In general, they differ between the two leads. The quantity Γ (see Fig. 1) measuring the width of the level resonance that arises through the interaction of the leads, and the dot is given in terms of the tunnel barrier heights to be $\Gamma=(V_1^2+V_2^2)/2$. Typically, $\Gamma/U\ll 1$ in the experiments of concern.[1–4]

Although the above-described experimental results have come relatively recently, the theoretical study of transport through impurities is much older. Appelbaum and Anderson both studied conductance anomalies present in tunnel junctions due to the presence of magnetic impurities.[6] However, their efforts were perturbative in nature and did not describe the strong-coupling nature of the Kondo effect. More recently, Ng and Lee[7] studied the linear-response conductance both in and out of a magnetic field using the Friedel sum rule. The Friedel sum rule relates the scattering phase of the electrons at the Fermi surface to the average number of electrons sitting on the dot. However, the Friedel sum rule is useful only in determining the linear-response conductance, a consequence of the rapid variation in the scattering phase as one moves away from the Fermi surface. In contrast to the linear-response conductance where the Friedel sum rule is an exact relationship, the techniques used to determine out-of-equilibrium transport are limiting in nature. In one approach, a noncrossing approximation[8,9] (NCA) was employed. The NCA approach has drawbacks. In order to implement the associated use of slave bosons, one must take $U=\infty$. Moreover, the NCA is in some sense a large-N approximation where N is the number of spin degrees of freedom of the impurity (in this case $N=2$). It is known to be remarkably accurate in computing thermodynamics. However, it is less accurate when it comes to transport quantities ($\sim$15% errors[9]) due to its less accurate prediction of behavior right at the Fermi surface. And as such these difficulties render it unusable in nonzero magnetic fields.[9] In another approach to computing nonequilibrium properties, a clever combination of the analysis of the equations of motion with perturbation theory was employed to study the differential magnetoconductance.[10] However, the truncation of the equations of motion necessary to perform the analysis in this work is in some sense an uncontrolled approximation. The authors of Ref. 10 indicate that their methodology underestimates the magnitude of the differential conductance. Another set of approaches has relied upon perturbation theory.[11–13] As with the results of Ref. 6, perturbation theory requires relatively small U (Coulomb repulsion) or, alternatively, temperatures far in excess of the Kondo temperature and so presumably can access, at best, qualitative, not quantitative, features of the strongly coupled physics found in the Kondo regime of quantum dots at low temperatures.

These inherent difficulties with the out-of-equilibrium Anderson were circumvented in the study of a nonequilibrium Kondo impurity at its Toulouse point.[14] At this point, the model can be mapped to a system of noninteracting fermions, thus permitting an exact solution. It is unclear, however, how the Toulouse limit affects the underlying physics. Although the ordinary Kondo model shares the same IR fixed point as its Toulouse counterpart, we are interested in

part in physics for large applied field, bias, and temperature: that is, in physics far away from this fixed point.

Given the limitations of these methods, one cannot help but notice that the Anderson model is exactly solvable. Indeed, this integrability has already been exploited through Bethe ansatz solutions to compute thermodynamic quantities[15,16] such as the specific heat and magnetic susceptibility. But what of transport quantities? A limited attempt to deduce information about transport properties from the Bethe ansatz solution of the *Kondo* model was made recently.[17] There the equilibrium impurity density of states that arises from the Bethe ansatz was studied. In general, the impurity density of states coming from the Bethe ansatz is unrelated to the spectral density of states arising from the dot correlator, $\mathrm{Im}\langle dd^\dagger\rangle$. Indeed, at zero temperature and zero field, it is clear the two are much different quantities (the heights of the zero-energy peaks in both quantities are controlled by far different energy scales). But in the methodology of Ref. 17, it is this latter quantity $\mathrm{Im}\langle dd^\dagger\rangle$ that is directly related to transport.[9,10,12] Moreover, the context of their computation, as determined in Refs. 9, 10, and 12, demands that the *nonequilibrium* properties of $\mathrm{Im}\langle dd^\dagger\rangle$ be computed. Given the general unavailability from the integrability of information about correlators such as $\mathrm{Im}\langle dd^\dagger\rangle$, a different approach is needed to extract transport properties from the exact solvability of the model. Here we advocate a Landauer-Büttiker approach to transport and so are instead faced with the task of identifying scattering states in the context of integrability.

The key feature of an integrable system is the exact knowledge of eigenfunctions of the fully interacting Hamiltonian. In turn, there is a well-defined notion of elementary excitations. In particular, these excitations have an infinite lifetime: integrability forbids any decay processes from occurring. This arises from the infinite series of nontrivial conservation laws in the model. In some sense an integrable system is a superior version of a Fermi liquid.

In the Anderson model, there is such a set of excitations, as detailed in Secs. III and IV. They are not on the face of it, however, particularly electronic. And if we are to understand the transport of the sea of electrons in the attached leads, we necessarily need scattering states which carry the quantum numbers of an electron. Rather, the excitations divide into separate spin and charge sectors. The closest they come to being electronic is in bound states between excitations which can be thought of as bound states of electrons. This is not so unnatural. If one were to bosonize the Anderson model, one would find that the degrees of freedom separate into spin and charge bosons. But this is only one problem with the excitations arising from integrability. These excitations, as explained in Sec. III, are a combination of degrees of freedom in *both* of the leads connected to the dot. And it is the case that this entanglement cannot always be simply reversed.

And so there is the difficulty. The scattering states are not necessarily electronic in nature and not confined to a single lead. Only if one can understand electronic excitations in an individual lead can one hope to make sense of scattering amplitudes off the dot. It is these two facts that have prevented the integrability of the Anderson model from being applied to transport quantities up to now.

However, we have managed to circumvent these problems in a number of cases. In particular, we have successfully described both scattering states at the Fermi surface for generic values of U, ε_d, and Γ and scattering at finite energies at the symmetric point of the Anderson model, $U=-\varepsilon_d/2$. There we argue that by correctly gluing together a spin and charge excitation, we are able to form an excitation that is electronic in nature. Moreover, the excitations are such that one can understand them in terms of the individual leads and so compute reflection and transmission amplitudes of the excitation off the dot. We do so in an argument akin to that used by Andrei[18] in computing the magnetoresistance in the Kondo model. There he argues that the scattering phase of an excitation can be identified with its impurity momentum. In turn, this momentum is related to the impurity density of states as it appears in the Bethe ansatz and so can be directly computed.

We now turn to how we use these excitations to compute transport quantities. All such quantities could be expressed in terms of the scattering of asymptotically free electrons (i.e., electrons in the attached leads) off the quantum dot. However, such scattering, in general, is not particularly simple. In general away from the Fermi surface such scattering will be inelastic and involve particle-hole production. We however recast the density of states of asymptotically free fermions in terms of the integrable excitations we have identified. Because of their integrability, their scattering is simple: their character does not change in scattering through the dot and their transport can be described individually: they scatter one by one through the dot.

It is, however, unlikely that the integrable electronic excitations we use in computing transport properties provide exact results in all cases—the issues involved here are subtle and will be discussed in detail in the next sections. In particular, it is unlikely the high-energy limit of the excitations we construct are entirely confined to a single lead. However, this methodology successfully passes a number of tests. The first test of our method comes in proving the Friedel sum rule. The Friedel sum rule relates the occupancy of spin $\uparrow/\downarrow$ electrons on the quantum dot, $n_{d\uparrow/\downarrow}$, to the scattering phase of an electron of the same spin, $\delta_{e\uparrow/\downarrow}$, at the Fermi surface:

$$\delta_{e\uparrow/\downarrow}=2\pi n_{\uparrow/\downarrow}. \tag{1.3}$$

It thus relates a dynamic quantity to a thermodynamic quantity. With this in hand, previous works have computed the linear-response conductance from the knowledge of this occupancy, at least at $H=0$.[19,20] However, such works do not make any attempt to explicitly identify the excitations that scatter according to the Friedel sum rule. Here we do so. We show that the scattering phase of the excitations we have identified to be the same as that predicted by the Friedel sum rule both in and out of a magnetic field. As we have reproduced the Friedel sum rule, we can say that the excitations we have identified coincide exactly with the free fermions *at the Fermi surface*.

Now, while the Friedel sum rule only deals with excitations at the Fermi surface, our methods goes beyond excitations directly at the Fermi surface, at least near the symmetric point of the Anderson model. To determine whether the

excitations we have identified together with their associated scattering amplitudes provide a complete solution of the problem, we compute the linear-response conductance at finite temperature. At finite temperature, the excitations needed for the linear-response conductance using a Landauer-Büttiker formalism exist over a range of energies. In particular, we compute the linear-response conductance at the symmetric point ($-U/2=\varepsilon_d$) of the Anderson model as a function of temperature T and compare it to the numerical renormalization group (NRG) computation of this quantity by Costi *et al.*[21] and find excellent agreement. We thus are able to conclude that using our excitations away from the Fermi surface is a valid procedure.

Although our finite-temperature computation suggests that we have correctly identified the low- (but finite-) energy excitations at the symmetric point, we do not claim that our result is *exact*. Again, our inability to make this claim hinges on the question of whether the integrable excitations we construct are entirely confined to a single lead and so make appropriate scattering states. Moreover, we know that our prescription for scattering fails once we leave the Kondo regime where approximately one electron sits on the dot and enter the mixed-valence regime of the Anderson model. This again suggests that near the symmetric point, our methods are merely highly accurate. The situation here is not dissimilar to form-factor computations of correlation and response functions, where integrable techniques can provide, if not the exact result (which would involve resumming an infinite number of contributions), controlled approximations of excellent accuracy, from the lowest energies through crossover regimes.[22,23]

The physical origin of the accurate reproduction of scattering at nonzero energies relative to the Fermi surface at the Anderson model's symmetric point lies in a separation of scales. At this point there are two relevant scales in the problem: one is the Kondo temperature T_k, while the other is $\sqrt{U\Gamma}$, a function of the Coulomb repulsion U and the resonance width of the dot level, Γ. At the symmetric point, $T_k \ll \sqrt{U\Gamma}$. We exploit this fact to make our identification of integrable scattering states. But in turn this means that we expect errors in transport quantities involving scattering away from the Fermi surface of $\mathcal{O}(T_k/\sqrt{U\Gamma})$.

Bootstrapping from our success with the finite-temperature linear response conductance, we look at the nonequilibrium conductance near the symmetric point both in and out of a magnetic field at zero temperature. In order to compute this conductance we again employ a Landauer-Büttiker formalism akin to that employed in computing the out-of-equilibrium conductance of interacting quantum Hall edges.[24] We imagine placing each lead at two differing chemical potentials μ_1 and μ_2. These differing voltages induce different populations of free electrons in the leads. As with the finite-temperature linear-response problem, we recast these electrons in terms of our integrable scattering states. We then compute the (equilibrium) scattering amplitudes of scattering states in the leads. These scattering amplitudes then provide the probability for a state to tunnel from one lead to the other. Although the system is interacting, its integrability again implies the states scatter one by one. It is important to understand that this means of computation introduces no additional error into the calculation. The sole source of uncertainty is found in whether the scattering states that we construct are entirely confined to a single lead. But because of the excellent agreement of the finite-T linear-response conductance with the previous NRG results, we expect this error to be similarly insignificant in our nonequilibrium computations.

It is important to understand that this approach to the nonequilibrium physics differs from that used in Refs. 9, 10, and 12 in a fundamental way. There the nonequilibrium conductance is expressed in terms of the nonequilibrium density of states of the impurity as determined from the correlator $\mathrm{Im}\langle dd^\dagger\rangle$. Here we have nothing direct to say about the nonequilibrium (or, indeed, the equilibrium) behavior of this quantity.

We must stress this as the reader may be confused by the fact we do use the impurity momentum (which is in turn related to the Bethe ansatz impurity density of states as explained in Sec. II) to compute the scattering amplitudes of excitations off the dot. This confusion may be heightened in that we employ the equilibrium Bethe ansatz density of states in computing the scattering matrices. It would thus seem legitimate to ask why we do not need to use a nonequilibrium impurity density of states in computing the out-of-equilibrium conductance.[25]

The answer lies in correctly understanding the basis of excitations by which we compute the conductance.[26] We are able to use the equilibrium scattering phases as we employ the basis that is naturally present when the system is equilibrated. However, because of the integrability of the system, we can continue to employ this basis when we move the system out of equilibrium. These particles continue to scatter as they do in equilibrium. We note that if one were to compute out-of-equilibrium scattering matrices, one would find that they differ from their in-equilibrium counterparts by an overall phase alone. As transport quantities depend upon the absolute value of the scattering, this overall phase would then have no effect.[26] While the application of finite voltage does not effect the scattering of the excitations, it does change their distribution in the leads. And indeed we must and do take this into account.

The rationale behind this understanding has been tested beyond the various checks of these ideas applied by Ref. 24 in their computations of conductances of quantum Hall edges. Generically, the thermodynamics of an integrable field theory can be computed using thermodynamic Bethe ansatz which employs zero-temperature S matrices (and not finite-temperature S matrices as might again be naively expected—the finite-temperature distribution might be thought to *necessarily* dress the scattering). With the thermodynamics, one can determine the finite-temperature scaling behavior of a field theory. If in the UV or IR limit the theory flows to a conformal field theory, the finite-scaling behavior in these limits is independently determined by the central charge c of the theory. That the two computations always agree provides strong evidence we are handling the problem correctly.

Turning to our nonequilibrium results, we find that they reproduce the expected gross features of the experimental

differential conductance. When $H=0$ and we are near the symmetric point, the differential conductance is sharply peaked about its linear-response value. The peak width is controlled by the scale T_k, the Kondo temperature. We find that the peak is roughly symmetrical about $V=0$ in accordance with experiment.[1]

In a nonzero field, Meir *et al.*[10] predicted that the differential conductance would peak at $eV=\pm H$. We find such peaks with our techniques, although our peaks are found shifted to values of $e|V|$ notably smaller than $|H|$. Even in the limit of fields much larger than T_k, we do not find the peaks at $|H|$. This is again consistent with experiment.[3] We should not necessarily expect the peaks to occur exactly at $eV=H$ as the prediction of Meir *et al.* is predicated in part upon a second-order perturbative result. Moreover, our construction of the scattering states suggests that in the particular case of the differential magnetoconductance, our results become exact in the limit of large applied fields.

A portion of the results of this paper have been reported in Ref. 27. Here in this work we provide far greater detail on the nature of our computations. The paper is organized as follows. In Sec. II we introduce the continuum version of the two-lead Anderson model. The two-lead Anderson model is integrable as is. However, we first map it onto a one-lead problem. If we were to explicitly solve the two-lead problem, we would find nevertheless that we would be implicitly implementing the map to the one-lead case. Having done this, we review the Bethe ansatz for the one-lead Anderson model together with the excitations necessary to form the ground state at zero temperature. The remaining portion of Sec. II is devoted to identifying the excitations (both at and away from the Fermi surface) that can be identified with scattering states and then computing their scattering amplitudes. We provide further details of the approximate nature of the scattering states so identified away from the Fermi surface. In the course of this discussion we demonstrate the Friedel sum rule.

In Sec. III we explore the behavior of the $T=0$ linear-response conductance both in and out of a magnetic field. Because Wiegmann and Tsvelick[28] computed expressions for the occupancy of the dot, $n_{d\uparrow/\downarrow}$, as a function of the gate voltage ε_d and H in a variety of regimes, and the Friedel sum rule relates the electron scattering phase to this occupancy, we can derive closed-form expressions for the linear-response conductance in these same regimes. Outside these regimes we compute the occupancy numerically. Using these results, we show how the linear-response conductance behaves as function of ε_d.

We plot the linear-response conductance as a function of the gate voltage ε_d in zero field in Fig. 4. However, the most interesting results of this section are found in our computations of the linear-response conductance at finite H. In Fig. 5 we plot the linear-response conductance as function of ε_d for a variety of values of H. As H is increased from zero, we see that the linear-response conductance is suppressed as a result of the destruction of the Kondo effect in a finite field. We also see the structure of the conductance peak evolve from its zero-field value to that of free fermions. With increasing H, the full width at half maximum becomes narrower, decreasing from its zero-field value of U to its free-fermion value of 2Γ. The peak height, in turn, decreases from its maximal value of $2e^2/h$ to e^2/h. And finally the location of the peak shifts from $\varepsilon_d=-U/2$ to $H/2$ (we scale H here and throughout this paper such that $g\mu_B=1$), appropriate to a spin-up free fermion with a field-induced, shifted chemical potential. These results are encoded in Fig. 6.

At the symmetric point $U/2=-\varepsilon_d$, we provide a simple closed-form expression for the conductance (see Sec. IV B). We then find that the conductance deviates from its unitary maximum for small fields via

$$G=2\frac{e^2}{h}\left(1-\frac{\pi^2}{16}\frac{H^2}{T_k^2}+\mathcal{O}(H^4/T_k)\right). \tag{1.4}$$

This deviation from the maximal conductance is quadratic, appropriate for the controlling $H=0$ strongly coupled Fermi-liquid fixed point. Here T_k, the Kondo temperature, is given in Eq. (3.16).

In Sec. IV we compute the finite-temperature linear-response conductance at the symmetric point, $U/2=-\varepsilon_d$. This requires recomputing the scattering of Sec. II. At finite temperature one must consider the thermal bath of all possible excitations. This highly nontrivial bath modifies the scattering. However, doing so leads us to a highly pleasing result. We are able to reproduce the NRG result of Costi *et al.* for G as a function of T (see Fig. 9). This is convincing evidence that we have correctly identified the scattering states (at least at the symmetric point of the dot). More specifically, we know the linear-response conductance will again have a Fermi-liquid form

$$G(T)=2\frac{e^2}{h}\left(1-c\frac{T^2}{T_k^2}+\mathcal{O}(T^4/T_k)\right). \tag{1.5}$$

Costi *et al.* demonstrated in perturbation theory that the constant c takes the value $c=\pi^4/16=6.088$. We compute in comparison $c=6.05\pm0.1$. Beyond the low-temperature Fermi-liquid regime, we emphasize we are able to describe accurately the conductance in the crossover regime $T\sim T_k$.

We also compare the scaling curve for the finite-temperature linear-response conductance with the experimental data found in Ref. 1. The comparison is plotted in Fig. 10. We find that the experimental measurements, even though taken away from the symmetric point of the dot (although still in its Kondo regime), agree well with our scaling curve. This suggests that the Kondo regime of the dot exists over a wide range of gate voltages (i.e., ε_d).

In Sec. V we move on to compute the nonequilibrium conductance at zero temperature. Again, the scattering amplitudes need to be recomputed to take into account the change in the distributions of electrons in the leads induced by the finite bias. We also discuss subtleties with understanding how to think of a finite-biased system in its one-lead formulation. We then present results of the differential conductance both in and out of a magnetic field as discussed above.

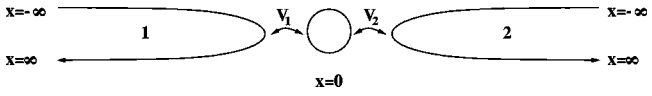

FIG. 2. Sketch of two leads attached to a quantum dot.

We are able to derive a number of simple closed-form results for the out-of-equilibrium conductance. The differential conductance in zero field at the symmetric point is computed to be

$$G(\mu_1,\mu_2)=2\frac{e^2}{h}\frac{1}{[1+\pi^2(\mu_1-\mu_2)^2/4T_k]}, \tag{1.6}$$

a remarkably simple result. This expression is expected to be valid for $\mu_1-\mu_2\lesssim T_k$. We are also able to characterize the peak in the differential conductance that develops in the presence of a magnetic field. The quantity most discussed in the literature—the bias at which the peak occurs—is given by the expression

$$eV_{\max}=-H\left(1-\frac{1}{2\pi}\tan^{-1}\frac{1}{I^{-1}-b}+\cdots\right),$$

$$I^{-1}-b=\frac{1}{\pi}\ln\left(\frac{H}{2T_k}\sqrt{\frac{\pi e}{2}}\right), \tag{1.7}$$

valid for $H\gg T_k$ and $H\ll\sqrt{U\Gamma}$. Because of the logarithmic dependence of b upon H, the position of the peak approaches $eV=|H|$ extremely slowly. In addition to the location of the peak, we are also able to describe both the peak width and height of the peak. The peak width is given by

$$e\Delta V=\frac{H}{2\pi}\left(\tan^{-1}\frac{1}{I^{-1}-1/2-b}-\tan^{-1}\frac{1}{I^{-1}+1/2-b}\right), \tag{1.8}$$

while the peak height is equal to

$$G_{\max}=\frac{e^2}{h}\left(\frac{3}{2}-\frac{(I^{-1}-b)}{\sqrt{4(I^{-1}-b)+1}}\right). \tag{1.9}$$

We see that the height of the conductance peak approaches e^2/h, one-half the unitary limit, in the asymptotic limit of large H. Interestingly, the nonequilibrium Kondo model in the Toulouse limit[14] also predicts a zero-temperature differential magnetoconductance peak at $eV=H$ which has a peak of e^2/h, one-half the unitary limit.

II. BASIC FORMALISM

A. Description of the system

Pictured in Fig. 2 is a sketch of the quantum dot connected to two leads. The Hamiltonian for this model in the continuum limit is given by

$$\mathcal{H}=\sum_{l\sigma}\int_{-\infty}^{\infty}dx\{-ic_{l\sigma}^{\dagger}(x)\partial_x c_{l\sigma}(x)+V_l\delta(x)[c_{l\sigma}^{\dagger}(x)d_\sigma+d_\sigma^{\dagger}c_{l\sigma}(x)]\}+\varepsilon_d\sum_\sigma n_\sigma+Un_\uparrow n_\downarrow, \tag{2.1}$$

where $n_\sigma=d_\sigma^{\dagger}d_\sigma$. Here Σ_l is a sum over the two leads ($l=1,2$). We have allowed for the possibility that the hopping matrix element V_l differs between the leads as is typical in any experimental realization. Rather than treating the leads as half-lines with both left- and right-moving fermions, we represent the leads as ''unfolded'' with fermions that are solely right moving. Fermions in either lead that are incident upon the dot are considered to lie in the region $x<0$, while those traveling away from the dot in either lead are found with $x>0$. We represent this in Fig. 2 by drawing the leads as elongated arcs.

We stress that there are no interactions in the leads (as opposed to the calculations in Ref. 24, for instance): the nontrivial physics of the problem arises solely from the strongly interacting dynamics of the dot.

It will be advantageous to reformulate this problem as a one-lead Anderson model (i.e., a single-lead model). To do so, we introduce even/odd electrons

$$c_{e/o}=\frac{1}{\sqrt{V_1^2+V_2^2}}(V_{1/2}c_1\pm V_{2/1}c_2). \tag{2.2}$$

Recasting $\mathcal{H}$ in this new basis, the odd electron c_o decouples and we are left with

$$\mathcal{H}=\sum_\sigma\int dx\{-c_{e\sigma}^{\dagger}(x)\partial_x c_{e\sigma}(x)+(V_1^2+V_2^2)^{1/2}\delta(x)\times[c_{e\sigma}^{\dagger}(x)d_\sigma+d_\sigma^{\dagger}c_{e\sigma}(x)]\}+\varepsilon_d\sum_\sigma n_\sigma+Un_\uparrow n_\downarrow. \tag{2.3}$$

We have thus reduced the problem to that solved using Bethe ansatz in a series of papers by Kawakami and Okiji[15] and Wiegmann, Filyov, and Tsvelick.[16]

With this reformulation of the model, we have to address the question of computing scattering amplitudes of electronic excitations in the original two lead problem. Naively it would seem we can do this. Let $T(\varepsilon)$ and $R(\varepsilon)$ be defined by

$T(\varepsilon)$, the transmission amplitude for an electronic excitation of energy ε to scatter from lead 1 to lead 2 (or 2 to 1), (2.4a)

$R(\varepsilon)$, reflection amplitude for an electronic excitation of energy ε to scatter from lead 1 to lead 1 (or 2 to 2). (2.4b)

Assuming that the amplitudes behave linearly under the even/odd map (2.2), we have (for $V_1=V_2$)

$$e^{i\delta_e(\varepsilon)}=R(\varepsilon)+T(\varepsilon),$$

$$e^{i\delta_o(\varepsilon)}=1=R(\varepsilon)-T(\varepsilon). \tag{2.5}$$

We then conclude that

$$T(\varepsilon)=\frac{e^{i\delta_e(\varepsilon)}-1}{2},$$

$$R(\varepsilon)=\frac{e^{i\delta_e(\varepsilon)}+1}{2}, \tag{2.6}$$

govern scattering in the two-lead problem. However, not all electronic excitations behave linearly under the map (2.2) and so things are not always this simple. We will consider this in more detail in Sec. II D and in particular Sec. II E.

As noted, in writing the above two equations, we have assumed $V_1=V_2$. If $V_1\neq V_2$, the transmission amplitude is scaled by the factor

$$\frac{2V_1V_2}{V_1^2+V_2^2}.$$

As this is a constant factor, it always possible to rescale results to take into account an asymmetry in the dot-lead couplings. As such, we will assume throughout the paper that $V_1=V_2$.

B. Bethe ansatz solution of the one-lead Anderson model

In order to understand the scattering between the two leads we will rely upon aspects of the one-lead Bethe ansatz solution found in Refs. 15 and 16. As such, we summarize briefly the results of this work. Applying the Bethe ansatz yields a set of quantization conditions describing a finite number of bare excitations in the system:

$$e^{ik_jL+i\delta(k_j)}=\prod_{\alpha=1}^{M}\frac{g(k_j)-\lambda_\alpha+i/2}{g(k_j)-\lambda_\alpha-i/2},$$

$$\prod_{j=1}^{N}\frac{\lambda_\alpha-g(k_j)+i/2}{\lambda_\alpha-g(k_j)-i/2}=-\prod_{\beta=1}^{M}\frac{\lambda_\alpha-\lambda_\beta+i}{\lambda_\alpha-\lambda_\beta-i}, \tag{2.7}$$

where

$$\delta(k)=-2\tan^{-1}\left(\frac{\Gamma}{(k-\varepsilon_d)}\right),$$

$$g(k)=\frac{(k-\varepsilon_d-U/2)^2}{2U\Gamma},$$

$$\Gamma=(V_1^2+V_2^2). \tag{2.8}$$

As in all problems with an SU(2) symmetry, there are two types of excitations: charge (with rapidities k) and spin (with rapidities λ). Here N is the total number of particles in the system, and M marks out the spin projection of the system, $2S_z=N-2M$ (in zero magnetic field $M=N/2$).

When $\varepsilon_d>-U/2$, the ground state of the system consists of the following set of excitations:

(i) $N-2M$ real k_j's,

(ii) M real λ_α's,

(iii) associated with each of the M λ_α's are two complex k's $k_\pm^\alpha$, described by

$$g(k_\pm^\alpha)=g[x(\lambda_\alpha)\mp iy(\lambda_\alpha)]=\lambda_\alpha\pm i/2,$$

$$x(\lambda)=U/2+\varepsilon_d-\sqrt{U\Gamma}\,[\lambda+(\lambda^2+1/4)^{1/2}]^{1/2},$$

$$y(\lambda)=\sqrt{U\Gamma}\,[-\lambda+(\lambda^2+1/4)^{1/2}]^{1/2}. \tag{2.9}$$

Although only valid for $\varepsilon_d>-U/2$, we can also understand the case $\varepsilon_d<-U/2$ through a particle-hole transformation. If we take the continuum limit of Eqs. (2.9), we no longer deal with discrete values of λ and k, but rather go over to smooth distributions $\rho(k)$ for the real k_j's and $\sigma(\lambda)$ for the λ_α's and their associated $k_\pm^\alpha$'s. To derive these distributions, we first take the logarithm of Eq. (2.7):

$$k_jL+\delta(k_j)=2\pi N_j-\sum_{\beta=1}^{M}\theta_1(g(k_j)-\lambda_\beta),$$

$$2\pi J_\alpha+\sum_{\beta=1}^{M}\theta_2(\lambda_\alpha-\lambda_\beta)+\sum_{j=1}^{N-2M}\theta_1(\lambda_\alpha-g(k_j))$$

$$=-2Lx(\lambda_\alpha)-2\,\mathrm{Re}\,\delta(x(\lambda_\alpha)+iy(\lambda_\alpha)),$$

$$\theta_n(x)=2\tan^{-1}\left(\frac{2}{n}x\right)+\pi. \tag{2.10}$$

N_j and J_α are the quantum numbers of the charge and spin excitations, respectively. Taking the thermodynamic limit (i.e., $N,M,L\to\infty$ with N/L and M/L finite), followed by derivatives of the above gives

$$\rho(k)=\frac{1}{2\pi}+\frac{\Delta(k)}{L}+g'(k)\int_Q^{\tilde{Q}}d\lambda\,a_1(g(k)-\lambda)\sigma(\lambda),$$

$$\sigma(\lambda)=-\frac{x'(\lambda)}{\pi}+\frac{\tilde{\Delta}(\lambda)}{L}-\int_Q^{\tilde{Q}}d\lambda'a_2(\lambda'-\lambda)\sigma(\lambda')$$

$$-\int_{-D}^{B}dk\,a_1(\lambda-g(k))\rho(k), \tag{2.11}$$

where

$$\Delta(k)=\frac{1}{2\pi}\partial_k\delta(k),$$

$$\tilde{\Delta}(\lambda)=-\frac{1}{\pi}\partial_\lambda\,\mathrm{Re}\,\delta(x(\lambda)+iy(\lambda)),$$

$$a_n(x)=\frac{1}{2\pi}\partial_x\theta_n(x)=\frac{2n}{\pi}\frac{1}{(n^2+4x^2)}. \tag{2.12}$$

Various limits appear in the above equations for the distributions. $-D$ marks the lower allowed limit of the k's while $\tilde{Q}$ marks out the bandwidth of the λ's. As each λ has a pair of complex k's, its associated energy is $2x(\lambda)$. We thus determine $\tilde{Q}$ by

$$x(\tilde{Q}) = -D. \tag{2.13}$$

Often, it will be possible to replace $\tilde{Q}$ and $-D$ by ∞ and $-\infty$. Here B and Q, on the other hand, give the spin and charge Fermi surfaces. They are determined by the constraints

$$\frac{N-2M}{L} = \int_{-D}^{B} dk\, \rho(k),$$

$$\frac{M}{L} = \int_{Q}^{\tilde{Q}} d\lambda\, \sigma(\lambda). \tag{2.14}$$

C. Determination of the scattering phase at the Fermi surface: The Friedel sum rule

In this section we examine the relationship between the scattering phase of electrons $\delta_e(\epsilon)$ at the Fermi surface and the number of electrons on the dot and so verify the Friedel sum rule.

To determine $\delta_e(\varepsilon)$, we employ an energetics argument of the sort used by Andrei in the computation of the magnetoresistance in the Kondo model.[18] Imagine adding an electron to the system. Through periodic boundary conditions, its momentum is quantized, $p = 2\pi n/L$. If the dot was absent, the quantization condition would be determined solely by the conditions in the bulk of the system and we would write $p_{\text{bulk}} = 2\pi n/L$. Upon including the dot, this bulk momentum is shifted by a term scaling as $1/L$. The quantization condition is then rewritten as

$$p = \frac{2\pi n}{L} = p_{\text{bulk}} + \frac{\delta_e(\varepsilon)}{L}, \tag{2.15}$$

where L is the system's length. The coefficient of the $1/L$ term is identified with the scattering phase of the electron off the dot.

As we are interested in expressing δ_e in terms of the number of electrons on the dot, it is useful to separate out from $\rho(k)$ and $\sigma(\lambda)$ the impurity contribution to the density of states. We thus write

$$\rho(k) = \rho_{\text{bulk}}(k) + \frac{1}{L}\rho_{\text{imp}}(k),$$

$$\sigma(\lambda) = \sigma_{\text{bulk}}(\lambda) + \frac{1}{L}\sigma_{\text{imp}}(\lambda). \tag{2.16}$$

$\rho_{\text{bulk}}/\sigma_{\text{bulk}}$ represents the bulk contribution to the densities while $\rho_{\text{imp}}/\sigma_{\text{imp}}$ determine the number of electrons of definite spin, $n_{d\uparrow}/n_{d\downarrow}$, sitting on the dot. From Eqs. (2.14) we have

$$n_{d\uparrow} = \int_{Q}^{\tilde{Q}} d\lambda\, \sigma_{\text{imp}}(\lambda) + \int_{-D}^{B} dk\, \rho_{\text{imp}}(k),$$

$$n_{d\downarrow} = \int_{Q}^{\tilde{Q}} d\lambda\, \sigma_{\text{imp}}(\lambda). \tag{2.17}$$

These relations will be key in verifying the Friedel sum rule. Substituting Eqs. (2.16) into Eqs. (2.11), we obtain separate equations for $\rho_{\text{bulk}}/\rho_{\text{imp}}$ and $\sigma_{\text{bulk}}/\sigma_{\text{imp}}$:

$$\rho_{\text{bulk}}(k) = \frac{1}{2\pi} + g'(k)\int_{Q}^{\tilde{Q}} d\lambda\, a_1(g(k)-\lambda)\sigma_{\text{bulk}}(\lambda),$$

$$\sigma_{\text{bulk}}(\lambda) = -\frac{x'(\lambda)}{\pi} - \int_{Q}^{\tilde{Q}} d\lambda' a_2(\lambda'-\lambda)\sigma_{\text{bulk}}(\lambda') - \int_{-D}^{B} dk\, a_1(\lambda - g(k))\rho_{\text{bulk}}(k) \tag{2.18}$$

and

$$\rho_{\text{imp}}(k) = \Delta(k) + g'(k)\int_{Q}^{\tilde{Q}} d\lambda\, a_1(g(k)-\lambda)\sigma_{\text{imp}}(\lambda),$$

$$\sigma_{\text{imp}}(\lambda) = \tilde{\Delta}(\lambda) - \int_{Q}^{\tilde{Q}} d\lambda' a_2(\lambda'-\lambda)\sigma_{\text{imp}}(\lambda') - \int_{-D}^{B} dk\, a_1(\lambda - g(k))\rho_{\text{imp}}(k). \tag{2.19}$$

In Appendix A we give alternative forms to the above equations governing the density functionals. These alternatives are far more amenable to numerical analysis and in practice, the ones used in solving for the densities.

Having obtained the equations governing the impurity densities of state, we now focus on the scattering phase itself. From Eqs. (2.10) we can read off the bulk momentum of a charge/spin excitation with quantum number N/J to be

$$p(k) = \frac{2\pi N}{L} = k + \int_{Q}^{\tilde{Q}} d\lambda\, \sigma_{\text{bulk}}(\lambda)\theta_1(g(k)-\lambda),$$

$$p(\lambda) = -\frac{2\pi J}{L} = 2x(\lambda) + \int_{Q}^{\tilde{Q}} d\lambda' \sigma_{\text{bulk}}(\lambda')\theta_2(\lambda-\lambda') + \int_{-D}^{B} dk\, \rho_{\text{bulk}}(k)\theta_1(\lambda - g(k)). \tag{2.20}$$

We assume here that $\tan^{-1}$ in $\theta_{1,2}$ varies from $\pi/2$ to $\pi/2$, thus ensuring a simple relationship between the momentum and energy functionals to be derived in the next subsection.

The impurity contribution to the momentum for each type of excitation can be similarly determined to be

$$p_{\text{imp}}(k) = \delta(k) + \int_{Q}^{\tilde{Q}} d\lambda\, \sigma_{\text{imp}}(\lambda)\{\theta_1(g(k)-\lambda) - 2\pi\},$$

$$p_{\rm imp}(\lambda)=2\,{\rm Re}\,\delta(x(\lambda)+iy(\lambda)) + \int_Q^{\tilde{Q}} d\lambda'\,\sigma_{\rm imp}(\lambda')[\,\theta_2(\lambda-\lambda')-2\pi] + \int_{-D}^{B} dk\,\rho_{\rm imp}(k)\{\theta_1(\lambda-g(k))-2\pi\}. \tag{2.21}$$

Here we have chosen a different range for $\tan^{-1}$ in $\theta_{1,2}$ for describing the impurity momentum. Shifting back to the original range leads then to the appearance of the 2π's. This choice is governed by our ultimate desire to give the scattering phases in terms of the impurity momentum. In particular, we want $p_{\rm imp}(k\to-\infty)=p_{\rm imp}(\lambda\to\infty)=0$.

According to Eq. (2.15), we identify $p_{\rm imp}(k)$ with the scattering phase of a charge excitation and $p_{\rm imp}(\lambda)$ with the scattering phase of a spin excitation. By differentiating these expressions and comparing to Eqs. (2.19), we obtain the relations

$$\partial_k p_{\rm imp}(k)=2\pi\rho_{\rm imp}(k),$$
$$\partial_\lambda p_{\rm imp}(\lambda)=-2\pi\sigma_{\rm imp}(\lambda). \tag{2.22}$$

Again, we have relations crucial to verifying the Friedel sum rule.

In order to determine the scattering phase of an electron (as opposed to a spin or charge excitation), we must specify how to glue together a spin and a charge excitation to form the electron. The situation is analogous to adding a single particle excitation in the attractive Hubbard model.[29] Adding a single spin $\uparrow$ electron to the system demands that we add a real $k>B$ (charge) excitation. In doing so we create a hole at $\lambda>Q$ in the spin distribution as the number of the available slots in the spin distribution is determined by the number of electrons in the system. Adding an electron to the system thus opens up an additional slot in the λ distribution.

The electron scattering phase off the impurity is then the difference of the right-moving k-impurity momentum $p_{\rm imp}(k)$ and the left-moving λ-hole–impurity momentum $-p_{\rm imp}(\lambda)$:

$$\delta_e^{\uparrow}=p_{\rm imp}^{\uparrow}=p_{\rm imp}(k)+p_{\rm imp}(\lambda) =2\pi\int_{-D}^{k}dk'\,\rho_{\rm imp}(k')+2\pi\int_{\lambda}^{\tilde{Q}}d\lambda'\,\sigma_{\rm imp}(\lambda'), \tag{2.23}$$

where we have used Eqs. (2.22) in writing the last line. If the excitations are added or removed at the Fermi surfaces, i.e., $k=B$, $\lambda=Q$, we obtain the Friedel sum rule for spin-up electrons,

$$\delta_e^{\uparrow}=2\pi\int_{-D}^{B}dk\,\rho_{\rm imp}(k)+2\pi\int_{Q}^{\tilde{Q}}d\lambda\,\sigma_{\rm imp}(\lambda)=2\pi n_{d\uparrow}, \tag{2.24}$$

where Eq. (2.17) has been used. The total energy of this excitation is $\varepsilon(k=B)+\varepsilon(\lambda=Q)=0$, as it should be.

To determine the scattering of a spin-down electron we employ particle-hole symmetry. A particle-hole transformation is implemented via

$$c_{\uparrow}^{\dagger}(k)\to c_{\downarrow}(-k),$$
$$c_{\downarrow}^{\dagger}(k)\to c_{\uparrow}(-k),$$
$$d_{\uparrow}^{\dagger}\to d_{\downarrow},$$
$$d_{\uparrow}^{\dagger}\to d_{\downarrow},$$
$$\varepsilon_d\to -U-\varepsilon_d. \tag{2.25}$$

Consequently, the scattering phase of a spin $\downarrow$ hole is related to that of a spin $\uparrow$ electron via

$$\delta_{\rm ho}^{\downarrow}(-U-\varepsilon_d)=\delta_e^{\uparrow}(\varepsilon_d). \tag{2.26}$$

The phase of this excitation is then

$$\delta_{\rm ho}^{\downarrow}(-U-\varepsilon_d)=2\pi\int_{\lambda}^{\tilde{Q}}d\lambda'\,\sigma_{\rm imp}(\lambda')+2\pi\int_{-D}^{k}dk'\,\rho_{\rm imp}(k') =2\pi n_{d\uparrow}(\varepsilon_d), \tag{2.27}$$

where the last equality holds if we take the hole to be at the Fermi surface, $\lambda=Q$ and $k=B$. As $n_{d\uparrow}(\varepsilon_d)=1-n_{d\downarrow}(-U-\varepsilon_d)$, we have

$$\delta_{\rm ho}^{\downarrow}(-U-\varepsilon_d)\,{\rm mod}\;2\pi=-n_{d\downarrow}(-U-\varepsilon_d). \tag{2.28}$$

At the Fermi surface, hole and electron scattering are identical (up to a sign) and so we verify the Friedel sum rule for spin-down electrons.

The reader may be puzzled why we rely on a particle-hole transformation in computing the scattering amplitude for spin-down electrons. Although it would be desirable to do this computation directly, it does not seem to be possible. To construct a spin $\downarrow$ electron at the Fermi surface, it is natural to remove a $k=B$ excitation while adding a $\lambda=Q$ excitation. The corresponding scattering phase is then given by

$$\delta_e^{\downarrow}=p_{\rm imp}^{\downarrow}=p_{\rm imp}(k)+p_{\rm imp}(\lambda) =2\pi\int_{-D}^{B}dk\,\rho_{\rm imp}(k)+2\pi\int_{Q}^{\tilde{Q}}d\lambda'\,\sigma_{\rm imp}(\lambda') =2\pi n_{d\uparrow}. \tag{2.29}$$

But this is obviously not what we want—a manifest violation of the Friedel sum rule. Rather by comparing Eq. (2.29) with Eq. (2.27), the scattering indicates that we have constructed a spin $\downarrow$ electron not at ε_d, but at the particle-hole conjugate point $-U-\varepsilon_d$. Why this is so it is not entirely clear. However, one can notice that the k excitations are not only charge excitations, but are in some sense unbound spin $\uparrow$ electrons (the number of k excitations is directly proportional to the magnetization of the system). So in removing a k excitation to form the spin $\downarrow$ electron, we are in some sense creating a spin $\uparrow$ hole. And a spin $\uparrow$ hole at chemical potential ε_d will scatter as a spin $\downarrow$ electron at $-U-\varepsilon_d$.

This entire discussion has concerned itself with proving the Friedel sum rule for the one-lead Anderson model. However, we can argue that it applies, appropriately revised, to the two-lead model. More precisely, we can argue that the excitations at the Fermi surface behave linearly under the map (2.2) and so have two-lead scattering amplitudes given by Eqs. (2.6). This will be detailed in the following two sections.

In Appendix B we give an alternate derivation of the scattering phase that focuses upon the impurity energy of an excitation as opposed to its impurity momentum. In doing so, we elucidate subtleties not explicitly discussed in Ref. 28. We also give a third derivation of the scattering phase in Appendix C by directly considering the dressing of the bare scattering.

D. Excitations away from the Fermi surface in the Kondo regime

In the previous section we were mainly concerned with scattering at the Fermi surface. However, as made clear by taking $k \neq B$, $\lambda \neq Q$, we can look at scattering above the Fermi surface.

It is tempting to ask first whether the noninteracting electrons in the lead can still be described in this formalism (by electrons we mean the standard plane-wave excitations of appropriate spin and charge). Here it is useful to recall some well-known results from many-body theory: Langreth, in verifying the Friedel sum rule for $H=0$,[30] computed the ratio of the elastic inverse lifetime $\tau_{\rm el}^{-1}$ of a plane-wave mode to that of its total inverse lifetime τ^{-1}, finding

$$\frac{\tau_{\rm el}^{-1}(\varepsilon)}{\tau^{-1}(\varepsilon)} = \frac{\Gamma}{2\,\mathrm{Im}\,\Sigma(\varepsilon)}, \tag{2.30}$$

where $\Sigma(\varepsilon)$ is the self-energy for the dot electron Green's function. At the Fermi surface,

$$\mathrm{Im}\,\Sigma(\varepsilon=0) = \frac{\Gamma}{2}, \tag{2.31}$$

and there are no inelastic processes. However, away from the Fermi surface,

$$\mathrm{Im}\,\Sigma(\varepsilon) = \frac{\Gamma}{2} + c\varepsilon^2, \quad c>0, \tag{2.32}$$

and $\tau_{\rm el}^{-1} < \tau^{-1}$, so electrons with energies above the Fermi surface do not scatter elastically.

On the other hand, the simple excitations we construct within the integrable description by gluing spin and charge excitations will necessarily scatter elastically: beyond the Fermi surface, they cannot be the free electrons one would initially like to describe. In and of itself, this does not matter as all we are interested in at the end is charge transport, irrespective of what kind of objects actually do carry this charge. A similar situation occurs in the fractional quantum Hall effect,[24] where the integrability approach uses quasiparticles which are neither electrons nor Laughlin quasiparticles. This approach merely provides a more convenient basis for the space of excitations, chosen such that scattering at the impurity is as simple as possible. However, we do have to concern ourselves with rewriting the original free electrons in terms of the integrable scattering basis. As indicated in the Introduction, we are not able to provide an answer to this problem in its entirety.

Our approach will then be to build excitations which are ''electronic,'' that is, carry the same quantum numbers as electrons, but scatter simply (i.e., elastically) at the impurity—they will also scatter in a simple, factorized way among themselves, although their S matrix is nontrivial (it is not $S=-1$ anymore). One can certainly think of these excitations as dressed electrons.

This being understood, another difficulty remains: the potential parameter space of electronic excitations, i.e., (k,λ), is two dimensional (provided we neglect other solutions of the Bethe ansatz: see Sec. II F), whereas we naturally want the space to be one dimensional. For the moment, we can only make the necessary dimensional reduction when we are in the Kondo regime of the Anderson model. The first step in doing so is to determine the energy-momentum of an excitation labeled by (k,λ).

We already know the momentum of the excitations from Eqs. (2.20). We thus must only compute the energies. To facilitate the calculation of excitation energies, it is useful to decompose $\rho(k)$ and $\sigma(\lambda)$ into particle and hole densities:

$$\rho_{p/h}(k) = \theta(\pm B \mp k)\rho(k),$$
$$\sigma_{p/h}(\lambda) = \theta(\mp Q \pm \lambda)\sigma(\lambda). \tag{2.33}$$

Now imagine varying $\rho_{p/h}$ and $\sigma_{p/h}$ and asking what is the corresponding variation in the energy. We can write this variation in two ways: one in terms of the bare energies and one in terms of new functions $\varepsilon^{\pm}(k)$ and $\varepsilon^{\pm}(\lambda)$ governing the dressed energies:

$$\begin{aligned}\delta E &= L\int dk\{\varepsilon^{+}(k)\delta\rho_p(k) - \varepsilon^{-}(k)\delta\rho_h(k)\} \\ &\quad + L\int d\lambda\{\varepsilon^{+}(\lambda)\delta\sigma_p(\lambda) - \varepsilon^{-}(\lambda)\delta\sigma_h(\lambda)\} \\ &= L\int dk\left(k-\frac{H}{2}\right)\delta\rho_p(k) + 2L\int d\lambda\, x(\lambda)\delta\sigma_p(\lambda).\end{aligned} \tag{2.34}$$

The variations on $\delta\rho_{p/h}$ and $\delta\rho_{p/h}$ are not independent. From Eqs. (2.11) we see

$$\begin{aligned}\delta\rho_p(k) + \delta\rho_h(k) &= g'(k)\int d\lambda\ \delta\sigma_p(\lambda)a_1(g(k)-\lambda), \\ \delta\sigma_p(\lambda) + \delta\sigma_h(\lambda) &= -\int d\lambda'\,\delta\sigma_p(\lambda')a_2(\lambda'-\lambda) \\ &\quad -\int dk\ \delta\rho_p(k)a_1(\lambda-g(k)).\end{aligned} \tag{2.35}$$

Substituting Eqs. (2.35) into Eq. (2.34), we obtain

$$\varepsilon^+(k)+\varepsilon^-(k)=k-\frac{H}{2}-\int d\lambda\,\varepsilon^-(\lambda)a_1(\lambda-g(k)),$$

$$\varepsilon^+(\lambda)+\varepsilon^-(\lambda)=2x(\lambda)-\int d\lambda'\varepsilon^-(\lambda')a_2(\lambda'-\lambda)+\int dk\,g'(k)\varepsilon^-(k)a_1(g(k)-\lambda). \tag{2.36}$$

$\varepsilon^{\pm}(\lambda)$ and $\varepsilon^{\pm}(k)$ are characterized by

$$\varepsilon^+(\lambda)=\theta(Q-\lambda)(\varepsilon^+(\lambda)+\varepsilon^-(\lambda))>0,$$

$$\varepsilon^-(\lambda)=\theta(\lambda-Q)(\varepsilon^+(\lambda)+\varepsilon^-(\lambda))<0,$$

$$\varepsilon^+(k)=\theta(k-B)(\varepsilon^+(k)+\varepsilon^-(k))>0,$$

$$\varepsilon^-(k)=\theta(B-k)(\varepsilon^+(k)+\varepsilon^-(k))<0. \tag{2.37}$$

The functions $\varepsilon=\varepsilon^++\varepsilon^-$ are continuous and monotonic. $\varepsilon^{\pm}$ have been defined such that $\varepsilon^+(k/\lambda)$ is the cost of adding an excitation at k/λ while $-\varepsilon^-(k/\lambda)$ is the energy needed to create a hole at k/λ. Again, in Appendix A, we give alternative forms to the above equations governing the energy functionals which are more amenable to numerical analysis.

Having determined the energy of the excitation, we can easily relate it to its corresponding momentum. We consider the case of $H=0$ first. Comparing Eqs. (2.20) and (2.36) and using $\partial_k\varepsilon(k)=2\pi\rho_{\rm bulk}(k)$ and $\partial_\lambda\varepsilon(\lambda)=-2\pi\sigma_{\rm bulk}(\lambda)$, we see that

$$p_{\rm bulk}(k)=\varepsilon(k),$$

$$p_{\rm bulk}(\lambda)=\varepsilon(\lambda), \tag{2.38}$$

where $p_{\rm bulk}$ is the portion of momentum not scaling as $1/L$.

With this in hand, we can parametrize the scattering phases of electronic excitations away from the Fermi surface. Suppose we want to characterize a spin $\uparrow$ electron with energy $\varepsilon_{\rm el}$. (This is sufficiently general for $H=0$ as we know spin $\downarrow$ electrons will scatter identically.) The possible k and λ forming this excitation must satisfy

$$\varepsilon(k)-\varepsilon(\lambda)=\varepsilon_{\rm el}. \tag{2.39}$$

Given Eqs. (2.38), this choice automatically satisfies $\varepsilon_{\rm el}=p_{\rm el}$ (up to $1/L$ corrections).

This parametrization leaves an unresolved issue. It does not in general uniquely specify a particular pair (k,λ), crucial if we are to actually compute quantities involving information away from the Fermi surface. We have schematically illustrated the degeneracy of choices in Fig. 3: as the energy is increased, the multiplicity of pairs (k,λ) correspondingly increases.

In certain cases, however, the specification is unique. At the Fermi surface, the degeneracy of pairs is lifted. This is already illustrated in Fig. 3. However, there is another case not captured by the cartoon in Fig. 3 where the specification is unique. We have only a single possible pair (k,λ) for each energy in the case of spin $\uparrow$ hole scattering in finite magnetic field at the symmetric point of the model. The reason behind the reduction of the parameter space for this case will be made clear in what follows.

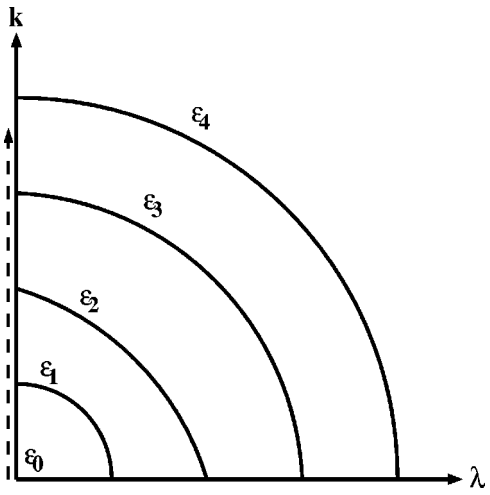

FIG. 3. Cartoon of the parameter space describing electronic excitations. The drawing supposes that $\varepsilon_0=0<\varepsilon_1<\varepsilon_2<\varepsilon_3<\varepsilon_4$. Each curve represents a set of the excitations that share the same energy ε. Only in the case $\varepsilon_0=0$, i.e., when we are at the Fermi surface, is the pair (k,λ) uniquely specified. The dashed line marks out the ansatz we employ in the Kondo regime.

For the other cases where the choice is not unique, the question becomes on what operative principle do we reduce the space. The key that we have identified to reducing the parameter space is determining how the excitations behave under the map (2.2). Only if they behave linearly under the map are they of use for it is only then that we can compute their scattering amplitudes in the two-lead picture via Eqs. (2.6).

Although we have refined the question, we cannot in general determine whether a given excitation unfolds linearly in the case when there are multiple possible pairs (k,λ). We can, however, make some progress when we are in the Kondo regime of the Anderson model (i.e., $U+2\varepsilon_d\sim 0$). In this regime we expect the scattering phase to vary on the scale of the Kondo temperature T_k. The electron scattering phase is determined by $\rho_{\rm imp}$ and $\sigma_{\rm imp}$, the two impurity densities. Of the two, only $\rho_{\rm imp}$ varies on scales on the order of T_k. In contrast, $\sigma_{\rm imp}$ is controlled by the much larger scale $\sqrt{U\Gamma}$. Thus, in computing electronic scattering phases away from the Fermi surface at zero temperature, it is natural to keep $\lambda=Q$, its Fermi surface value, and vary k. Specifically, to describe an electron of energy $\varepsilon_{\rm el}$, we chose (k,λ) such that

$$k \text{ particle}, \quad \varepsilon(k)=\varepsilon_{\rm el},$$

$$\lambda \text{ hole at } \lambda=Q. \tag{2.40}$$

With this ansatz, we then have restricted the two-dimensional phase space (λ,k) of potential excitations carrying the quan-

tum numbers of an electron to a one-dimensional subspace. Hence the scattering phases of electrons of energy $\varepsilon_{\rm el}$ above the Fermi surface at $H=0$ are given by

$$\delta_e^{\uparrow}(\varepsilon_{\rm el})=\delta_e^{\downarrow}(\varepsilon_{\rm el})=2\pi\int_{-D}^{k}dk'\rho_{\rm imp}(k')$$

$$+2\pi\int_{Q}^{\tilde{Q}}d\lambda\ \sigma_{\rm imp}(\lambda),\quad \varepsilon(k)=\varepsilon_{\rm el}. \quad (2.41)$$

When $H\neq 0$, we still have a simple relation between the energy and momentum, i.e., we have

$$\varepsilon(k)=p(k)-\frac{H}{2},$$

$$\varepsilon(\lambda)=p(\lambda). \quad (2.42)$$

Hence with $H\neq 0$ we are still faced with an oversized parameter space. But we conjecture similar relations to those in Eqs. (2.40) hold in constructing the electronic spin $\uparrow$ excitations:

$$\uparrow \text{ electron: } k \text{ particle},\quad \varepsilon(k)=\varepsilon_{\rm el},$$

$$\lambda \text{ hole at } \lambda=Q. \quad (2.43)$$

The scattering phase of this excitation is accordingly

$$\delta_e^{\uparrow}(\varepsilon_{\rm el})=2\pi\int_{-D}^{k}dk'\rho_{\rm imp}(k')+2\pi\int_{Q}^{\tilde{Q}}d\lambda\ \sigma_{\rm imp}(\lambda),$$

$$\varepsilon(k)=\varepsilon_{\rm el}. \quad (2.44)$$

With $H\neq 0$ and consequently $\varepsilon^{-}(k)$ not identically zero, we can construct spin $\uparrow$ hole states by removing a k state and a λ hole. The scattering phase of spin $\uparrow$ holes is then equal to

$$\delta_{\rm ho}^{\uparrow}(\varepsilon_{\rm ho}>0)=p_{\rm imp}(k)+p_{\rm imp}(\lambda),$$

$$=2\pi\int_{-D}^{k}dk'\rho_{\rm imp}(k')+2\pi\int_{Q}^{\tilde{Q}}d\lambda'\sigma_{\rm imp}(\lambda'),$$

$$\varepsilon(k)=-\varepsilon_{\rm ho}. \quad (2.45)$$

For this particular excitation we do not need the scattering ansatz. If we are to remove a λ hole, we must do it for $\lambda<Q$. However, at the symmetric point, $Q=-\infty$ and so the choice is unique. This fact will allow us to conclude that in the large-field limit, our computation of the differential magnetoconductance becomes exact. We also point out that as $\varepsilon(k)$ is bounded below, i.e., $\varepsilon(k=-D)=-H$, we are limited in the energy range ($[0,H]$) in which we can construct spin $\uparrow$ holes.

With $H\neq 0$, we must compute the scattering of spin $\downarrow$ objects separately. To do so we again employ a particle-hole transformation. We so obtain

$$\delta_e^{\downarrow}(\varepsilon_{\rm el},-U-\varepsilon_d)=\delta_{\rm ho}^{\uparrow}(\varepsilon_{\rm ho}=\varepsilon_{\rm el},\varepsilon_d),$$

$$\delta_{\rm ho}^{\downarrow}(\varepsilon_{\rm ho},-U-\varepsilon_d)=\delta_e^{\uparrow}(\varepsilon_{\rm el}=\varepsilon_{\rm ho},\varepsilon_d). \quad (2.46)$$

Unlike scattering at the Fermi surface where we could infer behavior at $\varepsilon_d>-U/2$ from behavior at $\varepsilon_d<-U/2$, we cannot do so for scattering away from the Fermi surface. Thus, when we need to compute explicitly the scattering of spin $\downarrow$ objects—say, in computing the magnetoconductance out of equilibrium—we will be restricted to the symmetric point $\varepsilon_d=-U/2$.

E. Returning to the two-lead problem

In this section we explore in more depth the map between the one- and two-lead models and its attendant problems. To review the map in more formal terms call $E_{e,o}$ the integrable excitations in the even and odd leads. We then describe the factorized scattering by the relations

$$E_eD=e^{i\delta_e}DE_e,$$

$$E_oD=e^{i\delta_o}DE_o, \quad (2.47)$$

where D is a formal symbol representing the impurity. Again, the phase δ_e is nontrivial, while $\delta_o=0$. Under the map (2.2), integrable excitations in the two-lead picture are given by

$$E_{1,2}=E_e\pm E_o. \quad (2.48)$$

Scattering of an excitation in the first lead is then described by

$$E_1D=RDE_1+TDE_2$$

or

$$(E_e+E_o)D=RD(E_e+E_o)+TD(E_e-E_o), \quad (2.49)$$

where consistency with Eqs. (2.47) demands that the transmission and reflection amplitudes R and T satisfy $R+T=e^{i\delta_e}$ and $R-T=e^{i\delta_o}$. An implicit assumption in this determination of the scattering in the two-lead picture is that the superposition E_o+E_e of an electronic excitation in the even sector and an electronic excitation in the odd sector carries unit charge in lead 1 and no charge in lead 2. For an arbitrary fermionic excitation in the even and odd leads this will not be the case. For example, imagine an electronic excitation in the even lead that if decomposed into a plane-wave basis of free electrons consists in part of particle-hole excitations:

$$E_e=\sum_k a_k c_{ek}^{\dagger}|\text{Fermi sea}\rangle$$

$$+\sum_{k,k_p,k_h}a_{kk_pk_h}c_{ek}^{\dagger}c_{ek_p}^{\dagger}c_{ek_h}|\text{Fermi sea}\rangle+\cdots, \quad (2.50)$$

where here c_{ek} is a plane-wave electron in the even lead with wave vector k. The linear combination E_e+E_o, where the excitation E_o is arrived at from Eq. (2.50) through $c_e\rightarrow c_o$, does then not carry unit charge in lead 1. Rather, it carries indefinite charge in both leads. In this case the excitation does not transform between the two pictures as indicated by Eq. (2.48) and its scattering cannot be expected to be de-

scribed by Eq. (2.49). If E_e was strictly a linear combination of terms of the form $c_{ek}^{\dagger}|\text{Fermi sea}\rangle$, this problem would not surface.

Thus, in order to exploit the map between the two pictures, we must limit ourself to excitations that behave linearly under the map as described in Eq. (2.48). There are then two questions to be answered. Do such excitations in general exist? And if they do exist, are they sufficient for our purposes, the description of transport properties. We have two arguments that excitations with scattering described by Eq. (2.48) do exist. More precisely, we have two arguments giving that excitations falling along some line in the two-dimensional (k,λ) parameter space have such scattering. Moreover, we argue that the scattering of such excitations is sufficient to determine transport properties.

The first argument relies upon the transformation properties of the Fermi field $c(x)$. Recall that in order to implement the map between the one- and two-lead pictures, it is $c(x)$ that is transformed, i.e.,

$$c_e(x) \to \frac{1}{\sqrt{2}}[c_1(x) \pm c_2(x)].$$

Thus any integrable excitation E_e that has a finite matrix element with c_e, i.e.,

$$\langle c_e | E_e \rangle \neq 0,$$

must also behave linearly under the map from one to two leads. To see this more explicitly imagine making a mode expansion of the field $c_e(x)$ in terms of the integrable excitations. As E_e couples to c_e, E_e must appear in this expansion:

$$c_e(x) = \sum_r a_r e^{ip_r x} E_{er} + \cdots, \tag{2.51}$$

where it suggests that E_e is one of the E_{er}'s. As c_e and E_e are linearly related, they must share the same transformation properties. This then would guarantee that any excitation appearing in the above mode expansion will have scattering described by Eq. (2.49).

But we can say more on the basis of the properties of $c_e(x)$. Because the underlying model is essentially free, we know the single-particle spectral function of the model will be given by

$$\langle c_e c_e \rangle(E,p) \propto \delta(E-p).$$

Thus, for any given energy $E=p$, we know that some integrable excitation with this energy and momentum must appear in the mode expansion (2.50). In terms of the two-dimensional parameter space (k,λ), this implies that there is at least one line in this space describing excitations transforming as Eq. (2.48) and scattering as Eq. (2.49).

The second argument for the existence of this line in the (k,λ) parameter space relies upon combining the properties of the low-energy sector of the theory with the equivalence of the integrable excitation we have constructed at the Fermi surface with the corresponding plane-wave electron excitation. Given our reliance on this equivalence, it deserves further exploration.

This equivalence is, of course, strongly suggested by our ability to reproduce the Friedel sum rule and the fact Langreth[30] demonstrated that plane-wave electrons at the Fermi surface scatter elastically, the hallmark of integrable excitations. Nevertheless, the statement that the integrable excitation coincides with a plane-wave electron needs further clarification. If we denote the wave function of the integrable excitation as $\psi_{\text{int}}(x,x_1,\ldots,x_N)$, where x is the coordinate of the excitation and the x_i are the coordinates of the electrons in the Fermi sea, and $\psi_{\text{free el}}(x,x_1,\ldots,x_N)$ as the many-body wave function of the corresponding plane-wave electron plus Fermi sea, we know that the orthogonality catastrophe implies the matrix element $\langle \text{int}|\text{free el}\rangle$ equals

$$\begin{aligned}\langle \text{int}|\text{free el}\rangle &= \int_{-\infty}^{\infty} dx\, dx_1 \cdots dx_N \psi_{\text{int}}^*(x,x_1,\ldots,x_N) \\ &\quad \times \psi_{\text{free el}}(x,x_1,\ldots,x_N) \\ &= \mathcal{O}(1/L),\end{aligned}$$

and so vanishes in the thermodynamic limit. Thus it would seem that in fact the two excitations do not coincide.

However, we are not interested in matrix elements involving full eigenstates of the Hamiltonian, but matrix elements involving asymptotic scattering states defined far from the impurity. These are the states of concern in applying a Landauer-Buttiker formalism. With such states, we would evaluate the above matrix elements by restricting $x,x_i \ll 0$ or $x, x_i \gg 0$, depending on whether the state is ingoing or outgoing. With such a restriction, the orthogonality catastrophe does not apply and

$$\langle \text{int}|\text{free el}\rangle = 1 + \mathcal{O}(1/L).$$

In this sense the excitations coincide.

With this equivalence so understood, the two excitations—the integrable and plane-wave excitations—share the same transformation property (2.48) under the map. We now exploit this fact by combining it with the behavior of the low-energy sector of the theory. In this sector we can take a scaling limit and obtain a relativistic theory invariant under Lorentz transformations. Under such transformations, we can imagine boosting the integrable excitations at the Fermi surface, obtaining in the process an excitation with finite energy and momentum. However, the transformation properties of the excitation cannot be altered by the boost. As such, the boosted excitation will still transform via Eq. (2.48) under the map. This again implies that there is a line in (k,λ) parameter space describing excitations transforming in the desired fashion. In this case moving along this line amounts to making a Lorentz boost.

Having argued that there do exist excitations transforming as Eq. (2.48), we now have to address whether the existence of such excitations is sufficient for our computations of transport properties. We can answer in the affirmative. To compute any given transport quantity in the Landauer-Buttiker approach, we need to sum up transmission amplitudes over some given energy range. For example, if we were to compute the zero-temperature out-of-equilibrium conductance, this energy range would be determined by the

difference of chemical potentials in the two leads. Now imagine looking at a particular infinitesimal energy interval within this range. As we know the density of states of the free electron in the lead and we know that the interactions in the problem do not affect this particular quantity, we know precisely how much charge lies in this interval. Now we are able to construct an integrable state that transforms via Eq. (2.48) with an energy in this interval and with the same density of states as the free particles. Thus our integrable state completely exhausts the charge lying within this infinitesimal interval. Given that we are able to compute its transmission amplitude (2.49), we can compute the contribution of this infinitesimal energy interval to the transport quantity.

As a corollary to this, the manifold of other integrable states arising from the Bethe ansatz equations are then not needed for the computation of transport properties. We do not need to account for the (k,λ) states that do not transform as Eq. (2.48). We also do not need to worry about states consisting of (k,λ) excitations together with particle-hole excitations of k and λ or, indeed, excitations involving more complicated string solutions of the Bethe ansatz equations. The inclusion of such states in the computation of any transport quantity would amount to a double counting, given that the line of (k,λ) states transforming as Eq. (2.48) completely exhausts the density of states of free electrons in the leads.

Given all of this, we still must stress that our computation of scattering amplitudes away from the Fermi surface is in general only approximate. Although we believe that there exists a line of excitations in the (k,λ) parameter space for which we understand and can compute scattering, we do not know which line. Rather, at the symmetric point of the model we have only an ansatz of how this line cuts through parameter space. However, we again stress that this ansatz is supported by the nature of the two scales in the Kondo regime, T_k and $\sqrt{U\Gamma}$. Moreover, our ansatz appears to be extremely good given its agreement with the NRG results of Costi *et al.*

Fortuitously, there is one case where this ansatz is exact: the description of spin $\uparrow$ holes. There the (k,λ) parameter space is one dimensional from the start and no ansatz is needed. We point out that the scattering of such holes provides by far and away the main contribution to the differential magnetoconductance at large fields H. As such, we expect the differential magnetoconductance to be exact at asymptotically large fields.

In order to determine for all cases how the line of linearly transforming excitations cuts through the (k,λ) parameter space we would have to have complete control of the change of basis between the free electrons and integrable excitations. There must presumably exist a complete set of such excitations providing a proper change of basis of the form

$$|E\rangle = \sum c_{n,F_1,\cdots F_k} |F_1,\ldots,F_k\rangle. \tag{2.52}$$

Here the notation is highly symbolic: E stands for any possible integrable excitation, while F_i stands for free electrons with some spin and energy with the sum over the number k, the types, and the energies of such excitations. Presumably, there are some complex selection rules making it possible to match the number of degrees of freedom on the left and on the right of Eq. (2.52). At this point, however, an exact understanding of Eq. (2.52) is beyond our reach.

III. LINEAR-RESPONSE CONDUCTANCE AT $T=0$

In this section we discuss the linear-response conductance both in and out of a magnetic field at zero temperature. We of course note that none of Sec. II is necessary to compute the linear-response conductance at $T=0$. Although we have demonstrated the Friedel sum rule using integrability, all we need for this quantity is the occupancy of the dot as a function of various parameters, something available from the original Bethe ansatz work on the one-lead Anderson model. However, the behavior of the linear-response conductance as predicted by the Bethe ansatz has never been adequately explored, particularly in the case with a magnetic field. Indeed, the original work of Ng and Lee[7] showing that the Friedel sum rule could be applied to quantum dots employs a Hartree-Fock approximation in estimating the dot occupancy and so obtains some qualitatively incorrect predictions as to the behavior of the conductance.

Generally, the linear-response conductance equals

$$G = \frac{e^2}{h}[|T_\uparrow(\varepsilon=0)|^2 + |T_\downarrow(\varepsilon=0)|^2], \tag{3.1}$$

where $T_{\uparrow/\downarrow}(\varepsilon=0)$ is the scattering amplitude at the Fermi surface:

$$|T_{\uparrow/\downarrow}(\varepsilon=0)|^2 = \sin^2(\pi n_{d\uparrow/\downarrow}). \tag{3.2}$$

In the case with $H=0$, the number of electrons on the dot as a function of ε_d, the gate voltage, can be computed exactly, as has been done by Ref. 28. When $H\neq 0$, the equations become more difficult to analyze and in general only numerical solutions are available. However, at the symmetric point, it is again possible to compute in closed form the number of spin $\uparrow/\downarrow$ electrons on the dot[28] and so arrive at an analytic expression for G. We first consider the case with $H=0$.

A. $H=0$ linear-response conductance

In this case the Friedel sum rule tells us that

$$|T_{\uparrow/\downarrow}|^2 = \sin^2\left(\frac{\delta_{\uparrow/\downarrow}(\varepsilon=0)}{2}\right), \tag{3.3}$$

where the phase $\delta_{\uparrow/\downarrow}$ is equal to

$$\delta_{\uparrow/\downarrow} = 2\pi n_{d\uparrow/\downarrow}. \tag{3.4}$$

The number of electrons, $n_{d\uparrow/\downarrow}$, on the dot when $H=0$ simplifies to

$$n_{d\uparrow/\downarrow} = \int_Q^{\tilde{Q}} d\lambda\, \sigma_{\rm imp}(\lambda). \tag{3.5}$$

$\sigma_{\rm imp}(\lambda)$ in turn is given by Eq. (2.19) with the charge Fermi surface B set to the bottom of the band $-D$:

$$\sigma_{\rm imp}(\lambda)=\tilde{\Delta}(\lambda)-\int_Q^{\tilde{Q}} d\lambda' a_2(\lambda'-\lambda)\sigma_{\rm imp}(\lambda'). \quad (3.6)$$

The Fermi surface Q of the spin excitations is determined by the equations

$$\frac{N}{L}=\int_Q^{\tilde{Q}} d\lambda\ \sigma(\lambda),$$

$$\sigma(\lambda)=-\frac{x'(\lambda)}{\pi}-\int_Q^{\tilde{Q}} d\lambda' a_2(\lambda'-\lambda)\sigma(\lambda'). \quad (3.7)$$

These equations are solved explicitly over most of the relevant parameter range in Ref. 28 using a Wiener-Hopf technique.

The solution breaks down into three cases according to the value of Q describing the Fermi surface

Case (i): If we are close to the symmetric point ($U/2+\varepsilon_d \ll \sqrt{(U\Gamma)}$), then $Q \ll 0$ (at the symmetric point, $Q=-\infty$) and we have

$$n_{d\uparrow/\downarrow}=\frac{1}{2}-\frac{1}{\pi\sqrt{2}}\sum_{n=0}^{\infty}\frac{(-1)^n}{(2n+1)}G_+(i\pi(2n+1))$$

$$\times\int_{-\infty}^{\infty} dk\ \Delta(k)e^{-(2n+1)\pi(g(k)-Q)}, \quad (3.8)$$

where G_+ arises in factoring the kernel of the integral equation (3.6):

$$G_+(\omega)=\frac{\sqrt{2\pi}}{\Gamma(\frac{1}{2}-i\omega/2\pi)}\left(\frac{-i\omega+\varepsilon}{2\pi e}\right)^{-i\omega/2\pi}. \quad (3.9)$$

We include above an extra factor of e omitted from Ref. 28 through a typo. Q is determined implicitly by the equation

$$\frac{2\varepsilon_d+U}{\sqrt{2U\Gamma}}=\frac{\sqrt{2}}{\pi}\sum_{n=0}^{\infty}\frac{(-1)^n}{(2n+1)^{3/2}}e^{\pi Q(2n+1)}G_+[i\pi(2n+1)]. \quad (3.10)$$

This differs from Ref. 28 by a factor of 2. This same factor of 2 is missing from Eq. 8.2.38 of Ref. 28, which should, we believe, read

$$\frac{1}{\pi}(\varepsilon_d+U/2)=\int_{-\infty}^{Q} d\lambda\ \sigma(\lambda). \quad (3.11)$$

Case (ii): In the next case the location of the Fermi surface satisfies the constraint

$$0<Q<I^{-1}\equiv\frac{U}{8\Gamma}-\frac{\Gamma}{2U}. \quad (3.12)$$

In this case $n_{d\uparrow/\downarrow}$ is computed to be

$$n_{d\uparrow/\downarrow}=2-\sqrt{2}+\frac{\pi}{6\sqrt{2}}(I^{-1}-Q)-\frac{\pi^2\sqrt{2}}{(24)^2}(I^{-1}-Q)^2$$

$$+\mathcal{O}((I^{-1}-Q)^3). \quad (3.13)$$

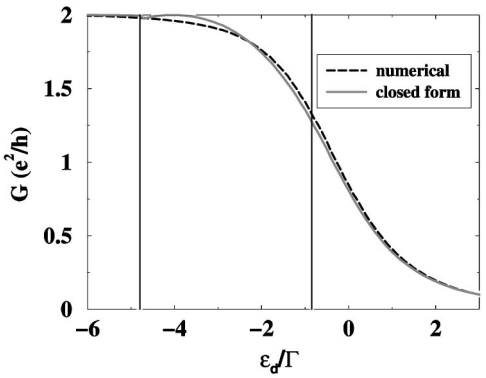

FIG. 4. Plot of the linear-response conductance at zero temperature in zero magnetic field. The parameters used are $U=0.75$ and $\Gamma=U/12$. The dashed line marks out the conductivity derived from a numerical solution of n_d while the solid line represents the closed-form solution described in this section.

The first two terms are found in Ref. 28, although we disagree by a factor of 2 in the term of $\mathcal{O}(I^{-1}-Q)$ while the remaining term was computed by the authors alone.

Case (iii): In the final case we are far from the symmetric point such that $(U/2+\varepsilon_d)\gg\sqrt{U\Gamma}$ and $Q>I^{-1}\equiv U/8\Gamma-\Gamma/(2U)$. We then have instead

$$n_{d\uparrow/\downarrow}=\frac{1}{2\pi^{3/2}}\int_0^{\infty}\frac{dw}{w}\Gamma(1/2+w)e^{2\pi w(1/I-Q)}$$

$$\times\sin(2\pi w)\left(\frac{w}{e}\right)^{-w}, \quad (3.14)$$

with Q in this case determined by

$$Q=q^*+\frac{1}{2\pi}\ln(2\pi e q^*),$$

$$\sqrt{q^*}=\frac{\varepsilon_d+U/2}{\sqrt{2U\Gamma}}. \quad (3.15)$$

In Fig. 4 is plotted the linear-response conductance as a function of the dot chemical potential, $\varepsilon_d>-U/2$ (for $\varepsilon_d<-U/2$ particle-hole symmetry tells us the plot is a mirror image about the $\varepsilon_d=-U/2$ axis), according to this closed-form solution. For the purposes of comparison, we also present the conductance derived from a numerical evaluation of the equations determining n_d. The vertical lines divide the plot according to the three cases of the closed-form solution. We see that this solution best matches the numerical solution in cases (i) and (iii). We also see that the solution makes a discontinuous transition from case (i) to case (ii), a consequence of the approximate nature of the solution in case (ii).

As expected, the linear-response conductance rises smoothly from zero at large, positive values of ε_d to its maximum possible value $2e^2/h$ at the symmetric point of the model, $U/2=-\varepsilon_d$. The ratio of the values of U and Γ chosen for this plot corresponds to that of the experimental realization of a quantum dot discussed in Ref. 1. (Note that our definition of Γ is related to that of Ref. 1 by $\Gamma=\Gamma/2$.)

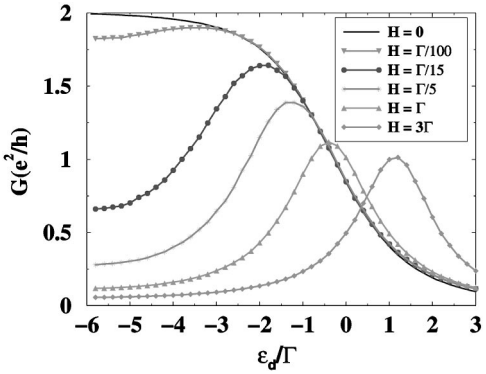

FIG. 5. Plot of the linear-response conductance at zero temperature for various values of the magnetic field. By particle-hole symmetry, the conductance for values of $\varepsilon_d < -U/2$ is obtained by taking the plot's mirror image about the axis $\varepsilon_d = -U/2$. The parameters used are $U = 0.75/\pi D$ (D being the bandwidth) and $\Gamma = U/12$. For these parameters, the Kondo temperature at the symmetric point is $T_k = 0.02508\Gamma$.

B. $H \neq 0$ linear-response conductance

1. Solution away from the symmetric point ($\varepsilon_d > -U/2$)

Again, the transmission amplitude of the electrons is given by Eqs. (3.3) and (3.4). But in this case,

$$n_{d\uparrow} = \int_{-D}^{B} dk\, \rho_{\rm imp}(k) + \int_{Q}^{\tilde{Q}} d\lambda\, \sigma_{\rm imp}(\lambda),$$

$$n_{d\downarrow} = \int_{Q}^{\tilde{Q}} d\lambda\, \sigma_{\rm imp}(\lambda), \tag{3.16}$$

where $\sigma_{\rm imp}$ and $\sigma_{\rm imp}$ are given by Eqs. (2.19).

In general, the equations for $\sigma_{\rm imp}$ and $\sigma_{\rm imp}$ cannot be solved analytically. Therefore, we resort to numerical solutions. In Fig. 5 we plot the result. Presented there is the linear-response conductance as a function of ε_d for a variety of magnetics fields ranging from $H = 0$ to $H = 3\Gamma$.

As H is increased from zero, we see two effects: the value of ε_d marking the conductance peak shifts away from the symmetric point, $\varepsilon_d = -U/2 (= -6\Gamma)$, while the magnitude of the peak decreases. This is as expected. The Kondo temperature for the model is given by Refs. 31 and 28 to be,

$$T_k = \sqrt{\frac{U\Gamma}{2}}\, e^{\pi[\varepsilon_d(\varepsilon_d+U)-\Gamma^2]/(2\Gamma U)}, \tag{3.17}$$

and so varies strongly as a function of the dot chemical potential. When $H > T_k$ we expect the Kondo effect to be suppressed and any consequent enhancement in G to disappear. For values of ε_d away from the symmetric point, T_k is relatively large and thus strong fields are needed to suppress the conductance. Closer to the symmetric point, T_k is exponentially suppressed and weak fields are sufficient to destroy the Kondo effect.

When $H = 0$, a conductance maximum of $2e^2/h$ occurs at the symmetric point. At the symmetric point, $n_{d\uparrow/\downarrow} = 1/2$, and so each spin species makes a corresponding e^2/h contribution to G. As H is increased to large positive values, the gate voltage ε_d at which $n_{d\uparrow/\downarrow} = 1/2$ splits, leading to a corresponding split in the conductance resonance. For example, for large H the resonance associated with the spin $\uparrow$ electrons is approximately e^2/h and occurs at $H/2$.

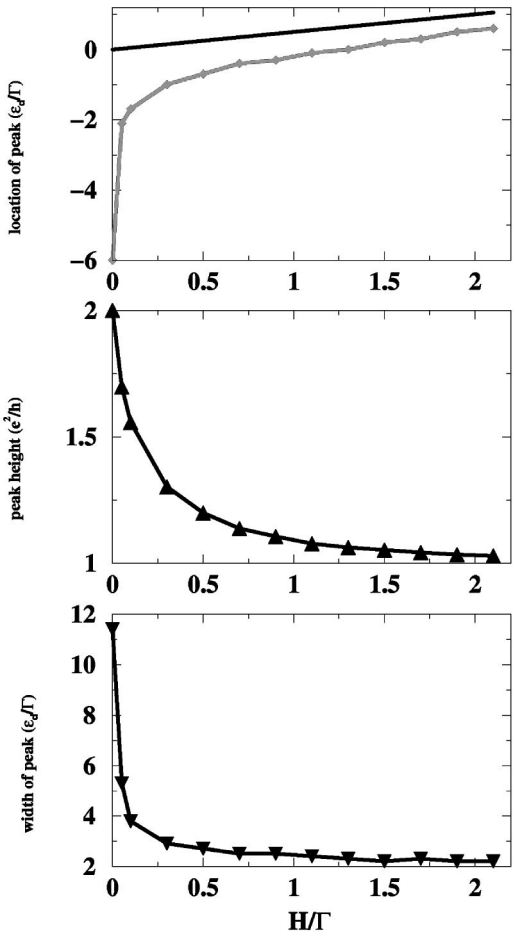

FIG. 6. Plots of how the conductance peak evolves with increasing magnetic field. In the top panel is a plot of the location of the peak while the middle panel records the peak height and the bottom panel gives the peak width. The parameters used are $U = 0.75/\pi D$ (D being the bandwidth) and $\Gamma = U/12$.

We see for example in Fig. 5 that when $H = \Gamma/100$ the Kondo temperature is never exceeded regardless of the value of the gate voltage and so we see little consequent suppression of the conductance. However, for the next largest value of H, $H = \Gamma/15$, the Kondo temperature is exceeded in the Kondo regime and we see a corresponding depression in the conductance in this regime. For the largest value of $H = 3\Gamma$, we see as expected that the peak value is approximately e^2/h and that it occurs roughly at $\varepsilon_d = H/2$.

We note that the linear-response conductance curves are symmetric about their peak value. This differs from the prediction based upon a Hartree-Fock computation of Ng and Lee.[7] But it is in agreement with Meir and Wingreen.[9]

The conclusions in the above discussion are reiterated in Fig. 6. There we plot the behavior of the conductance peak as the magnetic field is increased from zero. In the top panel of Fig. 6 we see that the location of the peak rapidly moves away from $\varepsilon_d = -U/2$ towards the large field value of $H/2$.

The straight line in this panel indicates the behavior of the peak if interactions were absent. Similarly, we see the peak height in the middle panel of Fig. 6 change from its maximal value of $2e^2/h$ at $H=0$ to e^2/h at large fields corresponding to a contribution to the conductance of a single spin species. And finally in the bottommost panel of Fig. 6 we examine the width of the peak. At $H=0$ the width of the peak is approximately 12Γ. However, in the large field limit this settles down to 2Γ appropriate to the conductance being governed by the Breit-Wigner formula,

$$G=\frac{e^2}{h}\frac{\Gamma^2}{\Gamma^2+(\varepsilon_d-H/2)^2}, \tag{3.18}$$

appropriate to a single noninteracting electron species.

2. Solution at the symmetric point ($\varepsilon_d=-U/2$)

Although we cannot in general express the magnetoconductance in closed form, we can do so at the symmetric point. At the symmetric point, the Fermi surface of the spin excitations, Q, goes to ∞. The density equations then simplify to

$$\rho_{\rm bulk}(k)=\frac{1}{2\pi}+g'(k)\int_{-\infty}^{\infty}d\lambda\, a_1(g(k)-\lambda)\sigma_{\rm bulk}(\lambda),$$

$$\sigma_{\rm bulk}(\lambda)=-\frac{x'(\lambda)}{\pi}-\int_{-\infty}^{\infty}a_2(\lambda'-\lambda)\sigma_{\rm bulk}(\lambda')-\int_{-D}^{B}dk\, a_1(\lambda-g(k))\rho_{\rm bulk}(k), \tag{3.19}$$

and

$$\rho_{\rm imp}(k)=\Delta(k)+g'(k)\int_{-\infty}^{\infty}d\lambda\, a_1(g(k)-\lambda)\sigma_{\rm imp}(\lambda),$$

$$\sigma_{\rm imp}(\lambda)=\tilde{\Delta}(\lambda)-\int_{-\infty}^{\infty}d\lambda\, a_2(\lambda'-\lambda)\sigma_{\rm imp}(\lambda')-\int_{-D}^{B}dk\, a_1(\lambda-g(k))\rho_{\rm imp}(k). \tag{3.20}$$

Here the limit B is determined by

$$\frac{2S_z}{L}=\frac{H}{2\pi}=\int_{-D}^{B}dk\,\rho(k). \tag{3.21}$$

As the electrons in the leads are noninteracting, the first equality is a result of Pauli paramagnetism.

The phase shifts are given by

$$\delta_{e\uparrow}=2\pi-\delta_{e\downarrow}=2\pi\int_{Q}^{\tilde{Q}}d\lambda\,\sigma_{\rm imp}(\lambda)+2\pi\int_{-\infty}^{B}dk\,\rho_{\rm imp}(k)$$

$$=\pi+\pi\int_{-\infty}^{B}dk\,\rho_{\rm imp}(k), \tag{3.22}$$

which follows as

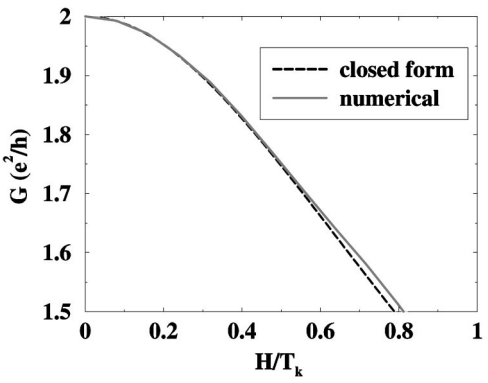

FIG. 7. Plot of the linear response conductance at zero temperature at the symmetric point ($\varepsilon_d=-U/2$) as a function of magnetic field. The parameters used are $U=0.75$ and $\Gamma=U/12$. The dashed line marks out the conductivity derived from a numerical solution of n_d while the solid line represents the closed-form solution described in this section.

$$\int_{-\infty}^{\infty}d\lambda\,\sigma_{\rm imp}(\lambda)=\frac{1}{2}-\frac{1}{2}\int_{-\infty}^{B}dk\,\rho_{\rm imp}(k). \tag{3.23}$$

This is established by integrating $\int_{-\infty}^{\infty}$, Eq. (3.20). We can thus focus solely upon the k distribution.

In order to evaluate the phase shift in the equation above, we are thus interested in computing the integral

$$\int_{-\infty}^{B}dk\,\rho_{\rm imp}(k)=2M_i, \tag{3.24}$$

which, as indicated, is directly related to the impurity magnetization M_i. Using the same Wiener-Hopf technique[28] determined this integral in the case $T_k>H$ to be

$$2M_i=\frac{\sqrt{2}}{\pi}\sum_{n=0}^{\infty}\frac{G_+(i\pi(2n+1))}{(2n+1)}(-1)^n e^{-\pi(2n+1)(b-1/I)},$$

$$b=\frac{1}{\pi}\ln\left(\frac{2}{H}\sqrt{\frac{U\Gamma}{\pi e}}\right). \tag{3.25}$$

Combining this with the expression for the Kondo temperature in Eq. (3.17), we have for the scattering phases at leading order in H/T_k

$$\delta_{e\uparrow}=2\pi-\delta_{e\downarrow}=\pi\left(1+\frac{H}{2T_k}\right), \tag{3.26}$$

which in turn gives the magnetoconductance as

$$G(H)=2\frac{e^2}{h}\left[1-\frac{\pi^2}{16}\left(\frac{H}{T_k}\right)^2+\mathcal{O}\left(\frac{H}{T_k}\right)^4\right]. \tag{3.27}$$

The quadratic deviation from the maximal conductance has the expected Fermi-liquid form.

In Fig. 7 is plotted how the magnitude of the linear-response conductance at the symmetric point changes as a function of H/T_k (for small H) according to this solution. We plot it against the numerical solution, and we obtain agreement at worst of 1.5%. The disagreement becomes larger as

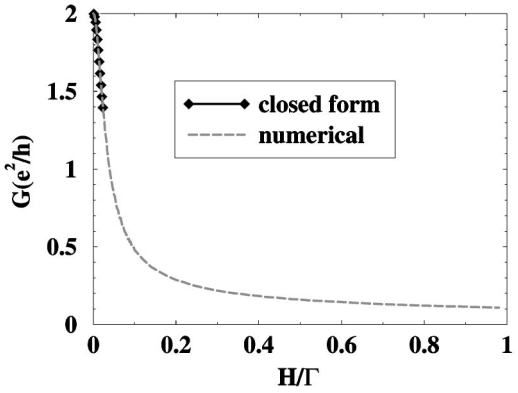

FIG. 8. Plot of the linear-response conductance at zero temperature at the symmetric point ($\varepsilon_d = -U/2$) as a function of magnetic field. The parameters used are $U=0.75$ and $\Gamma = U/12$. The dashed line marks out the conductivity derived from a numerical solution of n_d while the solid line represents the closed-form solution described in this section.

H increases as the closed-form solution is only valid at $H < T_k \propto e^{-1/I}$. Beyond $H > T_k$, we rely entirely on a numerical solution to determine the magnetoconductance. We plot the behavior of $G(H)$ in Fig. 8 up to $H=\Gamma$.

IV. LINEAR-RESPONSE CONDUCTANCE AT FINITE TEMPERATURE

In the previous section we focused upon scattering at the Fermi surface. In this section, we discuss a problem that requires us to understand scattering at finite energy: the linear-response conductance as a function of temperature. We compare it to the NRG results of Costi *et al.* and find excellent agreement. This is important as it indicates that we have an essentially correct description of the low-energy scattering states, i.e., an excellent approximation to the right-hand side of Eq. (2.52).

Computing the linear-response conductance at finite T is a complicated matter. Even though we only consider glued charge and spin excitations as explained in Sec. III, we now have to compute their scattering matrix—the $1/L$ correction of their associated momenta—in the presence of a ''thermalized ground state.'' This ground state is no longer composed of merely real k states and two-string bound states of spin and charge as it was at $T=0$. Rather, all the possible solutions of the Bethe ansatz equations of the model make an appearance. Thus, to begin the computation of the scattering amplitudes at finite T, we give the complete list of excitations in the model.

It is useful to understand how the following calculation differs from the exact computation of the conductances in the fractional quantum Hall problem.[24] The logic of Ref. 24 would first require the identification of all the excitations above the zero-temperature ground state. We then would need to compute both the bulk and impurity scattering matrices of these excitations. Having done this, the second step would be to turn on the temperature. The thermalized ground state would then consist of seas of all these excitations with their distributions determined by a thermodynamic Bethe ansatz, employing the zero-temperature S matrices. Finally, the conductance would be determined by the zero-temperature impurity scattering matrices as in Ref. 24. A potential difficulty in this approach would come in understanding the gluing necessary to form excitations carrying electronic quantum numbers as it only such excitations that can be mapped back to the two-lead picture.

Whatever the likelihood for success, one can see that this way of proceeding requires considerable technical expenditure. It turns out to be easier to determine the thermalized ground state directly from the Bethe ansatz, i.e., by dealing with bare excitations rather than first determining the zero-temperature ground state, classifying its ''physical'' or ''dressed'' excitations and expressing the thermalized ground state in terms of these excitations. On the other hand, with the quantum Hall edges, it was the natural way to proceed as the initial data one had at hand (with no calculations whatsoever) are precisely the excitations about the zero-temperature ground state together with their S matrices, both bulk and impurity.

To proceed then, the first step is to identify all solutions of the Bethe ansatz equations. These are of three types: real k states, spin complexes associated with complex k's (both of which we have seen as the ground state at zero temperature is composed of such excitations), and spin complexes not associated with complex k's. Below we give a more specific description together with the quantum numbers carried by each excitation. The spin quantum numbers are measured relative to a vacuum carrying spin $N/2$ where N is the number of particles in the system.

(i) Real k's: These appear in the ground state at $T=0$ in the presence of a magnetic field. They carry charge e and no spin.

(ii) n-spin complex with no associated k's: An n-complex involves n λ's organized as

$$\lambda^{nj} = \lambda^n + i\left(\frac{n+1}{2} - j\right), \quad j = 1, \ldots, n. \tag{4.1}$$

Here λ^n is a real rapidity and is known as the center of the complex. The n-spin complex carries spin $-n$.

(iii) n-spin complex with $2n$ associated complex k's: The n-complex is organized as before,

$$\lambda^{nj} = \lambda^n + i\left(\frac{n+1}{2} - j\right), \quad j = 1, \ldots, n, \tag{4.2}$$

but now there are two k's associated with each λ^{nj}:

$$g(k^{+nj}) = \lambda^n + i\left(\frac{n}{2} + 1 - j\right), \quad j = 1, \ldots, n,$$

$$g(k^{-nj}) = \lambda^n + i\left(\frac{n}{2} - j\right). \tag{4.3}$$

These excitations carry charge $2ne$ and spin $-n$. The simplest of these excitations ($n=1$) appear in the ground state at zero temperature. Now the claim is that these are solutions to the Bethe ansatz equations (2.7) and (2.8) and indeed they are in the thermodynamic limit (the object of our concern).[28]

We can derive equations constraining the particle-hole densities of these various excitations in the same fashion we arrive at Eqs. (2.11) from Eqs. (2.7) and (2.8). The result is

$$\rho_p(k)+\rho_h(k)=\frac{1}{2\pi}+\frac{\Delta(k)}{L}+g'(k)\sum_{n=1}^{\infty}\int_{-\infty}^{\infty}d\lambda a_n(g(k)-\lambda)[\sigma_{pn}(\lambda)+\sigma'_{pn}(\lambda)],$$

$$\sigma_{hn}(\lambda)=-\frac{x'_n(\lambda)}{\pi}+\frac{\widetilde{\Delta_n}(\lambda)}{L}-\int_{-\infty}^{\infty}a_n(\lambda-g(k))\rho_p(k)-\sum_{m=1}^{\infty}\int_{-\infty}^{\infty}d\lambda' A_{nm}(\lambda-\lambda')\sigma_{pm}(\lambda'),$$

$$\sigma'_{hn}(\lambda)=\int_{-\infty}^{\infty}a_n(\lambda-g(k))\rho_p(k)-\sum_{m=1}^{\infty}\int_{-\infty}^{\infty}d\lambda' A_{nm}(\lambda-\lambda')\sigma'_{pm}(\lambda'),$$

$$x_n(\lambda)=\sqrt{2U\Gamma}\,\mathrm{Re}\left(\lambda+i\frac{n}{2}\right)^{1/2}+n\left(\frac{U}{2}+\varepsilon_d\right)$$

$$\tilde{\Delta}_n(\lambda)=-\frac{1}{\pi}\partial_\lambda\delta_n(\lambda)\equiv-\frac{1}{\pi}\partial_\lambda\,\mathrm{Re}\delta\left(-\sqrt{2U\Gamma}\left(\lambda+i\frac{n}{2}\right)^{1/2}+U/2+\varepsilon_d\right)$$
$$-\frac{1}{2\pi}\partial_\lambda\sum_{k=1}^{n-1}\left\{\delta\left(-\sqrt{2U\Gamma}\left(\lambda+i\frac{i}{2}(n-2k)\right)^{1/2}+U/2+\varepsilon_d\right)+\delta\left(\sqrt{2U\Gamma}\left(\lambda+\frac{i}{2}(n-2k)\right)^{1/2}+U/2+\varepsilon_d\right)\right\}. \quad (4.4)$$

The kernels in the density equations are given by

$$a_n(\lambda)=\frac{2n}{\pi}\frac{1}{(n^2+4\lambda^2)},$$

$$A_{nm}(\lambda)=\delta_{nm}\delta(\lambda)+a_{|n-m|}(\lambda)+2\sum_{k=1}^{\min(n,m)-1}a_{|n-m|+2k}(\lambda)+a_{n+m}(\lambda). \quad (4.5)$$

Here $\rho_{p/h}$ is as before while $\sigma_{p/hn}$ denotes the particle/hole densities of n-strings associated with complex k's (in Sec. II we denoted $\sigma_{p/h1}$ by $\sigma_{p/h}$) and $\sigma'_{p/hn}$ denotes particle/hole densities of n-strings not so associated.

As stated in the introduction of this section, we construct the electronic excitations in the same fashion as at zero temperature, the only difference being that the excitations are now over the thermal ground state, not the $T=0$ ground state. In order to describe the scattering amplitudes we thus need to specify the impurity momentum of the $\rho(k)$ and $\sigma_1(\lambda)$ excitations. The finite-temperature momenta for such excitations are as follows [compare Eqs. (2.20)]:

$$p^{\mathrm{imp}}(k)=\delta(k)+\sum_{n=1}^{\infty}\int_{-\infty}^{\infty}\{\theta_n[g(k)-\lambda]-2\pi\}\times[\sigma^{\mathrm{imp}}_{pn}(\lambda)+\sigma'^{\mathrm{imp}}_{pn}(\lambda)],$$

$$p_1^{\mathrm{imp}}(\lambda)=2\delta_1(\lambda)+\int_{-\infty}^{\infty}dk\,\rho_p^{\mathrm{imp}}(k)\{\theta_1[\lambda-g(k)]-2\pi\}+\sum_{m=1}^{\infty}\int d\lambda'[\Sigma_{1m}(\lambda-\lambda')]\sigma^{\mathrm{imp}}_{pm}(\lambda'), \quad (4.6)$$

with Σ_{nm} given by

$$\Sigma_{nm}(\lambda)=(\theta_{|n-m|}(\lambda)-2\pi)+2\sum_{k=1}^{\min(n,m)-1}(\theta_{|n-m|+2k}(\lambda)-2\pi)+(\theta_{n+m}(\lambda)-2\pi). \quad (4.7)$$

We again can read off the $1/L$ contributions to the momenta and the densities and arrive at the all important relations

$$\partial_k p^{\mathrm{imp}}(k)=2\pi\rho^{\mathrm{imp}}(k),$$
$$\partial_\lambda p_1^{\mathrm{imp}}(\lambda)=-2\pi\sigma^{\mathrm{imp}}(\lambda), \quad (4.8)$$

still valid at finite temperatures. The scattering phases, as they are given (as in Sec. II) from the impurity momenta $p^{\mathrm{imp}}(k)$ and $p_1^{\mathrm{imp}}(\lambda)$, can be computed from a knowledge of ρ^{imp} and σ_1^{imp}. For example, a spin-up excitation constructed from a charge excitation k and a $n=1$ spin-charge complex λ has a scattering phase of the form

$$\delta_e^{\uparrow}=p^{\mathrm{imp}}(k)+p_1^{\mathrm{imp}}(\lambda)=2\pi\int_{-D}^{k}dk\,\rho^{\mathrm{imp}}(k)+2\pi\int_{\lambda}^{\tilde{Q}}d\lambda'\sigma_1^{\mathrm{imp}}(\lambda'), \quad (4.9)$$

identical to Eq. (2.23).

Another piece of the prescription of computing the scattering amplitudes at finite temperature is the energy associated with the charge and spin excitations. The energies of the various excitations can be derived as in Sec. II with the result

$$\varepsilon(k)=k+T\sum_{n=1}^{\infty}\int_{-\infty}^{\infty}d\lambda\,\ln\left(\frac{f(-\varepsilon_n'(\lambda))}{f(-\varepsilon_n(\lambda))}\right)a_n(\lambda-g(k)),$$

$$\ln[f(\varepsilon_n(\lambda))]=-\frac{2}{T}x_n(\lambda)-\int_{-\infty}^{\infty}dk\,g'(k)\ln(f(-\varepsilon(k)))\times a_n(g(k)-\lambda)+\sum_{m=1}^{\infty}\int d\lambda' A_{nm}(\lambda-\lambda')\times\ln(f(-\varepsilon_m(\lambda'))),$$

$$\ln(f(\varepsilon_n'(\lambda)))=-\int_{-\infty}^{\infty}dk\,g'(k)\ln(f(-\varepsilon(k)))a_n(g(k)-\lambda)+\sum_{m=1}^{\infty}\int d\lambda' A_{nm}(\lambda-\lambda')\ln(f(-\varepsilon_m'(\lambda'))),\tag{4.10}$$

where $f(\varepsilon)=[1+\exp(\varepsilon/T)]^{-1}$ is the Fermi distribution. These equations are arrived at by relating the densities to the energies via

$$\exp(\varepsilon(k)/T)=\rho_h(k)/\rho_p(k),$$

$$\exp(\varepsilon_n(\lambda)/T)=\sigma_{nh}(\lambda)/\sigma_{np}(\lambda),$$

$$\exp(\varepsilon_n'(\lambda)/T)=\sigma_{nh}'(\lambda)/\sigma_{np}'(\lambda).\tag{4.11}$$

This relation is chosen so that the energies determine the particle-hole distributions in the same fashion that they do in the case of noninteracting fermionic particles, i.e.,

$$\rho_p(k)=[\rho_p(k)+\rho_h(k)]f(\varepsilon(k)),\tag{4.12}$$

and likewise for $\sigma_{np/h}$ and $\sigma_{np/h}'$. This definition is completely consistent with that at zero temperature. Taking $T\to 0$ in the above recovers Eqs. (2.36). This is a general feature of energy functionals in a thermodynamic Bethe ansatz analysis. However, here the energies are related to the densities in an additional way indicative that the bulk of the system (i.e., the leads) is indeed noninteracting:

$$\rho_{p/h}(k)=\frac{1}{2\pi}\partial_k\varepsilon(k)f(\pm\varepsilon(k)),$$

$$\sigma_{np/h}(\lambda)=-\frac{1}{2\pi}\partial_\lambda\varepsilon_n(\lambda)f(\pm\varepsilon_n(\lambda)),$$

$$\sigma_{np/h}'(\lambda)=\frac{1}{2\pi}\partial_\lambda\varepsilon_n'(\lambda)f(\pm\varepsilon_n'(\lambda)).\tag{4.13}$$

Having specified the energy functionals, we can now determine the particular k and λ we choose in creating an electron. As $H=0$, we will simply focus on spin $\uparrow$ electrons. In forming a spin $\uparrow$ electron we add a k excitation in $\rho(k)$ and a λ hole in $\sigma_1(\lambda)$. The energy of the electron is then

$$\varepsilon_{\rm el}=\varepsilon(k)-\varepsilon(\lambda).\tag{4.14}$$

We again will only allow k to vary in varying $\varepsilon_{\rm el}$ while fixing λ to some λ_o. While at $T=0$ we fixed λ to be Q, its value at the Fermi surface, this is not appropriate at finite temperature as the Fermi surface has become blurred. However, we have another way to characterize the correct choice for λ, at least at the symmetric point, which we give in the following subsection.

We are now ready to specify the final equation governing the finite-temperature linear-response conductance. Given that we construct the electronic excitations by gluing together a fixed spin excitation λ_o and a range of k excitations, these excitations are distributed according to the Fermi distribution, as they must be. Thus the conductance at finite T is given by

$$G(T)=2\frac{e^2}{h}\int_{-\infty}^{\infty}d\varepsilon_{\rm el}(-\partial_{\varepsilon_{\rm el}}f(\varepsilon_{\rm el}))|T(\varepsilon_{\rm el})|^2,$$

$$|T(\varepsilon_{\rm el})|^2=\sin^2\left(\frac{1}{2}\delta_{\rm el}(\varepsilon_{\rm el}=\varepsilon(k)-\varepsilon(\lambda_o),T)\right).\tag{4.15}$$

Here the first formula is the standard Landauer-Büttiker formula applied to the electronic excitations discussed in Sec. II, while the second formula follows from the expression of $|T(\varepsilon_{\rm el})|^2$ in terms of phase shifts in the even and odd leads, and $\delta_{\rm el}$ is given by Eq. (4.9) with $\lambda=\lambda_o$. Finally, we have used the key result that the density of states (per unit of energy) for the electronic excitations is a constant as follows from Eq. (4.13).

Computation at the symmetric point

So far, we have discussed the computation of $G(T)$ in general terms. In this section we specialize to the symmetric point ($\varepsilon_d=-U/2$). There are two reasons to do so. At the symmetric point the equations become more amenable to analysis. However, more importantly, it is only at the symmetric point that we are able to compute the conductance, for it is only at this point that we can compute electron scattering for arbitrary energy, as required by Eqs. (4.15).

The problem is a technical one. The energy functional $\varepsilon(k)$ is bounded below. For example, as the analysis of Refs. 32–34 shows, at the symmetric point $\varepsilon(k)$ satisfies

$$\varepsilon(k)\geqslant -T\ln(3).\tag{4.16}$$

Thus we are unable to compute directly electron scattering phases for energies below $\varepsilon(k=-D)-\varepsilon(\lambda=\lambda_o)$. Rather, for energies below this, we must compute hole scattering and relate this to particle scattering via

$$\delta_e^{\uparrow}(\varepsilon_{\rm el},\varepsilon_d)=\delta_{\rm ho}^{\uparrow}(\varepsilon_{\rm ho}=\varepsilon_{\rm el},-U-\varepsilon_d),\tag{4.17}$$

valid when $H=0$. In order to exploit then this relation, we need $\varepsilon_d=-U-\varepsilon_d$, i.e., $\varepsilon_d=-U/2$. To compute $\delta_{\rm ho}^{\uparrow}$, we remove a k and a λ hole. Thus akin to Eq. (2.45) we have

$$\delta_{\rm ho}^{\uparrow}(\varepsilon_{\rm ho})=2\pi\int_{-D}^{k}dk'\rho_{\rm imp}(k')+2\pi\int_{\lambda_o}^{\tilde{Q}}d\lambda'\sigma_{\rm imp}(\lambda'),$$

$$\varepsilon(k)=-\varepsilon_{\rm ho}+\varepsilon(\lambda=\lambda_o), \tag{4.18}$$

with the difference $\lambda_o\neq Q$ and $\varepsilon(\lambda_o)\neq 0$.

With this, we can now consider the simplifications in the structure of the equations that arise at the symmetric point. Following Ref. 28, we can recast the equations defining the energy functionals in a universal form for energies comparable to T_k, the Kondo temperature. Define

$$\phi_n(\lambda)=\frac{1}{T}\varepsilon_n\left(\lambda-\frac{1}{\pi}\ln\left(\frac{2A}{T}\right)\right),$$

$$\phi_1'(g(k))=-\frac{1}{T}\varepsilon\left(-g(k)+\frac{1}{\pi}\ln\left(\frac{2A}{T}\right)\right),$$

$$\phi_{n+1}'(\lambda)=\frac{1}{T}\varepsilon_n'\left(-\lambda+\frac{1}{\pi}\ln\left(\frac{2A}{T}\right)\right),$$

$$A=\frac{\sqrt{2UT}}{2\pi}. \tag{4.19}$$

In our definition of ϕ_1', we rely upon the fact that in the energy range we are interested in, $\varepsilon(k)$ depends solely upon $g(k)$. With these definitions, ϕ_n and ϕ_n' satisfy the equations

$$\xi_n(\lambda)=-\int_{-\infty}^{\infty}d\lambda' s(\lambda-\lambda')\times\ln(f(T\xi_{n-1}(\lambda))f(T\xi_{n+1}(\lambda)))-\delta_{n1}e^{\pi\lambda}, \tag{4.20}$$

where $\xi_n=\phi_n$ or ϕ_n' and $s(\lambda)=\cosh^{-1}(\pi\lambda)/2$. These equations have been analyzed by Refs. 32–34. In practice, they are highly accurate in determining energies up to scales of tens of T_k's. This is a consequence of two scales existing in the problem, T_k and $\sqrt{U\Gamma}$. These equations focus on the first scale while throwing out information on the second. But because $T_k\ll\sqrt{U\Gamma}$ in the Kondo regime, this approximation is extremely good.

With these equations in hand, we can determine the choice of λ_o. At the symmetric point we expect the scattering phase to be symmetric in energy, i.e.,

$$\delta_{\rm el}(\varepsilon)=\delta_{\rm el}(-\varepsilon), \tag{4.21}$$

regardless of the temperature. We thus fix $\lambda=\lambda_o$ such that Eq. (4.21) is satisfied.

We now derive the specific equations for the impurity densities at the symmetric point. These equations have the initial form

$$\rho^{\rm imp}(k)=\Delta(k)+g'(k)\sum_{n=1}^{\infty}\int_{-\infty}^{\infty}d\lambda\, a_n(g(k)-\lambda)(\sigma_{pn}^{\rm imp}+\sigma_{pn}^{\rm imp})(\lambda),$$

$$\sigma_{hn}^{\rm imp}(\lambda)=\tilde{\Delta}_n(\lambda)-\int_{-\infty}^{\infty}dk\,\rho_p^{\rm imp}(k)a_n(\lambda-g(k))-\int_{-\infty}^{\infty}d\lambda'\sum_{m=1}^{\infty}A_{nm}(\lambda-\lambda')\sigma_{pm}^{\rm imp}(\lambda'),$$

$$\sigma_{hn}'^{\rm imp}(\lambda)=\int_{-\infty}^{\infty}dk\,\rho_p^{\rm imp}(k)a_n(\lambda-g(k))-\int_{-\infty}^{\infty}d\lambda'\sum_{m=1}^{\infty}A_{nm}(\lambda-\lambda')\sigma_{pm}'^{\rm imp}(\lambda'). \tag{4.22}$$

We will recast these equations in a simpler form. We use the inverse of the matrix A_{nm},

$$A_{nm}^{-1}(\lambda)=\delta_{nm}\delta(\lambda)-s(\lambda)(\delta_{nm+1}+\delta_{nm-1}), \tag{4.23}$$

together with the equalities

$$\delta_{n1}s(\lambda-\lambda'')=\int_{-\infty}^{\infty}d\lambda' A_{nm}^{-1}(\lambda-\lambda')a_m(\lambda'-\lambda''),$$

$$\tilde{\Delta}_n(\lambda)=\int_{-\infty}^{\infty}dk\,\Delta(k)a_n(\lambda-g(k)), \tag{4.24}$$

to rewrite Eqs. (4.22) as

$$\rho^{\rm imp}(k)=\Delta(k)+g'(k)\int_{-\infty}^{\infty}d\lambda\, s(\lambda-g(k))\tilde{\Delta}_1(\lambda)-g'(k)\int_{-\infty}^{\infty}d\lambda\, s(\lambda-g(k))[\sigma_{h1}^{\rm imp}(\lambda)+\sigma_{h1}'^{\rm imp}(\lambda)],$$

$$\sigma_{pn}^{\rm imp}(\lambda)+\sigma_{hn}^{\rm imp}(\lambda)=\int_{-\infty}^{\infty}d\lambda' s(\lambda-\lambda')[\sigma_{hn+1}^{\rm imp}(\lambda')+\sigma_{hn-1}^{\rm imp}(\lambda')]+\delta_{n1}\int_{-\infty}^{\infty}dk\,\rho_h^{\rm imp}(k)s(\lambda-g(k)),$$

$$\sigma_{pn}'^{\rm imp}(\lambda)+\sigma_{hn}'^{\rm imp}(\lambda)=\int_{-\infty}^{\infty}d\lambda' s(\lambda-\lambda')[\sigma_{hn+1}'^{\rm imp}(\lambda')+\sigma_{hn-1}'^{\rm imp}(\lambda')]+\delta_{n1}\int_{-\infty}^{\infty}dk\,\rho_p^{\rm imp}(k)s(\lambda-g(k)). \tag{4.25}$$

We can further simplify these equations. For energies $\ll\sqrt{U\Gamma}$, it is an excellent approximation to take

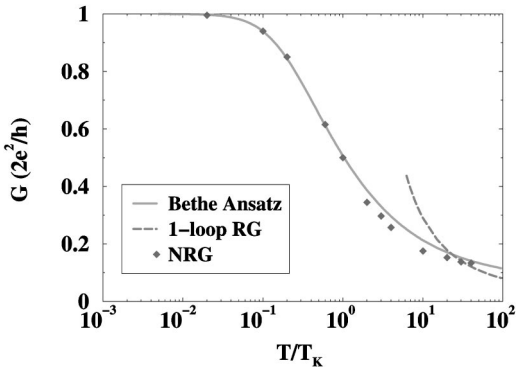

FIG. 9. Plot of the scaling curve for the conductance as a function of T/T_k. Here T_k is as defined in the work of Costi *et al.* and so there are no free parameters. Our computation was carried out at the symmetric point in the Anderson model, $U+2\varepsilon_d=0$.

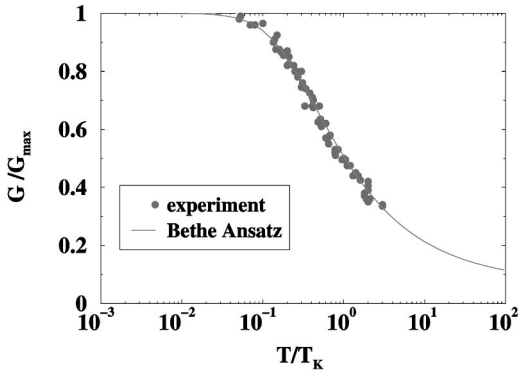

FIG. 10. Comparison of the data from Ref. 1 with the computed scaling curve for the conductance. We now plot on the abscissa the ratio of the conductance with the maximal possible conductance. For the experimental realization in Ref. 1, the dot-lead couplings $V_{1,2}$ are asymmetric and the conductance does not achieve its unitary maximum $2e^2/h$. However, the scaling behavior of $G/G_{\max}$ is expected to be the same.

$$-\frac{g'(k)}{2}\frac{1}{\cosh(\pi[g(k)-I^{-1}])}$$

$$=\Delta(k)+g'(k)\int_{-\infty}^{\infty}s(\lambda-g(k))\tilde{\Delta}_1(\lambda),$$

$$I^{-1}=\frac{U}{8\Gamma}-\frac{\Gamma}{2U}. \tag{4.26}$$

Together with this approximation we can take

$$\sigma_{h1}^{\mathrm{imp}}=0,$$

$$\sigma_m^{\mathrm{imp}}=0, \quad m>1. \tag{4.27}$$

These densities are identically zero at zero temperature and are governed by the energy scale $\sqrt{U\Gamma}$. Since we work at temperatures far below this scale, they can be safely approximated as zero. With this, the density and energy equations can be solved numerically through iteration.

We do so and plot, in Fig. 9, G as a function of T/T_k. Comparing to the NRG computation of Costi *et al.*, we find excellent agreement for energies up to several T_k, the regime where one would expect the NRG, by its very nature, to be most robust. We emphasize that this agreement is achieved with no fitting parameters. Our definition of the Kondo temperature T_k is the same as that used by Costi *et al.* Because of the Fermi-liquid nature of this problem, we know the functional form of the conductance at $T\ll T_k$ is

$$G(T/T_k)=\frac{2e^2}{h}\left(1-c\frac{T^2}{{T_k}^2}+\cdots\right). \tag{4.28}$$

Costi *et al.*,[21] based upon results borrowed from Refs. 35 and 36, computed c to be

$$c=\frac{\pi^4}{16}=6.088\ldots\ . \tag{4.29}$$

We find numerically

$$c=6.05\pm0.1. \tag{4.30}$$

We have arrived at this value by fitting the plot in the region $T/T_k<0.1$. The error is systematic in nature, arising from the arbitrary nature of deciding the region over which to fit.

We also compare our results in Fig. 9 with Ref. 13. It appears that the logarithmic dependence in G,

$$G\sim 1/\ln^2(T/T_k),$$

characteristic of weak coupling and arising from a one-loop RG,[13] should only be expected to become qualitatively descriptive for values of T/T_k in excess of about 20. This observation will play a role in our determination of the validity of our computation of the zero field differential conductance in the next section.

The quality of the fit is a good indicator of the validity of our approach in the Kondo regime. We expect from arguments given in Sec. II that our methodology should be characterized by errors of order $\mathcal{O}(T_k/\sqrt{U\Gamma})\ll 1$, and as such we should see an exact match between our scaling curve and the NRG results. We are thus uncertain whether the slight discrepancy between our results and the results of Costi *et al.* at large T is a consequence of the some unguessed shortcoming in our approach, some problem with the NRG, or some difficulty with our numerics. While we cannot speak to the first two, we do note that our handling of the numerics opens up the possibility for error at large T/T_k; the numerics are fashioned so to more readily reproduce the low-temperature behavior.

We end this section by comparing in Fig. 10 our scaling curve with the experimental results of Ref. 1. We see that we find excellent agreement. We point out, however, that while we compute the scaling curve at the symmetric point ($U/2+\varepsilon_d=0$) of the Anderson model, the data in Ref. 1 were taken away from the symmetric point, but still in the dot's Kondo regime. (The Kondo temperature obtains an exponentially suppressed minimum at the symmetric point and so is usually below the temperature that can be experimentally realized. In order to experimentally see Kondo physics one then must move away from the symmetric point.) The con-

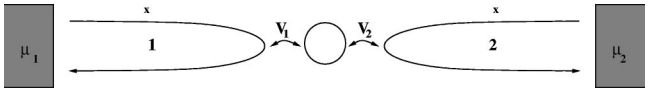

FIG. 11. Sketch of two leads attached to a quantum dot. Each lead is, as indicated, at differing chemical potentials.

tinuing applicability of our scaling curve suggests a certain robustness to the scaling behavior.

V. OUT-OF-EQUILIBRIUM CONDUCTANCE

A. Basic formalism

In order to compute the nonequilibrium conductance we imagine placing the reservoirs attached to each lead at differing chemical potentials as pictured in Fig. 11. This on the face of it poses a problem. In doing do we add a term to the Hamiltonian of the form

$$\mathcal{H}_{\mu}=\mu_1\int dx\, c_1^{\dagger}(x)c_1(x)+\mu_2\int dx\, c_2^{\dagger}(x)c_2(x). \tag{5.1}$$

This term does not behave well under the map into the even/odd electron basis in as much as the odd electron no longer decouples. It would thus seem it is not possible to employ the results of the previous sections in analyzing the out-of-equilibrium system.

However, we must ask what we need to compute the nonequilibrium conductance. We need to know the distribution of particles in each of the two reservoirs. And we need to know the scattering amplitudes of said particles. For the particle distributions, we note that the particles in the two reservoirs do not interact with one another. Knowledge of one distribution is not needed to determine the other. Thus, to compute the distribution of particles in reservoir 1, we can set μ_2 to be whatever is convenient and likewise for the determination of the distribution in reservoir 2. This is notably different from what occurs in the scattering of quasiparticles between quantum Hall edges. In the boundary sine-Gordon formulation of this problem, the two reservoirs—one reservoir of positive solitons and one of negative solitons—do interact with one another. The above device would thus not work in this context.

We emphasize again that the distribution of particles we compute are not the plane wave modes of an electron but rather are ''dressed'' electrons. But they do share several features with plane-wave electrons. Beyond carrying the same quantum numbers of electrons, they share the same constant density of states as a function of energy as the plane-wave electron modes. Moreover, their dispersion relationship is the same as the plane-wave modes.

Having dealt with the computation of the distributions, we now turn to the scattering. Here there is no problem. As we are using an integrable basis, we are able to compute the scattering in the context of the in-equilibrium model. The scattering of the basis of integrable excitations is unaffected by the differing chemical potentials in the leads. We could, if we wished, adopt a basis of (dressed) excitations that was aware of the finite voltage. Although technically challenging, we could also compute the corresponding scattering amplitudes. Such amplitudes, however, would only differ from the original by an overall phase. As the conductance depends upon the absolute value of the scattering matrices, our answer would go unchanged. The sole consequence of $\mu_1 \neq \mu_2$ is then felt in the distributions. In this sense, then, the problem *is* akin to scattering between quantum Hall edges.

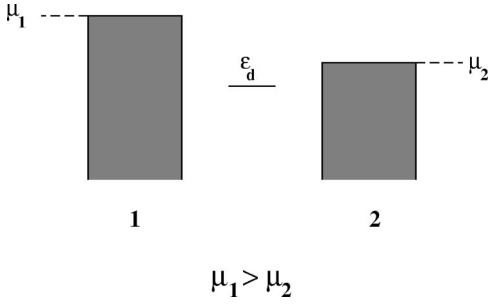

FIG. 12. Sketch of the distribution of particles in the leads when $\mu_1>\mu_2$.

We now proceed with the actual calculation. Here we keep μ_1 constant and imagine varying μ_2 alone. The computation divides itself into two cases: $\mu_1>\mu_2$ and $\mu_2>\mu_1$. We examine the former first.

The case $\mu_1>\mu_2$ is pictured in Fig. 12. As we are at zero temperature, particles will only diffuse from lead 1 to lead 2. The current is thus given by

$$J(\mu_1,\mu_2)=\frac{e}{h}\int_{\mu_2-\mu_1}^{0} d\varepsilon[|T_{\uparrow}^{1\to 2}(\varepsilon,\mu_1)|^2+|T_{\downarrow}^{1\to 2}(\varepsilon,\mu_1)|^2]. \tag{5.2}$$

We have expressed the current as an integral over all energies ranging from zero to $\mu_2-\mu_1$. We note that the above integral reflects that the density of states as a function of energy is constant. Our particular choice of limits in the above integral is a consequence of our conventions: our equations governing the energy of the excitations [see Eq. (2.36)] give the Fermi energy of lead 1 as 0. It is only in this energy range that particles are available to scatter in lead 1 and that are not Pauli blocked in lead 2. We choose energies to parametrize the particles as opposed to either of the parameters k or λ. These latter parameters are not convenient in determining Pauli blocking in that with $\mu_1\neq\mu_2$ the energy functionals for the leads are also not equal, i.e., $\varepsilon_1(k/\lambda) \neq \varepsilon_2(k/\lambda)$. We note that even though μ_1 and μ_2 are bare chemical potentials, they are the correct ones to use in determining the current. They are not renormalized by interactions, understandably, as there are no interactions in the bulk. [Technically this may be seen as follows. Changing the chemical potential in a lead by $\Delta\mu$ yields a change in the number of particles, $\Delta N=\Delta\mu/\pi$. The density of states per unit energy of the λ particles filling the ground state is $\sigma(\varepsilon)=1/2\pi$. As each λ particle is a bound state of two particles, the shift in the Fermi energy induced by the change in chemical potential is precisely $\Delta\mu$.]

It is worthwhile commenting on the dependence of the current J upon μ_1 and μ_2. Although the limits governing the energy range of excitations contributing to transport are a

function of the difference, $\mu_1-\mu_2$, of chemical potentials, the current's dependence upon μ_1 and μ_2 is more complicated. This reflects the dependence of the transmission amplitude $T^{1\to 2}$ upon μ_1 alone. In particular, in the Kondo regime of this problem, the Kondo temperature that appears in the expressions for the current will be a function of $\mu_1-\varepsilon_d$ and will not depend at all upon μ_2.

Appearing in Eq. (5.2) are the electron scattering probabilities $T^{1\to 2}$ from lead 1 to lead 2. The amplitude $T^{1\to 2}$ is given from Eq. (2.6):

$$|T^{1\to}(\varepsilon,\mu_1)|^2=\sin^2\left(\frac{1}{2}\,\delta^1(\varepsilon_{\rm ho}=-\varepsilon,\varepsilon_d-\mu_1)\right). \quad (5.3)$$

The phase for an electron below the Fermi surface, as indicated above, is computed by exciting the corresponding hole. As indicated in the introduction to this section, scattering in this case is determined solely by the dynamics in lead 1.

To compute $\delta_{\rm ho}$ involves exploiting particle-hole transformations. As such, it is worthwhile to consider the cases of zero H and nonzero H separately. With $H=0$, we can compute the scattering of a spin $\downarrow$ hole by relating it to a spin $\uparrow$ electron. According to Eqs. (2.25) and (2.41), we have

$$\begin{aligned}\delta^{1\downarrow}_{\rm ho}(\varepsilon_{\rm ho}>\mu_1,\varepsilon_d-\mu_1)&=\delta^{1\uparrow}_e(\varepsilon_{\rm el}=\varepsilon_{\rm ho},-U-\varepsilon_d+\mu_1)\\&=2\pi\int_{-D}^{k}dk\,\rho^1_{\rm imp}(k)+2\pi\int_Q^{\tilde Q}d\lambda\,\sigma^1_{\rm imp}(\lambda),\end{aligned}$$

$$\varepsilon^1(k)=\varepsilon_{\rm ho}-\mu_1. \quad (5.4)$$

Here the energies $\varepsilon_{\rm el}-\mu_1$ and $\varepsilon_{\rm ho}-\mu_1$ are measured relative to the Fermi surface in lead 1. By SU(2) spin symmetry we then know $\delta^{1\downarrow}_{\rm ho}(\varepsilon_{\rm ho})=\delta^{1\uparrow}_{\rm ho}(\varepsilon_{\rm ho})$. Because of the behavior of ε_d under a particle-hole transformation, we can only directly compute out-of-equilibrium conductances when $\varepsilon_d-\mu_1<-U/2$, unusual in that it is on the other side of the particle-hole symmetric point.

When H is nonzero the situation is more complicated. We no longer can equate spin $\uparrow$ and spin $\downarrow$ scattering. However, we now can compute spin $\uparrow$ hole scattering directly. From Eq. (2.45) we have

$$\begin{aligned}\delta^{1\uparrow}_{\rm ho}(\varepsilon_{\rm ho}>\mu_1,\varepsilon_d-\mu_1)&=2\pi\int_{-D}^{k}dk'\,\rho^1_{\rm imp}(k')+2\pi\int_Q^{\tilde Q}d\lambda\,\sigma^1_{\rm imp}(\lambda),\\ \varepsilon^1(k)&=-(\varepsilon_{\rm ho}-\mu_1).\end{aligned} \quad (5.5)$$

Because the bottom bound on $\varepsilon^1(k)$ is $-H$, we are limited to computing spin $\uparrow$ hole scattering for energies $0<\varepsilon<H$. For spin $\downarrow$ hole scattering we resort to the particle-hole transformation used above:

$$\begin{aligned}\delta^{1\downarrow}_{\rm ho}(\varepsilon_{\rm ho}>\mu_1,\varepsilon_d-\mu_1)&=\delta^{1\uparrow}_e(\varepsilon_{\rm el}=\varepsilon_{\rm ho}-U-\varepsilon_d+\mu_1)\\&=2\pi\int_{-D}^{k}dk'\,\rho^1_{\rm imp}(k')+2\pi\int_Q^{\tilde Q}d\lambda\,\sigma^1_{\rm imp}(\lambda),\\ \varepsilon^1(k)&=\varepsilon_{\rm ho}-\mu_1.\end{aligned} \quad (5.6)$$

We have no similar constraint on the energy range for spin $\downarrow$ scattering. But we can see another issue arises. We are able to compute spin $\uparrow$ hole scattering for a dot chemical potential $\varepsilon_d-\mu_1>-U/2$, while for spin $\downarrow$ hole scattering we can only perform the computation for $\varepsilon_d-\mu_1<-U/2$. We are thus limited in the case of nonzero H to the symmetric point $\varepsilon_d-\mu_1=-U/2$. But given our belief that our ansatz for the scattering states is only valid near the symmetric point, this constraint costs us little.

To compute the energy functional relating the parameter k to the energy we employ the equations

$$\begin{aligned}\varepsilon^1(k)&=k-\frac{H}{2}-\mu_1-\int_Q^{\tilde Q}d\lambda\,\varepsilon^1(\lambda)a_1(\lambda-g(k)),\\ \varepsilon^1(\lambda)&=2x(\lambda)-2\mu_1-\int_Q^{\tilde Q}d\lambda'\varepsilon^1(\lambda')a_2(\lambda'-\lambda)\\&\quad+\int_{-D}^{B}dk\,g'(k)\varepsilon^1(k)a_1(g(k)-\lambda).\end{aligned} \quad (5.7)$$

These equations are identical to those of Eqs. (2.36), but for the presence of μ_1. The Fermi surfaces Q and B are determined as before by

$$\begin{aligned}\varepsilon^1(\lambda=Q)&=0,\\ \varepsilon^1(k=B)&=0;\end{aligned} \quad (5.8)$$

that is, the energy functionals are defined such that the Fermi energy is always zero.

Computing the differential conductance then amounts to computing $-e\partial_{\mu_2}J$:

$$\begin{aligned}G(\mu_1,\mu_2)&=-e\partial_{\mu_2}J(\mu_1,\mu_2)\\&=\frac{e^2}{h}\Big[|T^{1\to 2}_\uparrow(\varepsilon=\mu_2-\mu_1,\mu_1)|^2\\&\quad+|T^{1\to 2}_\downarrow(\varepsilon=\mu_2-\mu_1,\mu_1)|^2\Big]\end{aligned} \quad (5.9)$$

As the particle distribution and correspondent scattering in lead 1 are, as discussed above, only dependent upon μ_1, G has a particularly simple form: there are no terms of the form $\partial_{\mu_2}|T|^2$.

In the second case $\mu_2>\mu_1$ (pictured in Fig. 13), such terms do come into play. Here the current has the form

$$\begin{aligned}J(\mu_1,\mu_2)=-\frac{e}{h}\int_{\mu_1-\mu_2}^{0}d\varepsilon\Big[&|T^{2\to 1}_\uparrow(\varepsilon,\mu_2)|^2\\&+|T^{2\to 1}_\downarrow(\varepsilon,\mu_2)|^2\Big].\end{aligned} \quad (5.10)$$

In this case particles scatter from lead 2 to lead 1. The choice

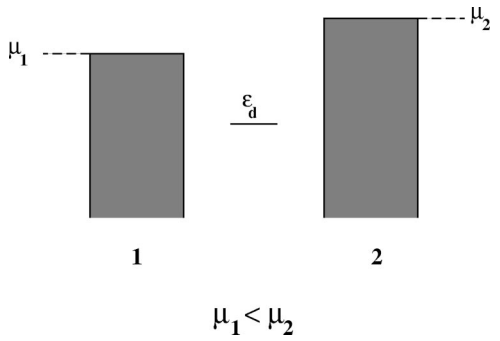

FIG. 13. Sketch of the distribution of particles in the leads when $\mu_1<\mu_2$.

of limits in the above integral now reflects that the Fermi energy in lead 2 has been taken to be zero. $T^{2\to1}$ can be determined by the same set of equations (5.3)–(5.6), but with the energies and densities defined in lead 2. The expression for the differential conductance is more complicated than previously as the scattering matrices are determined on the basis of distributions in leads 2 and so the scattering varies as μ_2 is varied. We thus have

$$G=-e\partial_{\mu_2}J=\frac{e^2}{h}\Big[|T^{2\to1}_{\uparrow}(\varepsilon=\mu_1-\mu_2,\mu_2)|^2+|T^{2\to1}_{\downarrow}(\varepsilon=\mu_1-\mu_2,\mu_2)|^2\Big]+\frac{e^2}{h}\int_{\mu_1-\mu_2}^{0}d\varepsilon\Big[\partial_{\mu_2}|T^{2\to1}_{\uparrow}(\varepsilon,\mu_2)|^2+\partial_{\mu_2}|T^{2\to1}_{\downarrow}(\varepsilon,\mu_2)|^2\Big]. \tag{5.11}$$

Here $T^{2\to1}$ is given by

$$|T^{2\to1}|^2=\sin^2\Big(\frac{1}{2}\,\delta_{\rm ho}(-\varepsilon,\varepsilon_d-\mu_2)\Big)=\sin^2\Big(\frac{1}{2}\,\delta_{\rm el}(-\varepsilon,-\varepsilon_d+\mu_2-U)\Big). \tag{5.12}$$

We thus see explicitly $\partial_{\mu_2}|T^{2\to1}|^2$ is nonzero. When $H\neq0$ recall we can only compute $T_\uparrow$ and $T_\downarrow$ only at the symmetric point. Given that we are varying μ_2 and so varying the effective dot chemical potential, we cannot compute the differential conductance for nonzero H in the case $\mu_2>\mu_1$. Moreover, we are restricted to the region where $\varepsilon_d-\mu_2<-U/2$, also as discussed previously.

We again comment upon the dependence of the current upon μ_1 and μ_2. As with the case $\mu_1>\mu_2$, the current is not simply a function of the difference of the two chemical potentials. In this case, however, the scattering amplitudes depend solely upon μ_2 not μ_1. In particular, in the Kondo regime, the Kondo temperature is determined by difference of μ_2 with the dot chemical potential ε_d.

As $\delta_{\rm ho}$ is given by an equation akin to Eq. (5.5), we can compute $\partial_{\mu_2}|T^{2\to1}|^2$ to be

$$\partial_{\mu_2}|T^{2\to1}(\varepsilon,\mu_2)|^2=\frac{1}{2}\sin(p_{\rm imp}(Q)+p_{\rm imp}(k))\times(\partial_{\mu_2}p_{\rm imp}(Q)+\partial_{\mu_2}p_{\rm imp}(k)),$$

$$\partial_{\mu_2}p_{\rm imp}(Q)=2\pi\int_Q^\infty d\lambda\;\partial_{\mu_2}\sigma_{\rm imp}(\lambda,-\varepsilon_d+\mu_2-U),$$

$$\partial_{\mu_2}p_{\rm imp}(k)=2\pi\int_{-\infty}^{k}dk'\,\partial_{\mu_2}\rho_{\rm imp}(k',-\varepsilon_d+\mu_2-U),$$

$$\varepsilon_2(k)=-\varepsilon. \tag{5.13}$$

From the density equations in Appendix A [see Eq. (A6)], we find that with $H=0$, $\partial_{\mu_2}\sigma_{\rm imp}(\lambda)$ and $\partial_{\mu_2}\rho_{\rm imp}(k)$ satisfy

$$\partial_{\mu_2}\sigma_{\rm imp}(\lambda)=0, \tag{5.14}$$

$$\partial_{\mu_2}\rho_{\rm imp}(k)=\partial_{\mu_2}\Delta(k,-\varepsilon_d+\mu_2-U)+\frac{1}{U\Gamma}\int_{-\infty}^{Q}d\lambda\;\sigma_{\rm imp}(\lambda)s(\lambda-g(k))-(\partial_k g(k))^2\int_{-\infty}^{Q}d\lambda\;\sigma_{\rm imp}(\lambda)s'(\lambda-g(k))-\frac{1}{U\Gamma}\int_{-\infty}^{\infty}dk'\Delta(k')R(g(k)-g(k'))-(\partial_k g(k))^2\int_{-\infty}^{\infty}dk'\Delta(k')R'(g(k)-g(k')), \tag{5.15}$$

where here $g(k)=(k+\varepsilon_d-\mu_2+U/2)^2/(2U\Gamma)$. In computing $\partial_{\mu_2}T$, we have neglected contributions from $\partial_{\mu_2}Q$. We can see from the energy equations (5.7) and (5.8) that

$$\partial_{\mu_2}Q\neq0. \tag{5.16}$$

However, Q, determining the Fermi surface relative to the bottom of the band, is reflective of energy scales on the order of the bandwidth whereas we consider changes in μ_2 of $\mathcal{O}(T_k)$. Hence $\partial_{\mu_2}Q$ is negligible.

B. Differential conductance at $H=0$

The differential conductance in zero field is expected to fall off rapidly with a scale $\sim T_k$ from its linear-response value near the symmetric point of $\sim 2e^2/h$. The characteristics of this peak are related to the peak, the Kondo resonance, in the spectral weight of the impurity density of states as determined by the Bethe ansatz. This is similar to the findings of Refs. 9, 10, and 12 where they cast all transport properties in terms of the impurity density of states though as determined by $\mathrm{Im}\langle dd^\dagger\rangle$. With the Landauer-Buttiker approach we have adopted, all scattering quantities are ultimately related to the equilibrium density of states; the nonequilibrium density of states plays no part in the computation marking an important difference with Refs. 9, 10, and 12. At the sym-

metric point we are able to derive in the case of negative bias $\mu_2 > \mu_1$ a closed-form expression for the differential conductance. Away from the symmetric point we must rely upon a numerical solution of the associated integral equations.

1. Results at the symmetric point

At the symmetric point (and hence only the case $\mu_1 > \mu_2$ assuming μ_2 is being varied), we derive a closed-form expression for the current and differential conductance. At the symmetric point, $\rho_{\rm imp}$ is given by[28]

$$\rho_{\rm imp}(k<0) = -\frac{g'(k)}{2}\frac{1}{\cosh(\pi[g(k)-I^{-1}])} - g'(k)\sum_{n=0}^{\infty} e^{-\pi g(k)(1+2n)} \times \int dk' e^{-\pi g(k')(1+2n)} \,\mathrm{Re}\,\Delta(ik'). \quad (5.17)$$

In order to make use of this expression we need to parametrize k in terms of the energy $\varepsilon(k)$. For energies not far in excess of T_k we find in solving Eq. (5.2) with $H=0$,

$$\varepsilon(k<0)-\mu_1 = \varepsilon^1(k<0) = \frac{\sqrt{2U\Gamma}}{\pi} e^{-\pi g(k)}. \quad (5.18)$$

Hence the scattering phase is given by

$$\begin{aligned}\delta^1_{\rm ho}(\varepsilon, \varepsilon_d-\mu_1 = -U/2) &= \delta^1_{\rm el}(\varepsilon, -U/2) \\ &= 2\pi\int_{-\infty}^{\infty} d\lambda\, \sigma_{\rm imp}(\lambda) + 2\pi\int_{-\infty}^{k} dk' \rho_{\rm imp}(k') \\ &= \frac{3}{2}\pi - \sin^{-1}\left(\frac{1-(\varepsilon-\mu_1)^2/\tilde{T}_k^2}{1+(\varepsilon-\mu_1)^2/\tilde{T}_k^2}\right) \\ &\quad + 2\sum_{n=0}^{\infty}\frac{1}{1+2n}\left(\frac{\pi(\varepsilon-\mu_1)}{\sqrt{2U\Gamma}}\right)^{1+2n} \\ &\quad \times \int dk\, e^{-\pi g(k)(1+2n)}\,\mathrm{Re}[\Delta(ik)], \end{aligned} \quad (5.19)$$

where

$$\tilde{T}_k = \frac{2}{\pi}T_k = \frac{2}{\pi}\sqrt{\frac{U\Gamma}{2}}\, e^{\pi[(\varepsilon_d-\mu_1)(\varepsilon_d-\mu_1+U)-\Gamma^2]/(2\Gamma U)}.$$

The latter term in the above is negligible when $(\varepsilon-\mu_1) \sim T_k$ as $T_k \ll \sqrt{U\Gamma}$.

With this we can compute the current and the differential conductance:

$$J(\mu_1,\mu_2) = -2\frac{e}{h}\tilde{T}_k \tan^{-1}\left(\frac{\mu_2-\mu_1}{\tilde{T}_k}\right),$$

$$G(\mu_1,\mu_2) = -e\partial_{\mu_2}J(\mu_2) = 2\frac{e^2}{h}\frac{1}{[1+(\mu_2-\mu_1)^2/\tilde{T}_k^2]}. \quad (5.20)$$

The simplicity of these results is striking. In our approach, it is directly related to the simple form of the dressed scattering phase (5.19), which only comes about at the end of a complex calculation. It is not clear to us whether there is a more direct way to obtain the results (5.20).

We observe that no $\ln(\mu/T_k)$ terms appear in the above expressions for the current and conductance whereas we might expect such terms for large μ/T_k. In this regime such terms appear in weak-coupling perturbative computations.[13] However, we have already established with our finite-temperature calculation that weak-coupling perturbation theory is not even qualitatively accurate until one exceeds scales of $T/T_k \sim 20$. We expect the differential conductance to be governed by similar considerations. Correspondingly, we would cautiously conclude that our scattering ansatz as applied to the zero-field differential conductance is at least good for energies up to $T/T_k \sim 0$.

Given that we are at the symmetric point, we would expect to be able to make contact with low-energy scattering in the Kondo model as this model should produce identical results to the Anderson model in the low-energy regime. At low energies we have

$$\begin{aligned}\delta^1_{\rm ho}(\varepsilon, \varepsilon_d-\mu_1 = -U/2) &= \frac{3}{2}\pi - \sin^{-1}\left(\frac{1-(\varepsilon-\mu_1)^2/\tilde{T}_k^2}{1+(\varepsilon-\mu_1)^2/\tilde{T}_k^2}\right), \\ &= \pi + 2\tan^{-1}[(\varepsilon-\mu_1)/\tilde{T}_k]. \end{aligned} \quad (5.21)$$

This latter form is identical to that found for spin excitations in the Kondo model.[28] In the exact solution of the Kondo model, the role assigned to ''charge'' and ''spin'' excitations differs from that of the Anderson model. In the Kondo model the charge excitations are noninteracting and so variations in the scattering phase occur solely because of changes in the spin sector. In this sense it is not surprising that we find the scattering phase of electronic excitations in the Anderson model is equal to the scattering phase of spin excitations in the Kondo model. If we were to compute transport properties directly in a two-lead Kondo model, this equivalence suggests how we would have to formulate the scattering ansatz that governs the gluing together of excitations from the two sectors (in the case of the Anderson model, this is discussed in detail in Sec. II). To compute the finite-energy scattering phase for the case of the Kondo model, we would leave k at its Fermi surface value while varying λ, the exact opposite of what we find in the Anderson model.

It is also instructive to recast the impurity density of states so that it is a function of energy:

$$\rho_{\rm imp}(\varepsilon) = \frac{1}{\pi\tilde{T}_k}\frac{1}{1+\varepsilon^2/\tilde{T}_k^2}. \quad (5.22)$$

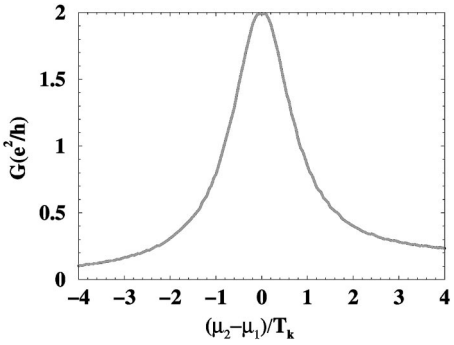

FIG. 14. Plot of the differential conductance in zero magnetic field. The value of the parameters used in the plot are $\Gamma=0.05$, $U=10\Gamma$, and $\varepsilon_d=-5.2\Gamma$, where we set the energy scale in terms of the bandwidth, $D=\pi$.

We see then that the impurity density of states is sharply peaked about zero energy with a peak height proportional to $1/\tilde{T}_k$. The spectral density of states as determined from the dot correlator $\mathrm{Im}\langle dd^\dagger\rangle$ is also sharply peaked around zero energy. In contrast, however, its peak height is proportional to $1/\Gamma$, a wildly different energy scale than the one governing the Bethe ansatz impurity density of states. The two quantities then are clearly different thus undermining an important premise of Ref. 17.

2. Results away from the symmetric point

Pictured in Fig. 14 is a plot of the differential conductance in zero magnetic field. We see that the expected qualitative features appear: namely, the differential conductance sharply varies on energy scales related to the Kondo temperature T_k.

Although we are not exactly at the symmetric point, we must remain close in order to keep true to our methodology of identifying scattering states. If, for example, we were to compute the differential conductance in the mixed-valence regime of the Anderson model, we would find our results unphysical. Our construction of the scattering states was predicated on the knowledge that in the Kondo regime the scattering phase varies on the smallest scale in the problem, the Kondo temperature, and that in turn, only the impurity density of states for the k excitations is governed by this scale. In the mixed-valence regime all of these assumptions break down.

We see that the differential conductance curve in Fig. 14 is asymmetric about $\mu_2-\mu_1=0$. This is a consequence of the asymmetry introduced by variations in the effective Kondo temperature. In the regime $\mu_1>\mu_2$, T_k does not vary as it is solely a function of $\mu_1-\varepsilon_d$ and we have assumed only μ_2 is changing. However, in the regime $\mu_2>\mu_1$, T_k now depends upon $\mu_2-\varepsilon_d$ and so changes in μ_2 lead to changes in T_k and hence the asymmetry in behavior.

C. Results at the symmetric point for $H\neq 0$

At the symmetric point we develop closed-form expressions for the differential conductance. As stated previously, the nature of our construction of the scattering states suggests that our results for the differential magnetoconductance become exact as H/T_k becomes large. Our results are in rough accordance with Ref. 10—we find that for fields $H>T_k$, the $H=0$ differential conductance peak at zero bias divides into two, one peak for each spin species. Roughly speaking, the origin of the split in the differential conductance arises from a similar bifurcation in the impurity density of states. The spectral weight of the Kondo resonance present at $\omega=0$ when $H=0$ divides into two resonances near $eV\sim\pm H$, again one associated with each spin species. The peak at negative bias $\mu_2<\mu_1$ corresponds to a spin $\uparrow$ resonance while the peak occurring with $\mu_2>\mu_1$ is associated with a spin $\downarrow$ resonance. Given our ability to work only at $\mu_2<\mu_1$ at the symmetric point, we explore the former alone.

For fields $H\gg T_k$, this peak is found at a bias close to $-H$. However, unlike Ref. 10 we find the differential conductance peak does not occur exactly at $eV=-H$. This is not surprising as this result was predicated upon a second-order perturbative computation. We find instead that the peak is shifted to values of $e|V|$ smaller than H. For large fields we can develop closed-form expressions for the position, height, and width of the conductance peaks. A related computation was done in Ref. 17 in the context of the Kondo model. However, there the analysis was restricted to the peaks in the *equilibrium-impurity density of states* as determined by the Bethe ansatz and not the conductance *per se*. As discussed previously, the two are not directly or obviously related, as indeed is clear from the work here.

In order to proceed with the computation, we review the constituent elements. The scattering phase for spin $\uparrow$ hole scattering is given by

$$\delta_{\mathrm{ho}}^{\uparrow}(\varepsilon_{\mathrm{ho}}>\mu_1)=2\pi\int_{-D}^{k}dk'\,\rho_{\mathrm{imp}}^{1}(k')+2\pi\int_{-\infty}^{\tilde{Q}}\sigma_{\mathrm{imp}}^{1}(\lambda),$$

$$\varepsilon^1(k)=-(\varepsilon_{\mathrm{ho}}-\mu_1). \tag{5.23}$$

Using Eq. (3.23), we can write the phase solely in terms of ρ_{imp}:

$$\delta_{\mathrm{ho}}^{\uparrow}(\varepsilon_{\mathrm{ho}}>\mu_1)$$

$$=2\pi\int_{-D}^{k}dk'\,\rho_{\mathrm{imp}}^{1}(k')+\pi\left(1-\int_{-D}^{B}dk\,\rho_{\mathrm{imp}}^{1}(k)\right),$$

$$\varepsilon^1(k)=-(\varepsilon_{\mathrm{ho}}-\mu_1). \tag{5.24}$$

The scattering phase for spin $\downarrow$ hole scattering is found to be

$$\delta_{\mathrm{ho}}^{\downarrow}(\varepsilon_{\mathrm{ho}}>\mu_1)$$

$$=2\pi\int_{-D}^{k}dk'\,\rho_{\mathrm{imp}}^{1}(k')+\pi\left(1-\int_{-D}^{B}dk\,\rho_{\mathrm{imp}}^{1}(k)\right),$$

$$\varepsilon^1(k)=\varepsilon_{\mathrm{ho}}-\mu_1. \tag{5.25}$$

through a particle-hole transformation.

For H satisfying $H\ll T_k$, we can arrive at a closed-form expression for the differential magnetoconductance. With $H\ll T_k$, the impurity density of states for the k excitations retains its zero-field form:

$$\rho_{\rm imp}(k) = -\frac{k}{U\Gamma}\frac{1}{2\cosh(\pi[g(k)-I^{-1}])}. \qquad (5.26)$$

The impurity density is unperturbed by the field at first approximation as its spectral weight is found at the scale T_k, while the presence of the field only affects energies far below this by assumption. On the other hand, the energy is shifted by a constant from its zero-field value (again taking $\mu_1 = 0$):

$$\varepsilon^1(k) = \frac{\sqrt{2UT}}{\pi} e^{-\pi g(k)} - H/2, \quad k \gg B,$$

$$\varepsilon^1(k) = \frac{\sqrt{2UT}}{\pi} e^{-\pi g(k)} - H, \quad k \ll B. \qquad (5.27)$$

For $k \gg B$ the energy is shifted by the bare energy of a spin in a magnetic field $H/2$. For $k \ll B$, the effect of the field upon $\varepsilon^1(k)$ can be determined by rewriting the energy $\varepsilon^1(k) \to \varepsilon^1(k) - H$ and substituting in Eq. (A11). We then find that the field H disappears from the the equation, leaving us to conclude that energy is shifted by a dressed magnetic energy H.

Using these forms for the energy and the impurity density, the spin $\uparrow$ scattering phase reduces to

$$\delta^{\uparrow}_{\rm ho}(\varepsilon_{\rm ho} > \mu_1) = \frac{5}{4}\pi - \sin^{-1}\left(\frac{1-(\varepsilon_{\rm ho}-\mu_1-H)^2/\tilde{T}_k^2}{1+(\varepsilon_{\rm ho}-\mu_1-H)^2/\tilde{T}_k^2}\right) + \frac{1}{2}\sin^{-1}\left(\frac{1-H^2/\tilde{T}_k^2}{1+H^2/\tilde{T}_k^2}\right), \qquad (5.28)$$

while for spin $\downarrow$ scattering, we have

$$\delta^{\downarrow}_{\rm ho}(\varepsilon_{\rm ho} > \mu_1) = \frac{5}{4}\pi - \sin^{-1}\left(\frac{1-(\varepsilon_{\rm ho}-\mu_1+H/2)^2/\tilde{T}_k^2}{1+(\varepsilon_{\rm ho}-\mu_1+H/2)^2/\tilde{T}_k^2}\right) + \frac{1}{2}\sin^{-1}\left(\frac{1-H^2/(4\tilde{T}_k^2)}{1+H^2/(4\tilde{T}_k^2)}\right). \qquad (5.29)$$

With this we can compute the differential conductance

$$G(\mu_1,\mu_2) = \frac{e^2}{h}\left[1 + \frac{1}{2}\frac{1+[H^2-(\mu_2-\mu_1)^2]/\tilde{T}_k^2}{(1+H^2/\tilde{T}_k^2)^{1/2}[1+(\mu_2-\mu_1+H)^2/\tilde{T}_k^2]} + \frac{1}{2}\frac{1+[H^2/4-(\mu_2-\mu_1)^2]/\tilde{T}_k^2}{(1+H^2/4\tilde{T}_k^2)^{1/2}[1+(\mu_2-\mu_1-H/2)^2/\tilde{T}_k^2]}\right],$$

$$\tilde{T}_k = \frac{2}{\pi}\sqrt{\frac{U\Gamma}{2}}\, e^{\pi[(\varepsilon_d-\mu_1)(\varepsilon_d-\mu_1+U)-\Gamma^2]/(2\Gamma U)}. \qquad (5.30)$$

Taking $H \to 0$ recovers Eq. (5.20).

For values of $H > T_k$, we must resort to a Wiener-Hopf analysis of the scattering phases. The details have been relegated to Appendix D where exact forms of the scattering phase and the energy $\varepsilon(k)$ can be found. Here however we summarize their asymptotic forms. For $k \ll B$ and $H \gg T_k$, the energy $\varepsilon^1(k)$ as given in Eq. (D8) takes the form

$$\varepsilon^1(k) = -H\left(1 - \frac{1}{2\pi}\tan^{-1}\left(\frac{1}{g(k)-b}\right) - \frac{1}{4\pi^2}\frac{1}{1+[g(k)-b]^2}\left[\frac{\psi(1/2)}{\Gamma(1/2)} + 1 - (g(k)-b)\tan^{-1}\left(\frac{1}{g(k)-b}\right) + \mathbf{C} + \frac{1}{2}\ln(4\pi^2(1+(g(k)-b)^2))\right]\right) + \frac{\sqrt{2\Gamma U}}{\pi^2}\left[\frac{1}{\sqrt{2e\pi}}\frac{e^{-b\pi}}{1+(g(k)-b)^2} + e^{-\pi g(k)}\tan^{-1}\left(\frac{1}{g(k)-b}\right)\right] + O([g(k)-b]^{-3}), \qquad (5.31)$$

where $C = 0.577\,216\ldots$ is Euler's constant and b is given by

$$b = \frac{1}{\pi}\ln\left(\frac{2}{H}\sqrt{\frac{UT}{\pi e}}\right). \qquad (5.32)$$

Note that only the first two terms in the above expansion are at leading order, but we need include the remaining terms in order to obtain reasonable estimates of the properties of the conductance peak. Under similar conditions for k and H we obtain an expression for $\int dk\, \rho_{\rm imp}$:

$$2\pi\int_{-\infty}^{k} dk\, \rho_{\rm imp} = \pi + 2\tan^{-1}(2(I^{-1} - g(k))),$$

$$I^{-1} = \frac{U}{8\Gamma} - \frac{\Gamma}{2U}, \qquad (5.33)$$

where again I^{-1} determines the Kondo temperature $T_k \sim e^{-\pi I}$.

Combining this analysis with numerical work and the results in Eqs. (5.30) allows us to plot in Fig. 15 the magnetoconductance for a variety of values of H/T_k. As explained earlier, we are able only able to compute the magneto-

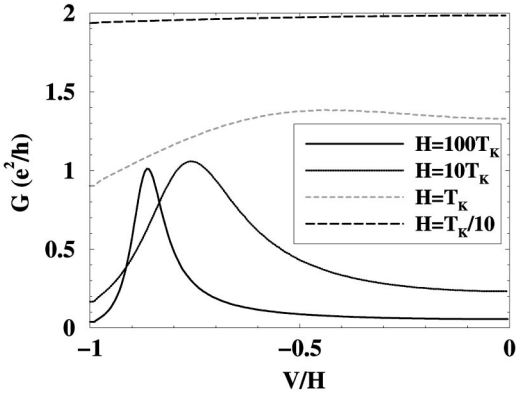

FIG. 15. Plot of the differential conductance in a magnetic field at the symmetric point. The value of the parameters used in the plot are $\Gamma=0.05$ and $U=10\Gamma$.

conductance for biases satisfying $\mu_2<\mu_1$. Nonetheless, we expect the differential conductance to be roughly symmetric about the $V=0$ axis.

We see that for $H\gg T_k$ the behavior of the differential conductance is in rough accordance with the predictions of Wingreen and Meir,[9] that is, there is a peak approximately at $\mu_2-\mu_1\sim H$ for $H\gg T_k$. However, as we have already noted, the peak occurs at a bias noticeably smaller than H while Ref. 10 finds the peak to occur exactly at H. As H is decreased, this peak moves to smaller ratios of $(\mu_1-\mu_2)/H$ before disappearing altogether at $H\sim T_k$. For values of $H\ll T_k$, the differential conductance does not appreciably change from its linear response value for voltage biases of the same order of magnitude as H. We also see that as H is increased the width of the peak narrows and the height of the peak approaches the value of e^2/h, indicating that only a single spin species (in this case spin $\uparrow$) is contributing to the conductance.

We now analyze the properties of the differential conductance peak for values of $H\gg T_k$. As we have already noted in Sec. III, we expect our results to be exact in the regime that H/T_k becomes asymptotically large. In this regime the differential magnetoconductance is determined solely by the spin $\uparrow$ hole scattering, which we are exactly able to determine: no scattering ansatz is needed here.

For $H/T_k\gg 1$, we can write the scattering phases as follows:

$$\begin{aligned}\delta^{\uparrow}_{\rm ho}(\varepsilon_{\rm ho}>\mu_1)&=2\pi\int_{-D}^{k}dk'\rho^1_{\rm imp}(k')\\&\quad+\pi\left(1-\int_{-D}^{B}dk\,\rho^1_{\rm imp}(k)\right)\\&\approx\pi+2\tan^{-1}(2(I^{-1}-g(k))),\\\delta^{\downarrow}_{\rm ho}(\varepsilon_{\rm ho}>\mu_1)&=2\pi\int_{-D}^{k}dk'\rho^1_{\rm imp}(k')\\&\quad+\pi\left(1-\int_{-D}^{B}dk\,\rho^1_{\rm imp}(k)\right)\\&\approx\frac{3}{2}\pi+\tan^{-1}(2(I^{-1}-b)).\end{aligned}\tag{5.34}$$

In the first of the above equations, the second integral has been neglected relative to the first, valid for $H\gg T_k$. We also make the approximation that the spin $\downarrow$ conductance varies inappreciably from its Fermi surface value as the bias is varied. Thus we set $k=B$ in the second of the equations. As the conductance of the spin $\downarrow$ species for large $eV\sim H\gg T_k$ is constant, the peak maximum occurs when

$$\delta^{\uparrow}_{\rm ho}(\varepsilon_{\rm ho}>\mu_1)=\pi.\tag{5.35}$$

This is turn implies the condition

$$g(k)=I^{-1},\tag{5.36}$$

and so from Eq. (5.31) the bias at which the maximum occurs is

$$\begin{aligned}eV_{\rm max}&=\varepsilon^1(k=-\sqrt{2U\Gamma}I^{-1})\\&=-H\left(1-\frac{1}{2\pi}\tan^{-1}\frac{1}{I^{-1}-b}+\cdots\right),\\I^{-1}-b&=\frac{1}{\pi}\ln\left(\frac{H}{2T_k}\sqrt{\frac{\pi e}{2}}\right),\end{aligned}\tag{5.37}$$

where the ellipsis indicates that we have not written out all the terms arising from Eq. (5.31). The half maxima of the peak occur when

$$\delta^{\uparrow}_{\rm ho}(\varepsilon_{\rm ho}>\mu_1)=\frac{\pi}{2}\Big/\frac{3\pi}{2},$$

which in turn implies

$$g(k)=I^{-1}\pm 1/2.\tag{5.38}$$

Hence the peak width equals

$$\begin{aligned}e\Delta V&=\varepsilon^1(k=-\sqrt{2U\Gamma}(I^{-1}-1/2))\\&\quad-\varepsilon^1(k=-\sqrt{2U\Gamma}(I^{-1}+1/2)),\\&=\frac{H}{2\pi}\left(\tan^{-1}\frac{1}{I^{-1}-\frac{1}{2}-b}-\tan^{-1}\frac{1}{I^{-1}+\frac{1}{2}-b}\right)+\cdots.\end{aligned}\tag{5.39}$$

Finally, we can estimate the peak height. The peak maximum will be characterized by the maximal conductance of the spin $\uparrow$ electrons (e^2/h) together with the associated conductance of the spin $\downarrow$ electrons. The latter will vary only slightly from its Fermi surface value as already discussed. Hence the height of the peak is given by

$$\begin{aligned}G_{\rm max}&=\frac{e^2}{h}\left[1+\sin^2\left(\frac{1}{2}\,\delta^{\downarrow}_{\rm ho}(\varepsilon=\varepsilon_F)\right)\right]\\&=\frac{e^2}{h}\left(\frac{3}{2}-\frac{(I^{-}-b)}{\sqrt{4(I^{-1}-b)^2+1}}\right).\end{aligned}\tag{5.40}$$

The results for the location and width of the differential conductance peak are similar to those found by Moore and Wen[17] to characterize the location and width of peaks ap-

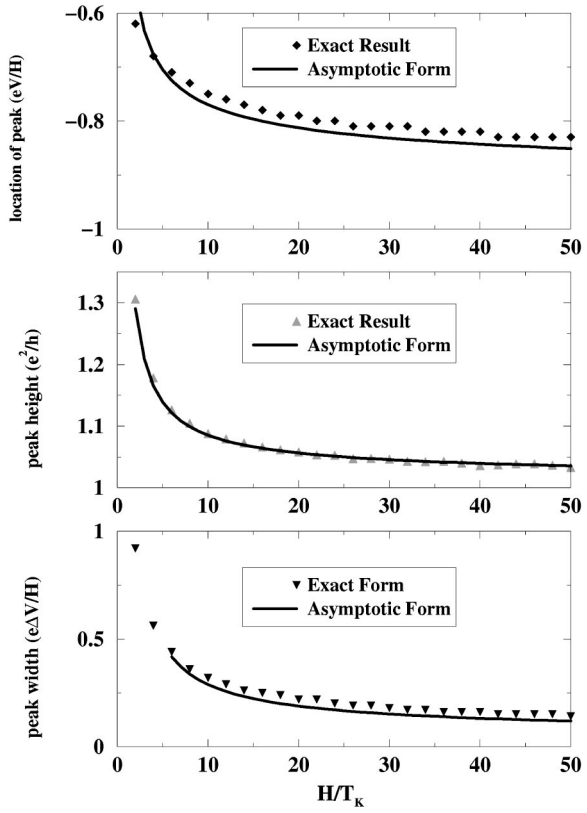

FIG. 16. Plots describing the evolution of the differential conductance peak with increasing magnetic field. In the top panel is a plot of the location of the peak while the middle panel records the peak height and the bottom panel gives the peak width. The parameters used are $U=0.75/\pi D$ (D being the bandwidth) and $\Gamma=U/12$.

pearing in the equilibrium Bethe ansatz impurity density of states for the Kondo model. In the large-H limit, the impurity density of states as found in the Bethe ansatz then evidently shares certain properties with the nonequilibrium spectral density of states defined from the dot correlator $\mathrm{Im}\langle dd^{\dagger}\rangle$, but, however,[17] makes no prediction as to the height of the differential conductance peak. We in general do not expect the height of the peak in the Bethe ansatz impurity density of states to be related to the height of the spectral density arising from $\mathrm{Im}\langle dd^{\dagger}\rangle$. We already know that no such relationship exists at $H=0$ (see Sec. V B 1), and there is no reason to expect it to appear at finite H.

In Fig. 16 we plot how peak characteristics evolve with increasing H. For comparison, we plot both the asymptotic forms [Eqs. (5.36)–(5.38)] for the peak characteristics against the exact results. We see that the location of the peak slowly approaches $eV=-H$ with increasing H. This approach will be logarithmic in H as

$$\frac{eV_{\max}}{H}+1\sim\frac{1}{2\pi}\frac{1}{I^{-1}-b}, \tag{5.41}$$

and $b\sim\ln(H)$. Similarly, the height of the peak approaches e^2/h, but again logarithmically in H. We note that the asymptotic forms reproduce the exact results with remarkable accuracy even in the region $H\sim T_k$, where the assumptions of their derivation do not necessarily hold.

VI. CONCLUDING REMARKS

Computing transport properties in a strongly interacting system is a difficult challenge. In this paper we have attacked the problem by combining a Landauer-Buttiker approach together with data from integrability. We have thus been able to provide a description of the scattering states in the theory that has led to several successes. We have verified the Friedel sum rule and provided a quantitative description of the linear response conductance at $T=0$ both in and out of a magnetic field. Our most striking result has, however, been the computation of the finite-temperature linear-response conductance scaling curve. This result is predicated upon an accurate description of the scattering states away from the Fermi surface. As such, we have also been able to compute the out-of-equilibrium current, again both in and out of a magnetic field. In particular, we have provided a quantitative description of the differential magnetoconductance. Given the nature of our construction of the scattering states, we believe our computation of this latter quantity to become exact in the large-field limit.

While our technique bears a degree of resemblance to the successful, exact treatment of interacting quantum Hall edges,[24] the technical complexity of the two-lead Anderson model has prevented us from finding a definitive solution of the problem in all regimes. However, we have still been able to use integrability to find extremely good approximations to the exact results in the cases of greatest experimental interest. The situation here is not altogether different from the use of form factors in calculating correlation functions: although the techniques of integrability do not (yet) generically lead to closed-form expressions, they are nevertheless a breakthrough, providing excellent approximations which are valid from the lowest energies through crossover regimes. These approximations are far different from the standard, mean-field ones, for they contain all the crucial features of low-dimensional, strong interactions. In particular, the results presented here represent an improvement on previous approximate methods found in the literature. The quality of our approach can be gauged from the excellent reproduction (with no fitting parameter) of the NRG finite-temperature linear-response curve of Costi *et al.* It is unlikely other analytical techniques could do the same.

Our work raises two kinds of questions. The first is whether higher-order approximations can be devised in the present problem, akin to taking higher-energy intermediate states into account in form-factor calculations of correlation functions. More precisely, is it possible to develop further the description of the fermions in terms of the integrable states found in Eq. (2.52)? The other, more practical question is whether similar calculations can be performed in other models of interest and so obtain excellent approximations of out-of-equilibrium transport properties based upon the exact solution of the thermodynamics and the proper identification of scattering states.

ACKNOWLEDGMENTS

The authors would like to thank T. Costi for sharing his NRG data. R.K. would like to thank Y. Meir, N. Wingreen, L. Glazman, and T. Costi for useful discussions. H.S. thanks N. Andrei and A. Georges for many useful discussions. R.K. has been supported by NSERC, the NSF through Grant No. DMR-9802813 and through the Waterman Award under Grant No. DMR-9528578, and the University of Virginia Physics Department. H.S. has been supported by the Packard Foundation, the NYI Program, and the DOE (H.S.). H.S. also acknowledges hospitality and support from the LPTHE (Jussieu) and LPTMS (Orsay). A.W.W.L. has been supported by the NSF through Grant No. DMR-00-75064. A.W.W.L. also acknowledges hospitality and partial support from NWO, University of Amsterdam (the Netherlands).

APPENDIX A: PRACTICAL COMPUTATION OF DENSITY AND ENERGY FUNCTIONALS

Here we present equations for the energy and density functionals that are more amenable to numerical analysis. The original density equations are given by

$$\rho_p(k)+\rho_h(k) = \frac{1}{2\pi}+\frac{\Delta(k)}{L}+g'(k)\int d\lambda\, a_1(g(k)-\lambda)\sigma_p(\lambda),$$

$$\sigma_p(\lambda)+\sigma_h(\lambda) = -\frac{x'(\lambda)}{\pi}+\frac{\tilde{\Delta}(\lambda)}{L} - \int d\lambda' a_2(\lambda'-\lambda)\sigma_p(\lambda') - \int dk\, a_1(\lambda-g(k))\rho_p(k). \quad \text{(A1)}$$

Expressing these equations in terms of the Fourier transform of $\sigma(\lambda)$ gives us

$$\rho_p(k)+\rho_h(k) = \frac{1}{2\pi}+\frac{\Delta(k)}{L}+g'(k)\int \frac{d\omega}{2\pi} e^{-i\omega g(k)} e^{-|\omega|/2}\sigma_p(\omega),$$

$$\sigma_p(\omega)+\sigma_h(\omega) = -\frac{x'(\omega)}{\pi}+\frac{\tilde{\Delta}(\omega)}{L} - e^{-|\omega|}\sigma_p(\omega) - \int dk\, e^{i\omega g(k)} e^{-|\omega|/2}\rho_p(k). \quad \text{(A2)}$$

Solving for $\sigma_p(\omega)$ and substituting into the right-hand side (RHS) of both of the above equations gives

$$\begin{aligned}\rho_p(k)+\rho_h(k) &= \frac{1}{2\pi}+\frac{\Delta(k)}{L}-g'(k)\int d\lambda\, \sigma_h(\lambda)s(\lambda-g(k)) \\ &\quad -g'(k)\int \frac{d\omega}{2\pi} e^{-i\omega g(k)}\left(\frac{x'(\omega)}{\pi}-\frac{\tilde{\Delta}(\omega)}{L}\right) \\ &\quad \times\frac{1}{2\cosh(\omega/2)} \\ &\quad \times -g'(k)\int dk'\rho_p(k')R(g(k)-g(k')),\end{aligned}$$

$$\begin{aligned}\sigma_p(\lambda)+\sigma_h(\lambda) &= -\frac{x'(\lambda)}{\pi}+\int d\lambda' R(\lambda'-\lambda)\frac{x'(\lambda')}{\pi}+\frac{\tilde{\Delta}(\lambda)}{L} \\ &\quad -\int d\lambda' R(\lambda'-\lambda)\frac{\tilde{\Delta}(\lambda')}{L}+\int d\lambda'\sigma_h(\lambda')R(\lambda'-\lambda) \\ &\quad -\int dk\,\rho_p(k)s(\lambda-g(k)),\end{aligned} \quad \text{(A3)}$$

where $R(\lambda)$ and $s(\lambda)$ are given by

$$R(\lambda)=\frac{1}{2\pi}\int d\omega\frac{e^{-i\omega\lambda}}{1+e^{|\omega|}},$$

$$s(\lambda)=\frac{1}{2\cosh(\pi\lambda)}=\frac{1}{2\pi}\int d\omega\frac{e^{-i\omega\lambda}}{2\cosh(w/2)}. \quad \text{(A4)}$$

We can further simplify the first of the equations in Eqs. (A3) by using the relations

$$-\frac{x'(\lambda)}{\pi}=\int dk\frac{d\omega}{(2\pi)^2}e^{-i\omega(\lambda-g(k))}e^{-|\omega|/2};$$

$$\tilde{\Delta}(2)=\int dk\frac{d\omega}{2\pi}\Delta(k)e^{-i\omega(\lambda-g(k))}e^{-|\omega|/2}. \quad \text{(A5)}$$

Then

$$\begin{aligned}\rho_p(k)+\rho_h(k) &= \left(\frac{1}{2\pi}+\frac{\Delta(k)}{L}+g'(k)\int dk' R(g(k)-g(k'))\right. \\ &\quad \left.\times\left(\frac{1}{2\pi}+\frac{\Delta(k')}{L}\right)\right)-g'(k)\int d\lambda\,\sigma_h(\lambda)s(\lambda-g(k)) \\ &\quad -g'(k)\int dk'\rho_p(k')R(g(k)-g(k')),\end{aligned}$$

$$\sigma_p(\lambda)+\eta_h(\lambda)=\int dk\left(\frac{\Delta(k)}{L}+\frac{1}{2\pi}\right)s(\lambda-g(k))+\int d\lambda' \sigma_h(\lambda')R(\lambda'-\lambda)-\int dk\,\rho_p(k)s(\lambda-g(k)). \tag{A6}$$

These forms of the equations are better behaved numerically as

$$\int d\lambda\, R(\lambda)=\frac{1}{2}, \tag{A7}$$

while

$$\int d\lambda\, a_n(\lambda)=1. \tag{A8}$$

Hence, when we go to solve these equations iteratively, successive iterations grow increasingly small as $(1/2)^n$, whereas before we would not necessarily expect convergence.

We can now derive new equations for the energy functional. As in Eq. (2.34), we find

$$\delta E=L\int dk(\varepsilon^+(k)\delta\rho_p(k)-\varepsilon^-(k)\delta\rho_h(k))+L\int d\lambda(\varepsilon^+(\lambda)\delta\sigma_p(\lambda)-\varepsilon^-(\lambda)\delta\sigma_h(\lambda))$$
$$=L\int dk\left(k-\frac{H}{2}\right)\delta\rho_p(k)+2L\int d\lambda\, x(\lambda)\delta\sigma_p(\lambda). \tag{A9}$$

But now from Eqs. (A6) we have

$$\delta\rho_p(k)+\delta\rho_h(k)=-g'(k)\int d\lambda\ \delta\sigma_h(\lambda)s(\lambda-g(k))-g'(k)\int dk'\,\delta\rho_p(k')R(g(k)-g(k')),$$
$$\delta\rho_p(\lambda)+\delta\rho_h(\lambda)=\int d\lambda'\,\delta\sigma_h(\lambda')R(\lambda'-\lambda)-\int dk\ \delta\rho_p(k')s(\lambda-g(k)) \tag{A10}$$

Solving for $\delta\sigma_p/\delta\rho_h$ and substituting into Eq. (A9) leaves us with

$$\varepsilon^+(k)+\varepsilon^-(k)=k-\frac{H}{2}-2\int d\lambda\, x(\lambda)s(\lambda-g(k))+\int d\lambda\ \varepsilon^+(\lambda)s(\lambda-g(k))-\int dk'g'(k')\varepsilon^-(k')R(g(k)-g(k')),$$
$$\varepsilon^+(\lambda)+\varepsilon^-(\lambda)=2x(\lambda)-2\int d\lambda' R(\lambda-\lambda')x(\lambda')+\int d\lambda'\varepsilon^+(\lambda')R(\lambda-\lambda')+\int dk\, g'(k)\varepsilon^-(k)s(g(k)-\lambda). \tag{A11}$$

APPENDIX B: COMPUTING SCATTERING VIA THE IMPURITY ENERGY

In this appendix we compute the scattering phase of the electronic excitations through examining the impurity energy. To do so we will relate the impurity energy to the impurity momentum and then use the already established relations in Sec. II. In doing so, we will bring out subtleties in defining the impurity energy for the purposes of deriving scattering phases.

To determine the impurity energy of the excitations, we play a game similar to that used previously in deriving $\varepsilon(k)/\varepsilon(\lambda)$. The total impurity energy has the form [from Eq. (2.10)]

$$E_{\rm imp}=-\int d\lambda\ \sigma_p(\lambda)(2\Gamma(\lambda))-\int dk\,\rho_p(k)\delta(k), \tag{B1}$$

where $\Gamma(\lambda)=\mathrm{Re}\,\delta(x(\lambda)+iy(\lambda))$. Hence the bulk energy is given by

$$E_{\rm bulk}=E-\frac{1}{L}E_{\rm imp}=L\int d\lambda\ \sigma_p(\lambda)2\left(x(\lambda)+\frac{\Gamma(\lambda)}{L}\right)+L\int dk\,\rho_p(k)\left(k-\frac{H}{2}+\frac{\delta(k)}{L}\right). \tag{B2}$$

We can thus derive equations for the bulk energy of the excitations:

$$\varepsilon^+_{\rm bulk}(k)+\varepsilon^-_{\rm bulk}(k)=k-\frac{H}{2}+\frac{\delta(k)}{L}-\int d\lambda\ \varepsilon^-_{\rm bulk}(\lambda)a_1(\lambda-g(k)),$$
$$\varepsilon^+_{\rm bulk}(\lambda)+\varepsilon^-_{\rm bulk}(\lambda)=2\left(x(\lambda)+\frac{\Gamma(\lambda)}{L}\right)-\int d\lambda'\varepsilon^-_{\rm bulk}(\lambda')a_2(\lambda'-\lambda)+\int dk\, g'(k)\varepsilon^-_{\rm bulk}(k)a_1(g(k)-\lambda). \tag{B3}$$

When we add particles to the system, we want to add them relative to the Fermi surface as determined by the host system (in other words, we add them far from the impurity). In light of this, we have another constraint determining the locations Q and B of the two Fermi surfaces:

$$\varepsilon_{\rm bulk}(k=B)=\varepsilon_{\rm bulk}(\lambda=Q)=0. \tag{B4}$$

Of course, any bulk quantity will not distinguish between a Fermi surface set as above or a Fermi surface determined by

$$\varepsilon(k=B)=\varepsilon(\lambda=Q)=0. \tag{B5}$$

The difference between the two amounts to $1/L$ corrections. However, this difference is important if one is looking at impurity quantities. See in contrast Ref. 28 in the context of the Kondo problem.

We are now in a position to relate the impurity energy to the impurity density of states. Differentiating the above leads to

$$\partial_k\varepsilon^+_{\rm bulk}(k)+\partial_k\varepsilon^-_{\rm bulk}(k)$$

$$=1+\frac{\delta'(k)}{L}-g'(k)\int d\lambda\ \partial_\lambda\varepsilon^-_{\rm bulk}(\lambda)a_1(\lambda-g(k)),$$

$$\partial_\lambda\varepsilon^+_{\rm bulk}(\lambda)+\partial_\lambda\varepsilon^-_{\rm bulk}(\lambda)$$

$$=2\left(x'(\lambda)+\frac{\Gamma'(\lambda)}{L}\right)-\int d\lambda'\partial_{\lambda'}\varepsilon_{\rm bulk}(\lambda')a_2(\lambda'-\lambda)$$

$$+\int dk\ \partial_k\varepsilon^-_{\rm bulk}(k)a_1(g(k)-\lambda). \tag{B6}$$

Writing

$$\partial\varepsilon_{\rm bulk}=\partial\varepsilon-\frac{1}{L}\partial\varepsilon_{\rm imp}, \tag{B7}$$

where $\varepsilon_{\rm imp}$ is the $1/L$ contribution to the energy of the excitation, and comparing to Eq. (2.19) leads to the relations

$$\partial_\lambda\varepsilon_{\rm imp}(\lambda)=-\partial_\lambda p_{\rm imp}(\lambda)=2\pi\sigma_{\rm imp}(\lambda),$$

$$\partial_k\varepsilon_{\rm imp}(k)=-\partial_k p_{\rm imp}(k)=-2\pi\rho_{\rm imp}(k). \tag{B8}$$

Hence, for spin $\uparrow$ electrons, the scattering phase is given by

$$\delta_e^\uparrow=-\varepsilon_{\rm imp}(k)-\varepsilon_{\rm imp}(\lambda). \tag{B9}$$

Moreover, we have

$$\varepsilon_{\rm imp}(\lambda)=-2\pi\int_\lambda^{\tilde{Q}}\sigma_{\rm imp}(\lambda),$$

$$\varepsilon_{\rm imp}(k)=-2\pi\int_{-D}^{k}\rho_{\rm imp}(k), \tag{B10}$$

allowing us to prove the Friedel sum rule. Note that these relationships only hold due to our choice in defining the Fermi surface as in Eq. (B4).

APPENDIX C: DIRECT COMPUTATION OF THE SCATTERING PHASE

It is possible to provide another derivation of the Friedel sum rule that involves a direct computation of the scattering phase (as opposed to working through the mediating agent of the impurity densities). For (purely technical) simplicity we restrict ourselves to the case of a vanishing magnetic field where there are no real k's in the ground state.

As we discussed in Sec. II, the computation of an electron scattering phase involves the phases of a k particle and a λ hole. As we work in the zero-field limit, the k-particle phase is zero and we can focus solely upon the phase of the λ hole. To this end, we consider the bulk density of the λ_α's, $\sigma_{\rm bulk}(\lambda)$. In the ground state, $\sigma_{\rm bulk}(\lambda)$ obeys the equation

$$\sigma_{\rm bulk}(\lambda)+\int_Q^\infty d\lambda' a_2(\lambda-\lambda')\sigma_{\rm bulk}(\lambda')=-\frac{1}{\pi}x'(\lambda). \tag{C1}$$

Following the discussion in Ref. 37, the key quantity in the following will be the shift of this distribution when a particle or a hole is created at rapidity Λ. To study this quantity, we go back to the discrete form of the Bethe ansatz equations, which read

$$2\pi J_\alpha+\sum_{\beta=1}^{M}\theta_2(\lambda_\alpha-\lambda_\beta)=-2Lx(\lambda_\alpha). \tag{C2}$$

If a hole is made at Λ, the rapidities shift $\lambda_\alpha\to\lambda_\alpha^{(1)}$ and the above equation becomes

$$2\pi J_\alpha+\sum_{\beta=1}^{M}\theta_2(\lambda_\alpha^{(1)}-\lambda_\beta^{(1)})-\theta_2(\lambda_\alpha^{(1)}-\Lambda)=-2Lx(\lambda_\alpha^{(1)}). \tag{C3}$$

Setting

$$\sigma_{\rm bulk}(\lambda_\alpha)[\lambda_\alpha^{(1)}-\lambda_\alpha]\equiv\frac{1}{L}F(\lambda_\alpha|\Lambda), \tag{C4}$$

it easily follows using the equation for $\sigma_{\rm bulk}(\lambda)$ in Eq. (1) that

$$F(\lambda|\Lambda)+\int_Q^\infty d\lambda' a_2(\lambda-\lambda')F(\lambda'|\Lambda)=-\frac{1}{2\pi}\theta_2(\lambda-\Lambda), \tag{C5}$$

where $\theta_2(x)=2\tan^{-1}(x)-\pi$. To proceed, it is convenient to introduce the integral operators $\hat{K}$ and $\hat{L}$ defined by

$$\hat{K}(f(\lambda))\equiv-\int_Q^\infty d\lambda' a_2(\lambda-\lambda')f(\lambda') \tag{C6}$$

and

$$(\hat{I}-\hat{K})(\hat{I}+\hat{L})=\hat{I}. \tag{C7}$$

From Eq. (C7) and the fact that

$$a_2(\lambda)=\frac{1}{2\pi}\frac{d}{d\lambda}\theta_2(\lambda),$$

it follows that

$$F(\lambda|\Lambda)=\int_{\Lambda}^{\infty}d\lambda' L(\lambda,\lambda'). \tag{C8}$$

A similar formula with a minus sign would hold if a particle were created in lieu of a hole at Λ. One can represent $\hat{L}$ as a power series if one wishes:

$$L(\lambda,\lambda')=-a_2(\lambda-\lambda')+\int_{Q}^{\infty}d\lambda'' a_2(\lambda-\lambda'')a_2(\lambda''-\lambda') +\cdots \tag{C9}$$

Hence, in particular, $L(\lambda,\lambda')=L(\lambda',\lambda)$.

Now consider the impurity density of states, $\sigma_{\rm imp}$. It obeys

$$\sigma_{\rm imp}(\lambda)+\int_{Q}^{\infty}d\lambda' a_2(\lambda-\lambda')\sigma_{\rm imp}(\lambda')=\tilde{\Delta}(\lambda), \tag{C10}$$

from which it follows that

$$\int_{Q}^{\infty}d\lambda\ \sigma_{\rm imp}(\lambda)=-\frac{1}{2\pi}\phi(Q)+\int_{Q}^{\infty}d\lambda\ F(\lambda|Q)\tilde{\Delta}(\lambda), \tag{C11}$$

having set $\phi(\lambda)\equiv -2\ \mathrm{Re}\ \delta[x(\lambda)+iy(\lambda)]$ and where we have used that $\phi(\infty)=0$. As

$$n_d=2\int_{Q}^{\infty}d\lambda\ \tilde{\sigma}_{\rm imp}(\lambda), \tag{C12}$$

we find

$$n_d=-\frac{1}{\pi}\phi(Q)+2\int_{Q}^{\infty}d\lambda\ \tilde{\Delta}(\lambda)F(\lambda|Q), \tag{C13}$$

the key formula of this appendix. The RHS of the above equation is highly suggestive: the first term is proportional to the bare scattering phase of the electron while the second term represents the dressing of the bare phase that results from the nontrivial ground state of the system.

To complete this section we now explicitly demonstrate the Friedel sum rule. To do so we first imagine scattering the unperturbed ground state through the impurity. The entire scattering phase is then

$$\sum_{\beta=1}^{M}\phi(\lambda_\beta). \tag{C14}$$

Now we imagine scattering the ground state plus hole through the impurity with a resultant total phase

$$-\phi(\Lambda)+\sum_{\beta=1}^{M}\phi(\lambda_\beta^1). \tag{C15}$$

The difference of the two defines the scattering phase of the electron:

$$\delta_{\rm el}=-\phi(\Lambda)+2\pi\int_{Q}^{\infty}d\lambda' F(\lambda'|\Lambda)\tilde{\Delta}(\lambda'). \tag{C16}$$

Comparing Eq. (C13) with Eq. (C16) shows that with $\Lambda=Q$ we arrive at $\delta_{\rm el}=\pi n_d=2\pi n_{d\uparrow/\downarrow}$, the Friedel sum rule in the particular case when the magnetic field vanishes.

APPENDIX D: WIENER-HOPF ANALYSIS AT THE SYMMETRIC POINT

1. Alternative equation for $\varepsilon^1(k)$

We first solve the equation governing $\varepsilon^1(k)$, the energy of excitations in lead 1 relative to the Fermi surface. To do so we cast it in a different form than found in Eq. (5.7). For simplicity, we assume that μ_1 is zero. However, finite μ_1 does not change the expression for ε^1 provided $\mu_1\ll D$.

Now $\varepsilon^1(k)$ is the energy associated with adding or removing a k excitation. Thus imagine removing a $k_0<B$. This induces a change in the densities $\rho(k)$ and $\sigma(\lambda)$. At the symmetric point, the unperturbed densities have the form [see Eq. (6)]

$$\rho(k)=\rho_o(k)-g'(k)\int_{-\infty}^{B}dk'\rho(k')R(g(k)-g(k')),$$

$$\sigma(\lambda)=\sigma_o(\lambda)-\int_{-\infty}^{B}dk\,\rho(k)s(\lambda-g(k)), \tag{D1}$$

while the perturbed densities $\rho_1(k)$ and $\sigma_1(\lambda)$ due to the hole at k_0 are

$$\rho_1(k)=\rho_o(k)-\frac{1}{L}\delta(k-k_0)-g'(k)\times\int_{-\infty}^{B}dk'\rho_1(k')R(g(k)-g(k')),$$

$$\sigma_1(\lambda)=\sigma_o(\lambda)-\int_{-\infty}^{B}dk\,\rho_1(k)s(\lambda-g(k)), \tag{D2}$$

where L is the system size. Rewriting ρ_1 as

$$\rho_1(k)\to\rho_1(k)-\frac{1}{L}\delta(k-k_0),$$

yields

$$\rho_1(k)=\rho_o(k)+\frac{1}{L}g'(k)R(g(k_0)-g(k))-g'(k)\int_{-\infty}^{B}dk'\rho_1(k')R(g(k)-g(k')),$$

$$\sigma_1(\lambda)=\sigma_o(\lambda)+\frac{1}{L}s(\lambda-g(k_0))-\int_{-\infty}^{B}dk\,\rho_1(k)s(\lambda-g(k)). \tag{D3}$$

And so changes in the density, apart from the $\delta(k-k_0)/L$ term already scaled out, are governed by

$$\begin{aligned}\delta\rho(k) &\equiv L(\rho_1(k)-\rho(k))\\ &= g'(k)R(g(k_0)-g(k))\\ &\quad - g'(k)\int_{-\infty}^{B} dk'\,\delta\rho(k')R(g(k)-g(k')),\end{aligned}$$

$$\begin{aligned}\delta\sigma(\lambda) &\equiv L(\sigma_1(\lambda)-\sigma(\lambda))\\ &= s(\lambda-g(k_0))-\int_{-\infty}^{B} dk\;\delta\rho(k)s(\lambda-g(k)).\end{aligned} \tag{D4}$$

The energy of the excitation can be expressed in terms of $\delta\rho$ and $\delta\sigma$:

$$\begin{aligned}-\varepsilon^1(k_0) &= -\left(k_0-\frac{H}{2}\right)+\int dk(k-H/2)\,\delta\rho(k)\\ &\quad +2\int d\lambda\, x(\lambda)\,\delta\sigma(\lambda),\\ &= -\left[(k_0-H/2)-2\int d\lambda x(\lambda)s(\lambda-g(k_0))\right]\\ &\quad +\int dk\;\delta\rho(k)\\ &\quad \times\left[k-\frac{H}{2}-2\int d\lambda x(\lambda)s(\lambda-g(k))\right];\end{aligned} \tag{D5}$$

We see that $\varepsilon^1(k_0)$ depends now only upon $\delta\rho$. That this form for $\varepsilon^1(k_0)$ is equivalent to the equations in Sec. III or Appendix A can be shown using the technology found in Appendix C.

Provided $B<0$, we can introduce a change of variables that simplifies matters:

$$\rho(z)\equiv -\frac{\rho(k)}{g'(k)},\quad z\equiv g(k),\quad k<0. \tag{D6}$$

At energies not far in excess of the Kondo temperature we have

$$(k-H/2)-2\int d\lambda\, x(\lambda)s(\lambda-g(k))\approx\frac{\sqrt{2U\Gamma}}{\pi}e^{-\pi g(k)}-\frac{H}{2}. \tag{D7}$$

The above then simplifies to

$$\begin{aligned}\delta\rho(z) &= -R(z-g(k_0))+\int_b^\infty dz'\,\delta\rho(z')R(z-z'),\\ b &= \frac{B^2}{2U\Gamma},\\ -\varepsilon^1(k_0) &= -\left[\frac{\sqrt{2U\Gamma}}{\pi}e^{-\pi g(k_0)}-\frac{H}{2}\right]\\ &\quad +\int dz\;\delta\rho(z)\left[\frac{\sqrt{2U\Gamma}}{\pi}e^{-\pi z}-\frac{H}{2}\right],\\ &= -\frac{\sqrt{2U\Gamma}}{\pi}[e^{-\pi g(k_0)}-\delta\rho(\omega=i\pi)]\\ &\quad +\frac{H}{2}[1-\delta\rho(\omega=0)],\end{aligned} \tag{D8}$$

where in the last line we have expressed $\varepsilon^1(k)$ in terms of the Fourier transform of $\delta\rho$. It is to the equation for $\delta\rho$ that we actually apply the Wiener-Hopf analysis.

The expression for $\varepsilon^1(k)$ is valid provided we have removed a particle, i.e., $g(k_0)>b$ or $k<B$. If we instead add a particle at $k>B$ or $g(k_0)<b$, we obtain in a similar fashion the following description of $\varepsilon^1(k)$:

$$\begin{aligned}\delta\rho(z) &= R(z-g(k_0))+\int_b^\infty dz'\,\delta\rho(z')R(z-z'),\\ b &= \frac{B^2}{2U\Gamma},\\ \varepsilon^1(k_0) &= \frac{\sqrt{2U\Gamma}}{\pi}(e^{-\pi g(k_0)}+\delta\rho(\omega=i\pi))\\ &\quad -\frac{H}{2}(1+\delta\rho(\omega=0)).\end{aligned} \tag{D9}$$

2. Review of the Wiener-Hopf analysis

We so review the technique as presented in Ref. 28 on equations of the general form

$$f(z)=\int_A^\infty dz'\,f(z')h(z-z')+g(z). \tag{D10}$$

Writing $f^{\pm}(z)=f(z)\,\theta(\pm z\mp A)$, the Fourier transform of the above equation yields

$$f^+(\omega)+f^-(\omega)=f^+(\omega)h(\omega)+g(\omega), \tag{D11}$$

where Fourier transforms are defined by

$$a(\omega)=\int d\omega\, e^{i\omega z}a(z). \tag{D12}$$

The key step in the analysis is writing $1-h(\omega)$ as a product of functions $G^{\pm}$, which are analytic in the upper and lower planes, respectively:

$$1-h(\omega)=\frac{1}{G^+(\omega)G^-(\omega)}. \tag{D13}$$

We can then write Eq. (D11) as

$$e^{-i\omega A}\frac{f^+(\omega)}{G^+(\omega)}+e^{-i\omega A}f^-(\omega)G^-(\omega)=g(\omega)G^-(\omega)e^{-i\omega A}. \tag{D14}$$

Given $e^{-i\omega A}f^{\pm}(\omega)$ is analytic in the upper and lower half-planes, applying the operators

$$\pm\frac{1}{2\pi i}\int d\omega'\frac{1}{\omega'-(\omega\pm i\delta)} \tag{D15}$$

to Eq. (D14) yields solutions for both f^+ and f^-:

$$f^+(\omega)=G^+(\omega)\frac{e^{i\omega A}}{2\pi i}\int d\omega'\frac{1}{\omega'-(\omega+i\delta)}\times g(\omega')G^-(\omega')e^{-i\omega' A},$$

$$f^-(\omega)=-\frac{e^{i\omega A}}{G^-(\omega)}\frac{1}{2\pi i}\int d\omega'\frac{1}{\omega'-(\omega-i\delta)}\times g(\omega')G^-(\omega')e^{-i\omega' A}. \tag{D16}$$

3. Determination of $\delta\rho$

Applying the above analysis to Eq. (D8), appropriate to the case of removing a particle, $z>b$ ($k<B$), we have

$$\delta\rho^+(\omega)=-e^{i\omega b}\frac{G^+(\omega)}{2\pi i}\int d\omega'\frac{e^{i\omega'(z_o-b)}}{\omega'-(\omega+i\delta)}\times R(\omega')G^-(\omega'),$$

$$G^{\pm}(\omega)=\sqrt{2\pi}\,\frac{\left(\frac{\mp i\omega+\delta}{2\pi e}\right)^{\mp i\omega/2\pi}}{\Gamma\left(\frac{1}{2}\mp\frac{i\omega}{2\pi}\right)},$$

$$1-R(\omega)=\frac{1}{G_+(\omega)G_-(\omega)},$$

$$b=\frac{1}{\pi}\ln\left(\frac{2}{H}\sqrt{\frac{U\Gamma}{\pi e}}\right). \tag{D17}$$

If $\omega=0$, we can continue the ω' contour into the upper half plane about the branch cut of $G^-(\omega)$ while picking up the pole at $\omega'=0$:

$$\delta\rho(\omega=0)=-1+\frac{1}{\pi^{3/2}}\int_0^\infty d\omega'\frac{\sin(2\pi\omega')}{\omega'}\left(\frac{\omega'}{e}\right)^{-\omega'}\times\Gamma\left(\frac{1}{2}+\omega'\right)e^{-2\pi\omega'[g(k_0)-b]}. \tag{D18}$$

With $\omega=i\pi$, we find instead

$$\delta\rho(\omega=i\pi)=e^{-\pi g(k_0)}+e^{-\pi b}\frac{1}{\pi\sqrt{2e}}\int_0^\infty d\omega'\frac{\sin(2\pi\omega')}{\omega'-\frac{1}{2}}\left(\frac{\omega'}{e}\right)^{-\omega'}\times\Gamma\left(\frac{1}{2}+\omega'\right)e^{-2\pi\omega'[g(k_0)-b]}. \tag{D19}$$

If we now instead add a particle at $k>B$ or $g(k_0)<b$, we obtain from the Wiener-Hopf analysis of Eq. (D9) the following equations:

$$\delta\rho(\omega=0)=\frac{1}{\sqrt{\pi}}\int_0^\infty\frac{d\omega'}{\omega'}e^{2\pi\omega'[g(k_0)-b]}\frac{\tan(\pi\omega')}{\Gamma(\frac{1}{2}+\omega')}\left(\frac{\omega'}{e}\right)^{\omega'},$$

$$\delta\rho(\omega=i\pi)=\frac{e^{-\pi b}}{\sqrt{2e}}\int_0^\infty\frac{d\omega'}{\omega'+\frac{1}{2}}e^{2\pi\omega'[g(k_0)-b]}\frac{\tan(\pi\omega')}{\Gamma(\frac{1}{2}+\omega')}\left(\frac{\omega'}{e}\right)^{\omega'}. \tag{D20}$$

4. Determination of $\delta(k)=2\pi\int dk\,\rho_{\rm imp}$

The impurity density of states, $\rho_{\rm imp}(k)$, obeys an equation of the form

$$\rho_{\rm imp}(z)=\int_b^\infty dz'\rho_{\rm imp}(z')R(z-z')+\frac{1}{2}\frac{1}{\cosh(\pi(z-I^{-1}))},$$

$$\rho_{\rm imp}(z)\equiv-\frac{\rho_{\rm imp}(k)}{g'(k)},\quad z=g(k), \tag{D21}$$

provided $B<0$, i.e., $H\ll\sqrt{U\Gamma}$. As we are interested in the scattering phase, we want to compute

$$\delta(k)=2\pi\int_{-\infty}^k dk'\rho_{\rm imp}(k'). \tag{D22}$$

If $z>b$, appropriate for when we are computing the phase of a hole, $\delta(k)$ becomes

$$\delta(k)=2\pi\int\frac{d\omega}{2\pi}\frac{-ie^{-i\omega g(k)}}{\omega-i\delta}\rho^+(\omega). \tag{D23}$$

In this case Wiener-Hopf gives the solution of $\rho^+(\omega)$ as

$$\rho^+_{\rm imp}(\omega)=\frac{e^{i\omega b}G^+(\omega)}{2\pi i}\int d\omega'\frac{1}{\omega'-(\omega+i\delta)}\times\rho_o(\omega')G^-(\omega')e^{-i\omega' b},$$

$$\rho_o(\omega)=\frac{e^{i\omega I^{-1}}}{2\cosh\frac{\omega}{2}}. \tag{D24}$$

Provided we assume $H>T_k$ or roughly, equivalently, $I^{-1}>b$, this simplifies to

$$\delta(k)=2\tan^{-1}(2[I^{-1}-g(k)])+\pi-\frac{1}{\pi^2}\int_0^\infty d\omega \times\frac{e^{-2\pi\omega(g(k)-b)}}{\omega}\sin(2\pi\omega)\left(\frac{\omega}{e}\right)^{-\omega}\Gamma\left(\frac{1}{2}+\omega\right) \times\int_0^\infty d\omega'\frac{e^{-2\pi\omega'(I^{-1}-b)}}{\omega'+\omega}\sin(\pi\omega') \times\left(\frac{\omega'}{e}\right)^{-\omega'}\Gamma\left(\frac{1}{2}+\omega'\right). \quad \text{(D25)}$$

If, on the other hand, we are interested in the phase of an added particle (i.e., $z<b$), we compute $\delta(k)$ via

$$\delta(k)=2\pi\int_{-\infty}^{k}dk'\rho_{\rm imp}(k') =2\pi-2\pi\int_{-\infty}^{g(k)}dz\,\rho_{\rm imp}(z) =2\pi-2\pi\int\frac{d\omega}{2\pi}\frac{e^{-i\omega g(k)}}{-i\omega+\delta}\rho^-(\omega). \quad \text{(D26)}$$

The Wiener-Hopf analysis then yields for $\rho^-(\omega)$

$$\rho^-_{\rm imp}(\omega)=-\frac{e^{i\omega b}}{2\pi i G^-(\omega)}\int d\omega'\frac{1}{\omega'-(\omega-i\delta)} \times\rho_o(\omega')G^-(\omega')e^{-i\omega' b}. \quad \text{(D27)}$$

This gives the scattering phase as

$$\delta(k)=\frac{3\pi}{2}-\sin^{-1}(\tanh(\pi(g(k)-I^{-1}))) +\frac{1}{2\pi}\mathbf{P}\int d\omega\,\frac{e^{2\pi\omega(g(k)-b)}}{\omega}\frac{\tan(\pi\omega)}{\Gamma(\frac{1}{2}+\omega)}\left(\frac{\omega}{e}\right)^{\omega} \times\mathbf{P}\int d\omega'\frac{e^{-2\pi\omega'(I^{-1}-b)}}{\omega'-\omega}\sin(\pi\omega') \times\left(\frac{\omega'}{e}\right)^{-\omega'}\Gamma\left(\frac{1}{2}+\omega'\right), \quad \text{(D28)}$$

where **P** indicates the principal value of the integral is to be taken.

[1] D. Goldhaber-Gordon, J. Göres, M. Kastner, H. Shtrikman, D. Mahalu, and U. Meirav, Phys. Rev. Lett. **81**, 5225 (1998).

[2] S. Cronenwett, T. Oosterkamp, and L. Kouwenhoven, Science **281**, 540 (1998).

[3] D. Goldhaber-Gordon, H. Shtrikman, D. Mahalu, D. Abusch-Magder, U. Meirav, and M. Kastner, Nature (London) **391**, 156 (1998).

[4] W. G. van der Wiel, S. De Franceschi, T. Fujisawa, J. Elzerman, S. Tarucha, and L. Kouwenhoven, Science **289**, 2105 (2000).

[5] J. Nygard, D. Cobden, and P. Lindelof, Nature (London) **408**, 342 (2000).

[6] J. Appelbaum, Phys. Rev. Lett. **17**, 91 (1966); P. Anderson, *ibid.* **17**, 95 (1966).

[7] T. Ng and P. Lee, Phys. Rev. Lett. **61**, 1768 (1988).

[8] M. Hettler, J. Kroha, and S. Hershfield, Phys. Rev. Lett. **73**, 1967 (1994); Phys. Rev. B **58**, 5649 (1998).

[9] N. Wingreen and Y. Meir, Phys. Rev. B **49**, 11 040 (1994).

[10] Y. Meir, N. Wingreen, and P. Lee, Phys. Rev. Lett. **70**, 2601 (1993).

[11] N. Sivan and N. Wingreen, Phys. Rev. B **54**, 11 622 (1996).

[12] S. Hershfield, J. Davies, and J. Wilkins, Phys. Rev. B **46**, 7046 (1992).

[13] A. Kaminski, Y. Nazarov, and L. Glazman, Phys. Rev. B **62**, 8154 (2000).

[14] A. Schiller and S. Hershfield, Phys. Rev. B **51**, 12 896 (1995); **58**, 14 978 (1998).

[15] N. Kawakami and A. Okiji, Phys. Lett. **86A**, 483 (1982); J. Phys. Soc. Jpn. **51**, 1143 (1982); Solid State Commun. **43**, 365 (1982); A. Okiji and N. J. Kawakami, J. Phys. Soc. Jpn. **51**, 3192 (1982).

[16] P. Wiegmann, V. Filyov, and A. Tsvelick, JETP Lett. **35**, 77 (1982); P. Wiegmann and A. Tsvelick, *ibid.* **35**, 100 (1982); J. Phys. C **16**, 2281 (1982); A. Tsvelick and P. Wiegmann, Phys. Lett. **89A**, 368 (1982); J. Phys. C **16**, 2281 (1983); V. Filyov, A. Tsvelick, and P. Wiegmann, Phys. Lett. **89A**, 157 (1982).

[17] J. Moore and X. Wen, Phys. Rev. Lett. **85**, 1722 (2000).

[18] N. Andrei, Phys. Lett. **87A**, 299 (1982).

[19] J. von Delft, U. Gerland, T. Costi, and Y. Oreg, Phys. Rev. Lett. **84**, 3710 (2000).

[20] D. Meyer, T. Wegner, M. Potthoff, and W. Nolting, Physica B **270**, 225 (1999).

[21] T. Costi, A. Hewson, and V. Vlatic, J. Phys.: Condens. Matter **6**, 2519 (1994); T. Costi, Phys. Rev. Lett. **85**, 1504 (2000).

[22] J. Cardy and G. Mussardo, Nucl. Phys. B **410**, 451 (1993); G. Delfino and G. Mussardo, *ibid.* **455**, 724 (1995); G. Delfino and J. Cardy, Nucl. Phys. B **519**, 551 (1998); J. Cardy and G. Mussardo, Nucl. Phys. B **410**, 451 (1993).

[23] F. Lesage, H. Saleur, and S. Skorik, Phys. Rev. Lett. **76**, 3388 (1996); Nucl. Phys. B **474**, 602 (1996).

[24] P. Fendley, A. W. W. Ludwig, and H. Saleur, Phys. Rev. Lett. **74**, 3005 (1995); **75**, 2196 (1995); Phys. Rev. B **52**, 8934 (1995).

[25] S. Skorik, cond-mat/9708163 (unpublished).

[26] P. Fendley, A. Ludwig, and H. Saleur, cond-mat/9710205 (unpublished).

[27] R. M. Konik, H. Saleur, and A. W. W. Ludwig, Phys. Rev. Lett. **87**, 236801 (2001).

[28] A. Tsvelick and P. Wiegmann, Adv. Phys. **32**, 453 (1983).

[29] N. Andrei, cond-mat/9408101 (unpublished).

[30] D. Langreth, Phys. Rev. **150**, 516 (1966).

[31] D. Haldane, Phys. Rev. Lett. **40**, 416 (1978).

[32] H. Desgranges and K. Schotte, Phys. Lett. **91**, 240 (1982).
[33] J. Johnson and B. McCoy, Phys. Rev. A **6**, 1613 (1972).
[34] M. Gaudin (unpublished).
[35] J. Nozières, J. Low Temp. Phys. **17**, 31 (1974).
[36] K. Yamada, Prog. Theor. Phys. **53**, 970 (1975).
[37] V. Korepin, N. Bogoliubov, and A. Izergin, *Quantum Inverse Scattering Method and Correlation Functions* (Cambridge University Press, Cambridge, England, 1993).